



Delft University of Technology

## Flocculation and consolidation of cohesive sediments under the influence of coagulant and flocculant

Ibanez Sanz, Maria

### DOI

[10.4233/uuid:6e96db66-1df0-4ed1-b343-92939d58d864](https://doi.org/10.4233/uuid:6e96db66-1df0-4ed1-b343-92939d58d864)

### Publication date

2018

### Document Version

Publisher's PDF, also known as Version of record

### Citation (APA)

Ibanez Sanz, M. (2018). Flocculation and consolidation of cohesive sediments under the influence of coagulant and flocculant DOI: [10.4233/uuid:6e96db66-1df0-4ed1-b343-92939d58d864](https://doi.org/10.4233/uuid:6e96db66-1df0-4ed1-b343-92939d58d864)

### Important note

To cite this publication, please use the final published version (if applicable). Please check the document version above.

### Copyright

Other than for strictly personal use, it is not permitted to download, forward or distribute the text or part of it, without the consent of the author(s) and/or copyright holder(s), unless the work is under an open content license such as Creative Commons.

### Takedown policy

Please contact us and provide details if you believe this document breaches copyrights. We will remove access to the work immediately and investigate your claim.

# Flocculation and consolidation of cohesive sediments under the influence of coagulant and flocculant

Thesis

presented for the degree of doctor  
at Delft University of Technology,  
under the authority of the Vice-Chancellor,  
Prof.dr.ir. T.H.J.J. van der Hagen,  
Chairman of the Board of Doctorates,  
to be defended in public in the presence of a committee on

Wednesday, July 4<sup>th</sup>, 2018 at 15:00 o'clock

by

Maria Eugenia Ibanez Sanz

Ingenieria de Caminos  
Universidad Politecnica de Madrid

Born in Soria, Spain

This thesis is approved by the promotor:

Prof. dr. J.C. Winterwerp

Supervisor:

Dr. C. Chassagne

Composition of Examination Committee:

Rector Magnificus	Technische Universiteit Delft, chairman
Prof. dr. J.C. Winterwerp	Technische Universiteit Delft, promotor
Dr. C. Chassagne	Technische Universiteit Delft, copromotor

Independent members:

Prof. dr. C. Jommi	Technische Universiteit Delft
Prof. dr. A. Manning	University of Plymouth
Dr. ir. G. Di Emidio	Universiteit Gent
Prof. dr. M. van Konningsveld	Technische Universiteit Delft
Prof. Wim Uijtewaal	Technische Universiteit Delft
Prof.dr.ir. Z.B. Wang	Technische Universiteit Delft, reserve member

© Maria E Ibanez Sanz, 2018

ISBN 978 94 6233 988 0

All rights reserved. The author encourages the communication of scientific contents and explicitly allows reproduction for scientific purposes, provided the proper citation of the source. Parts of the thesis are published in scientific journals and copyright is subject to different terms and conditions.

To my mum and my brother.



# Contents

<b>List of Contents</b>	<b>13</b>
<b>1 Introduction</b>	<b>17</b>
1.1 Background and motivation . . . . .	17
1.2 Aim and Outline of this research . . . . .	20
References . . . . .	20
<b>2 Particle Size Distribution measurements by Static Light Scattering</b>	<b>25</b>
2.1 Introduction . . . . .	26
2.2 Materials . . . . .	27
2.2.1 Clay . . . . .	27
2.2.2 Sand . . . . .	28
2.2.3 Kaolinite . . . . .	28
2.2.4 Water . . . . .	29
2.3 Methods . . . . .	29
2.3.1 Static Light Scattering (SLS) . . . . .	29
2.3.2 Sieves . . . . .	30
2.3.3 Hydrometer . . . . .	31
2.3.4 Sedigraph . . . . .	32
2.3.5 Summary . . . . .	33
2.4 Results and discussion . . . . .	33
2.4.1 Static Light Scattering . . . . .	34
2.4.2 Comparison between devices . . . . .	41
2.4.3 Application of the new protocol . . . . .	45

2.5	Conclusions . . . . .	51
	References . . . . .	52
<b>3</b>	<b>Experiments: Electrophoretic mobility.</b>	<b>55</b>
3.1	Introduction . . . . .	57
3.2	Materials . . . . .	57
3.2.1	Particles . . . . .	57
3.3	Methods . . . . .	58
3.3.1	Apparatus . . . . .	58
3.3.2	Protocol . . . . .	59
3.4	Theory and Models . . . . .	60
3.4.1	Relation between surface charge and surface potential . . . . .	60
3.4.2	Relation between surface charge and mobility . . . . .	63
3.5	Results and discussion . . . . .	64
3.5.1	Monovalent salt (KCl) . . . . .	64
3.5.2	Wall zeta potential . . . . .	69
3.5.3	Divalent salt (MgCl <sub>2</sub> ) . . . . .	70
3.6	Conclusions . . . . .	73
	References . . . . .	74
<b>4</b>	<b>Effect of polyelectrolytes on the electrokinetic surface potential and flocculation behaviour of cohesive sediments</b>	<b>77</b>
4.1	Introduction . . . . .	79
4.2	Materials . . . . .	80
4.2.1	Clay . . . . .	80
4.2.2	Flocculant . . . . .	81
4.3	Methods . . . . .	81
4.3.1	Particle Size Distribution . . . . .	81
4.3.2	$\zeta$ - Potential . . . . .	84
4.4	Particle size evolution as function of time . . . . .	84
4.4.1	Cationic flocculant (Zetag 7587) . . . . .	85
4.4.2	Anionic flocculant (Zetag 4110) . . . . .	91
4.5	The reversibility of growth and break-up of flocs under applied shear stress. . . . .	96

4.5.1	Cationic flocculant (Zetag 7587)	96
4.5.2	Anionic flocculant (Zetag 4110)	99
4.6	The electrophoretic mobility.	103
4.6.1	Cationic flocculant (Zetag 7587)	104
4.6.2	Anionic flocculant (Zetag 4110)	108
4.7	Conclusions	111
	References	113

## **5 Study of flocculated clay settling rates as function of polyelectrolyte charge, concentration and shear history 121**

5.1	Introduction	123
5.2	Materials	124
5.2.1	Clay	124
5.2.2	Flocculant	124
5.2.3	Water	125
5.3	Methods	125
5.3.1	Settling columns	125
5.3.2	Mixing methods and mixing times	125
5.3.3	Standard procedure to determine the optimum flocculant dose	126
5.4	Settling rate	127
5.4.1	Cationic flocculant	128
5.4.2	Anionic flocculant	131
5.5	Settling time	133
5.5.1	Influence of mixing method	135
5.5.2	Influence settling column size	147
5.6	Conclusions	151
	References	155

## **6 Consolidation of flocculated clay as function of polyelectrolyte charge. 161**

6.1	Introduction	162
6.2	Materials	163
6.2.1	Clay	163
6.2.2	Flocculant	163
6.2.3	Water	163



6.3	Methods . . . . .	164
6.3.1	Experimental set-up . . . . .	164
6.4	Results and discussions. . . . .	164
6.4.1	Hindered settling . . . . .	164
6.4.2	Initial phase of consolidation . . . . .	166
6.4.3	Final phase of consolidation . . . . .	176
6.5	Conclusions . . . . .	179
	References . . . . .	182
<b>7</b>	<b>Application: use of electrophoretic mobility measurements to understand the stability of fine tailings suspensions</b>	<b>187</b>
7.1	Introduction . . . . .	189
7.2	Materials . . . . .	190
7.2.1	Thin fine tailings . . . . .	190
7.2.2	Kaolinite . . . . .	190
7.3	Methods . . . . .	192
7.3.1	XRD measurements . . . . .	192
7.3.2	ESEM measurements . . . . .	192
7.3.3	Particle size from static light scattering . . . . .	192
7.3.4	Electrophoretic mobility measurements . . . . .	193
7.3.5	CO <sub>2</sub> bubbling . . . . .	194
7.4	Results and discussion . . . . .	194
7.4.1	Particle size . . . . .	194
7.4.2	Electrophoretic mobility . . . . .	195
7.4.3	Difference between changing pH with HCl and CO <sub>2</sub> . . . . .	202
7.4.4	Effect of pH on SP02 and kaolinite in the presence of monovalent and divalent electrolyte. . . . .	206
7.5	Conclusions . . . . .	209
	References . . . . .	210
<b>8</b>	<b>Conclusions</b>	<b>215</b>
8.1	Achievements of this research and recommendations . . . . .	215
8.1.1	Accuracy of the measurements . . . . .	216
8.1.2	Effect of polyelectrolyte on the flocculation, settling and consolidation . . . . .	217

	13
8.2 Application to oil sands . . . . .	219
<b>Summary</b>	<b>221</b>
<b>Samenvatting</b>	<b>223</b>
<b>Acknowledgments</b>	<b>225</b>
<b>Curriculum Vitae</b>	<b>229</b>



# Chapter 1

## Introduction

### 1.1 Background and motivation

In estuarine systems, the behaviour of fine grained sediments ( $\leq 10 \mu\text{m}$ ) is of importance to understand the transport and deposition of clayey material. Unlike silt ( $\leq 63 \mu\text{m}$ ) and sand ( $\leq 2 \text{mm}$ ) particles of fine grained sediment have a dynamic particle size distribution, as the particles can aggregate or break depending on the environmental conditions (salinity, pH, shear stress...). In an unaggregated state, i.e. when the particles are not *flocculated* or *coagulated*, their mean particle size is very small ( $\mu\text{m}$  or nm range).

Coagulation	aggregation of colloidal particles by an electrolyte.
Flocculation	aggregation of colloidal particles by flocculating agents like polymers.

These very small particles can be transported over very large distances, and their presence in the whole water column leads to an increased turbidity. The resulting light obscuration can be harmful for the biological activity in the water. A recent example is Lake Markermeer, where the presence of fines in the water column has led to a strongly reduced biological diversity in the lake [De Lucas Pardo, 2014].

On the other hand, when the transition from unaggregated to ag-

gregated state occurs, the light penetration in the water column is increasing as the larger particles settle down. Since this transition occurs in region where driving gradients are present -such as salinity gradients- this is the reason that the settling of flocculated sediments leads to estuarine siltation, hereby leading to an increased dredging activity in harbors. Salinity is responsible for *coagulation* (aggregation by salt) and the presence of organic matter for *flocculation* (aggregation by polymer and polyelectrolyte). Depending on the scientific community, the term flocculation is also used for coagulation. Organic matter can easily adhere to the clay particles of the sediment and induce bridging or patching flocculation between the clay particles [Lagaly et al., 2013]. The influence of organic matter, pH and salinity on natural sediment aggregation has been studied in situ [Manning et al., 2011, Kranck and Milligan, 1992, Liss et al., 2005] and in the laboratory [Gregory, 1988, Tombacz and Szekeres, 2004, Tombácz and Szekeres, 2006, Mietta et al., 2009, Lee et al., 2012, Lagaly et al., 2013, Liss et al., 2004]. Organic matter can be composed of various substances like polysaccharides, lipides, hydrocarbons, and humic acids [Winterwerp and Van Kesteren, 2004]. The variability of organic matter components makes it complicated to understand the flocculation processes. Therefore synthetic flocculants, which have well defined properties, are used in the present thesis to study the different flocculation mechanism due to the different type of surface charge (cationic / anionic) of the polyelectrolyte.

Synthetic flocculants have been studied extensively in disciplines like sanitary engineering (drinking water treatment) and biochemistry [Ackroyd et al., 1986, Mortimer, 1991, Stewart and Thompson, 1997, McLaughlin and Bartholomew, 2007, Sojka et al., 2007]. Anionic polyelectrolytes are abundant in nature, they are also widely used as flocculating agents in industry, in combination with coagulants (inorganic salts). Anionic flocculants need a cationic agent to bind to the sediment [Lee et al., 2012]. This cationic agent is provided by the dissolved inorganic salts in the system. In natural environments, where particles migrate from fresh water to saline water (or opposite), flocculation is influenced by the mixing order of the flocculating agents (flocculants and coagulants). Cationic polyelectrolytes exist in nature, in the form of

linear polysaccharides such as chitosan [Bolto and Gregory, 2007]. For cationic polyelectrolyte in the presence of negatively charged clays, electrostatic attraction is the main driving mechanism [Tripathy and De, 2006, Goodwin, 2009]. Polymer bridging in this case leads to stronger and larger aggregates than those formed by coagulation (aggregation by salt).

Turbulent shear stresses are an important variable for the flocculation process. Flocs formed in natural environments are subject to different limitations than flocs created in an industrial context. The shear stresses experienced by the flocs are very different, as the shear rates in-situ are much lower than those encountered in process plants where slurries are transported through pipes. Shear stresses in-situ are also spatially and seasonally varying. The shear stress determines the growth and break-up of the flocs.

In order to predict flocculation, the surface charge of particles is an important parameter. This can be evaluated by "zeta-potential measurements", where the zeta-potential is a parameter, linked to the surface charge, that helps to understand the aggregation ability of a suspension. This has been confirmed by studies on the coagulation of kaolinite [Mietta, 2010] and flocculation of sediments [Lee et al., 2011, Gregory and Barany, 2011, Yu and Somasundaran, 1996, Narkis et al., 1991]. Most of these studies are done for a given salinity (sea water salinity) but less studies so far have been performed in fresh water conditions, which are representatives for rivers and lake conditions. The link between flocculation and properties of the settled bed needs also to be more investigated. Also in industry has not been investigated, because this is not of interest for industry where the particles are transported through pipes. For sediment dynamics in open water, this link is very important as the transport of sediment and its availability in the water column is linked to its deposition / re-suspension. Being able to describe quantitatively the structure and strength of the bed as function of the properties of the settled particles is therefore essential.

## 1.2 Aim and Outline of this research

Several research questions have been identified that are at the origin of this thesis. In order to develop process-based knowledge, model systems were primarily studied (clay and synthetic flocculant). The results were subsequently applied in the framework of a project related to the dewatering of fine tailing of importance in the soil sand industry. The general aim of the study is to better understand the cohesive sediment processes in the water column and investigate the flocculation behavior and de-watering of fine sediments as function of anionic and cationic polymers.

Specifically, the tasks related to this thesis were:

1. To *measure* systematically the changes in floc sizes over time as function of flocculant, coagulant, and shear stresses using Static Light Scattering (SLS). In chapter 2, the particle size distribution results from SLS are compared to other particle size distribution techniques. The measurements of floc sizes for different estuarine conditions are given in chapter 4.
2. To *predict* the flocculation ability of a suspension based on  $\zeta$ -potential measurements as function of flocculant, coagulant and sediment type. First two  $\zeta$ -potential meter are compared in chapter 3. The  $\zeta$ -potential measurements with fine natural sediments are given in chapter 4; the results are discussed using particle size distribution measurements. The application of  $\zeta$ -potential measurements to a case study (oil sand sediment) is given in chapter 7.
3. To *link* flocculation (particle size distribution), settling and consolidation as function of flocculant, coagulant and sediment type. For this study natural clay was used and the results are shown in chapter 5 and chapter 6.

## References

- [Ackroyd et al., 1986] Ackroyd, D., Bale, A., Howland, R., Knox, S., Millward, G., and Morris, A. (1986). Distributions and behaviour of dissolved cu, zn and mn in the tamar estuary. *Estuarine, Coastal and Shelf Science*, 23(5):621–640.
- [Bolto and Gregory, 2007] Bolto, B. and Gregory, J. (2007). Organic polyelectrolytes in water treatment. *Water research*, 41(11):2301–2324.
- [De Lucas Pardo, 2014] De Lucas Pardo, M. (2014). *Effect of biota on fine sediment transport processes: A study of Lake Markermeer*. PhD thesis, TU Delft, Delft University of Technology.
- [Goodwin, 2009] Goodwin, J. (2009). *Colloids and interfaces with surfactants and polymers*. John Wiley & Sons.
- [Gregory, 1988] Gregory, J. (1988). Polymer adsorption and flocculation in sheared suspensions. *Colloids and Surfaces*, 31:231–253.
- [Gregory and Barany, 2011] Gregory, J. and Barany, S. (2011). Adsorption and flocculation by polymers and polymer mixtures. *Advances in colloid and interface science*, 169(1):1–12.
- [Kranck and Milligan, 1992] Kranck, K. and Milligan, T. (1992). Characteristics of suspended particles at an 11-hour anchor station in san francisco bay, california. *Journal of Geophysical Research: Oceans (1978–2012)*, 97(C7):11373–11382.
- [Lagaly et al., 2013] Lagaly, G., Ogawa, M., Dekany, I., Bergaya, F., and Lagaly, G. (2013). Handbook of clay science, part a: Fundamentals. *Bergaya, F*, pages 245–328.



- [Lee et al., 2012] Lee, B. J., Schlautman, M. A., Toorman, E., and Fetsweis, M. (2012). Competition between kaolinite flocculation and stabilization in divalent cation solutions dosed with anionic polyacrylamides. *Water research*, 46(17):5696–5706.
- [Lee et al., 2011] Lee, B. J., Toorman, E., Molz, F. J., and Wang, J. (2011). A two-class population balance equation yielding bimodal flocculation of marine or estuarine sediments. *Water research*, 45(5):2131–2145.
- [Liss et al., 2004] Liss, S. N., Droppo, I. G., Leppard, G. G., and Milligan, T. G. (2004). *Flocculation in natural and engineered environmental systems*. CRC Press.
- [Liss et al., 2005] Liss, S. N., Milligan, T. G., Droppo, I. G., and Leppard, G. G. (2005). Methods for analyzing floc properties. *Flocculation in natural and engineered environmental systems*, pages 1–21.
- [Manning et al., 2011] Manning, A., Spearman, J., Baugh, J., Whitehouse, R., and Soulsby, R. (2011). *Cohesive sediment flocculation and the application to settling flux modelling*. INTECH Open Access Publisher.
- [McLaughlin and Bartholomew, 2007] McLaughlin, R. A. and Bartholomew, N. (2007). Soil factors influencing suspended sediment flocculation by polyacrylamide. *Soil Science Society of America Journal*, 71(2):537–544.
- [Mietta, 2010] Mietta, F. (2010). *Evolution of the floc size distribution of cohesive sediments*. TU Delft, Delft University of Technology.
- [Mietta et al., 2009] Mietta, F., Chassagne, C., and Winterwerp, J. (2009). Shear-induced flocculation of a suspension of kaolinite as function of pH and salt concentration. *Journal of colloid and interface science*, 336(1):134–141.
- [Mortimer, 1991] Mortimer, D. A. (1991). Synthetic polyelectrolytes—a review. *Polymer International*, 25(1):29–41.

- [Narkis et al., 1991] Narkis, N., Ghattas, B., Rebhun, M., and Rubin, A. (1991). Mechanism of flocculation with aluminium salts in combination with polymeric flocculants as flocculant aids. *Water supply*, 9(1):37–44.
- [Sojka et al., 2007] Sojka, R., Bjorneberg, D., Entry, J., Lentz, R., and Orts, W. (2007). Polyacrylamide in agriculture and environmental land management. *Advances in Agronomy*, 92:75–162.
- [Stewart and Thompson, 1997] Stewart, C. and Thompson, J. (1997). Vertical distribution of butyltin residues in sediments of british columbia harbours. *Environmental Technology*, 18(12):1195–1202.
- [Tombacz and Szekeres, 2004] Tombacz, E. and Szekeres, M. (2004). Colloidal behavior of aqueous montmorillonite suspensions: the specific role of ph in the presence of indifferent electrolytes. *Applied Clay Science*, 27(1):75–94.
- [Tombácz and Szekeres, 2006] Tombácz, E. and Szekeres, M. (2006). Surface charge heterogeneity of kaolinite in aqueous suspension in comparison with montmorillonite. *Applied Clay Science*, 34(1):105–124.
- [Tripathy and De, 2006] Tripathy, T. and De, B. R. (2006). Flocculation: a new way to treat the waste water.
- [Winterwerp and Van Kesteren, 2004] Winterwerp, J. C. and Van Kesteren, W. G. (2004). *Introduction to the physics of cohesive sediment dynamics in the marine environment*. Elsevier.
- [Yu and Somasundaran, 1996] Yu, X. and Somasundaran, P. (1996). Role of polymer conformation in interparticle-bridging dominated flocculation. *Journal of Colloid and Interface Science*, 177(2):283–287.



## Chapter 2

# Particle Size Distribution measurements by Static Light Scattering

### Abstract

In this chapter, the particle size distribution (PSD) of different samples (clay, sand, clay and sand) are analyzed. The PSD were obtained using 3 different techniques (static light scattering, sedigraph and hydrometer tests). It is known that a discrepancy exists between the PSD's found using these different techniques. In the present chapter, the cause of these differences are discussed. As the static light scattering (SLS) technique is an easy-to-use technique to get a full PSD in 30 seconds, it is a very useful technique for measuring the evolution of PSD's as function of time. A protocol was therefore derived to get PSD's by SLS that are as representative for the PSD's obtained by the other techniques as possible.

## 2.1 Introduction

Cohesive sediments (mud) are a mixture of water, silt, sand, clay and organic matter. Characterization of cohesive sediments by grain size distribution is needed for the understanding of sediments dynamic processes (transport, erosion and deposition). Some standard methods to analyze Particle Size Distributions (PSD) make use of the sedimentation rates for the fine fractions (hydrometer and sedigraph techniques) and sieving for the coarse particles [Gee and Bauder, 1986]. These standard methods have some disadvantages: they are time-consuming, the sample has to be treated before the analysis, and quite a large amount of sample is needed. Among the alternative methods that have been developed, static light scattering (SLS) is a promising one as it enables to measure a full particle size spectra (2 nm - 2 mm) in 30 seconds. No pre-treatment of the sample is apriori needed. As the measurements are so fast, SLS gives the possibility to study the aggregation of particles in time, which is not possible by the sedimentation techniques [Muggler et al., 1997].

The different techniques can give different PSD's. The fine range fraction ( $< 10$  microns) is the range that gives the most pronounced discrepancies. Many authors [Berlamont et al., 1993, Beuselinck et al., 1998, Loizeau et al., 1994, McCave et al., 1986, Singer et al., 1988, Vdović et al., 2010, Di Stefano et al., 2010] have found that the SLS technique underestimates the amount of fines compared to the sedimentation techniques. Sedimentation techniques like the Sedigraph and Hydrometer tests give nearly always very comparable results. Even though the differences between sieving and SLS seem not to be as pronounced as between SLS and sedimentation techniques, we will show in the present chapter that discrepancies exist.

The aim of this chapter is to present and validate a protocol for the SLS technique to find a "correct" PSD of samples that are representative for samples found in-situ, i.e. usually with a broad PSD. We use three different samples, i.e. river clay, kaolinite and fine sand.

## 2.2 Materials

### 2.2.1 Clay

The clay used in all the experiments is known as K-10.000, was purchased from the company VE-KA (The Netherlands). The clay was always dispersed in demi-water, the obtained mixture having conductivity less than 0.005 mS/cm. The original clay has a water content of 35.7% and a sand content of 21%. The water content is calculated as a percentage of the dry sample. The Atterberg Limits of the clay are shown in table 2.1. The organic matter or carbonates were not removed from the sample before performing the particle size analysis.

**Table 2.1** – Atterberg Limits of river clay sample

Property	Clay [%]
Liquid Limit	53
Plastic Limit	24
Plasticity Index	29

X-ray measurements were performed in the X-ray diffraction facilities of the Faculty of Mechanical, Maritime and Materials Engineering (3mE), TUDelft. The diffractometer is manufactured by Bruker-AXS and PANalytical. X-ray powder diffraction (XRPD) patterns were recorded in a Bragg-Brentano geometry in a Bruker D5005 diffractometer equipped with Huber incident-beam monochromatic and Braun PSD detector. Data collection was carried out at room temperature using monochromatic  $\text{CuK}\alpha_1$  radiation ( $\lambda = 0.154056$  nm) in the  $2\theta$  region between  $5^\circ$  and  $90^\circ$ , step size  $0.038^\circ 2\theta$ . All samples were measured under identical conditions. The samples of about 20 milligrams were deposited on a Si  $\langle 510 \rangle$  wafer and were rotated during measurement. Data evaluation was done with the Bruker program EVA. From X-ray diffraction (XRD) measurement, the composition of the clay sample is quartz, calcite, anorthite and muscovite.

The clay was also analyzed with a Philips XL30 Environmental Scanning Electron Microscope (ESEM), from Microlab in the Faculty of Civil Engineering and Geosciences, TUDelft. During the ESEM measure-

ments the sample was under vacuum, with a beam acceleration voltage of 20 kV, with back scattered electrons imaging mode and a spot size of 4. The magnification is shown in figure 2.1. Figure 2.1 shows an ESEM picture of the sample, which shows particles with size (around 6  $\mu\text{m}$ ) similar to the Particle Size Distribution found from light scattering, using a Malvern Mastersizer 2000.

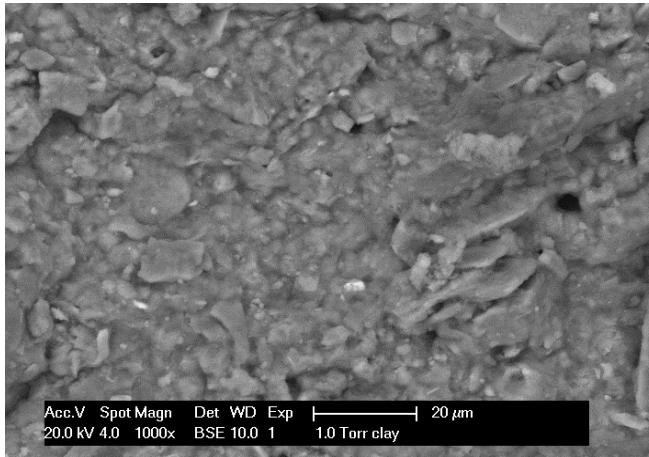


**Figure 2.1** – ESEM picture of the river clay sample. The typical length scale of the particles is about 6 microns, in accordance with Static Light Scattering results.

### 2.2.2 Sand

Two samples of sand from the Dutch coast, named s1 and s2 are used in this chapter. S1 has a mean particle size between 45 and 53  $\mu\text{m}$  and s2 a mean particle size between 63 and 75  $\mu\text{m}$ . These sizes were obtained from sieving.

### 2.2.3 Kaolinite

Experiments have been performed using a 1:1 type kaolinite in powder form from VE-KA Ltd. The Netherlands. Its composition is given in

table 2.2.

**Table 2.2** – Composition of the kaolinite sample.

Composition	$\text{Al}_2\text{O}_3\text{-}2\text{SiO}_2\text{-}2\text{HO}_2$
$\text{Al}_2\text{O}_3$	34.7%
$\text{SiO}_2$	48.5%
$\text{K}_2\text{O}$	3.3%
$\text{Fe}_2\text{O}_3$	< 1%
$\text{CaO}$	< 0.3%

## 2.2.4 Water

Tap water was used in all the experiments presented in this chapter. The relevant tap water specifications are listed in table 2.3. These specifications were obtained from the local drinking water company Evides for the months during which the experiments were performed.

**Table 2.3** – Water Specifications

Parameter	Value	Units
pH	8.2 - 8.7	-
$\text{HCO}_3^-$	188 - 225	mg/L
$\text{SO}_4^{2-}$	24 - 30	mg/L
$\text{Na}^+$	51 - 59	mg/L
$\text{Ca}^{2+}$	45 - 49	mg/L
$\text{Mg}^+$	8.2 - 8.4	mg/L
$\text{CL}^-$	48.6 - 49.1	mg/L

## 2.3 Methods

### 2.3.1 Static Light Scattering (SLS)

The particle size distribution of the samples was measured by Static Light Scattering by means of a Malvern Mastersizer 2000 [[www.malvern.com](http://www.malvern.com)],



2015]. The principle of the laser diffraction technique is that particles of a given size diffract light at a given angle and the angle of diffraction is inversely proportional to particle size. Figure 2.2 shows a schematic view of the laser diffraction technique. Mie theory for spherical particles is the basis of the Malvern software [www.malvern.com, 2015]. Mie theory is used in all the measurements done in this thesis. Mie theory uses as input parameter the refractive index (RI) of the material. The RI is function of the composition of the material. In all the tests the RI was chosen to be 1.57, which is a recommended value for clay.

The description of the set-up is given in chapter 3.

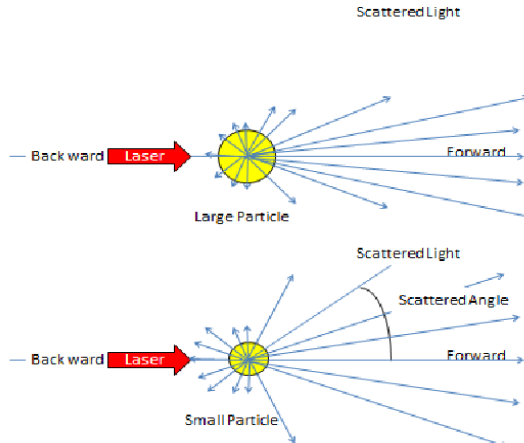


**Figure 2.2** – Schematic of laser diffraction technique.

### 2.3.2 Sieves

Following the British standards (BS 1377: Part 2: 1990), sieves from 2 mm to 63  $\mu\text{m}$  size are used to sieve the dry material before the particle size distribution is analyzed by any other device.

### 2.3.3 Hydrometer

The hydrometer indicates the ratio of the density of the tested fluid to the density of water, this ratio is called specific gravity. The height  $H_e$  of the hydrometer (see figure 2.3) is recorded as function of time and is a measure for the specific gravity. From Stokes' law the size of particles that at given time  $t$  are above  $H_e$  are the particles with a diameter  $D$  that is smaller than:

$$D = \sqrt{\frac{18v\eta}{(\rho - \rho_w)g}} \quad (2.3.1)$$

with

$$v = \frac{H_e}{t} \quad (2.3.2)$$

where  $\eta$  is the viscosity of water in Pa.s,  $\rho$  the density of the particle,  $\rho_w$  the density of water ( $\text{g}/\text{cm}^3$ ),  $g = 9.81 \text{ m}/\text{s}^2$   $H_e$  is the effective depth,  $t$  is the time in seconds at which the observation is done,  $t = 0$  being the beginning of sedimentation. The density of the particles is usually taken to be the density of quartz ( $2.66 \text{ g}/\text{cm}^3$ ).

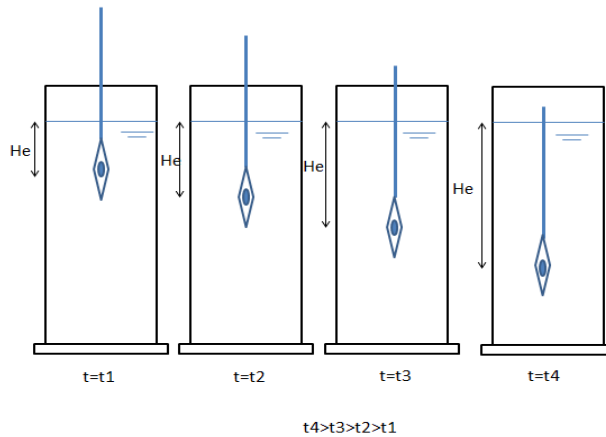


**Figure 2.3** – Sketch of the hydrometer test, in which the height  $H_e$  is increasing as function of time.

Corrections for temperature and mixture viscosity are made by taking a hydrometer reading of a blank solution (calibration of the hydrometer). The blank solution is a solution of clean water at a known temperature. The sample preparation and the test were done following the British standards (BS 1377: Part 2: 1990). Equipment needed to perform the test is: soil hydrometer (we used an AST 152H), set of sedimentation cylinders, analytical balance of resolution 0.01 g, thermometer, stopwatch, dispersing agent (Sodium Hexametaphosphate), and stirrer.

The sample is first dried at 105°C over night in the oven to remove water. After drying, it is ground with a mortar and pestle, then dispersed in a dispersant agent (Sodium Hexametaphosphate) for 16 hours following the British Standards BS 1377: Part2: 1990.

### 2.3.4 Sedigraph

The Sedigraph method of particle size analysis is based on Stokes' Law equation 2.3.1. The Sedigraph uses a parallel X-ray beam to detect changes in suspended sediment concentration during settling, at different vertical distances in the analysis cell, and at specific times during settling. Hence, the time required for a particle to settle a known distance is measured and the velocity is determined by distance divided by time. The device used is a SediGraph III Plus from Micromeritics [www.micromeritics.com, 2015]. The sample preparation was done following the British standards (BS 1377: Part 2: 1990). Equipment needed to perform the test are: Sedigraph, analytical balance of resolution 0.01 g, and dispersing agent (Sodium Hexametaphosphate). For this test the sample is dried over night in the oven as for the hydrometer test. After drying it is ground and dispersed in 1% Sodium Hexametaphosphate for 16 hours. The density of the (clay) particles can then be assumed to be equal to 2.66 g/cm<sup>3</sup> as most of the organic matter is removed.

### 2.3.5 Summary

Table 2.4 below shows the differences by the different techniques used in this chapter to analyze the particle size distribution.

**Table 2.4** – Different techniques

Techniques	Range	Protocol	Theory	Limitations
SLS (Malvern)	2 nm - 2 mm	-	Mie	finest < 10 $\mu\text{m}$ are not well detected
Hydrometer	> 2 $\mu\text{m}$	BS 1377	Stokes	particles < 2 $\mu\text{m}$ are not detected. Protocol might be an issue
Sedigraph	> 2 $\mu\text{m}$	BS 1377	Stokes	particles < 2 $\mu\text{m}$ are not detected. Protocol might be an issue
Sieve	> 63 $\mu\text{m}$	-	-	Strongly anisotropic particles might be a limitation

The samples are tested wet, without being dried overnight for the SLS technique. The effect of using a disperse agent was analyzed with the Malvern.

## 2.4 Results and discussion

As can be seen in table 2.4, the SLS technique provides the largest range in particle sizes. The measurement technique is easy and fast to

use. Measurements are taken every 30 seconds which enables to monitor the change of particle size in time as will be shown in the next chapters. Another advantage is that SLS enables to measure the very fine particle size range (2 nm - 2  $\mu\text{m}$ ). This is a range where particles do not settle and therefore no PSD can be obtained from hydrometer and sedigraph. However the traditional techniques (sieve, hydrometer, sedigraph) are still the most widely used in industry and it is therefore important to assess whether they give similar results compared to SLS. Some authors have already studied and compared different techniques [Berlamont et al., 1993, Beuselinck et al., 1998, Loizeau et al., 1994, McCave et al., 1986, Singer et al., 1988, Vdović et al., 2010, Di Stefano et al., 2010]. They all have found in particular that the SLS technique underestimates the amount of fines.

### 2.4.1 Static Light Scattering

#### Effect of concentration

The static light scattering technique (SLS) gives PSD's that are normalized to 100%. This implies that in theory the PSD's will not depend on the concentration of particles, but only on their relative ratio. In practice only a range of concentration is measurable. If the concentration is too low, no particles will be detected, whereas if the concentration is too high laser obscuration will occur. In both cases a warning will be issued by the equipment.

For sand particles in the range 125-150  $\mu\text{m}$  see figure 2.4, it was found that the PSD was independent of any concentration within the accepted range of the equipment. The particle size range (125-150  $\mu\text{m}$ ) was found by sieving. The  $D_{50}$  found by SLS is 175  $\mu\text{m}$ . The  $D_{10}$  is found to be 127  $\mu\text{m}$  (corresponding to the lowest sieve value) but the  $D_{90}$  is 240  $\mu\text{m}$ , much higher than the highest sieve value of 150  $\mu\text{m}$ . In general, it was found for all sand fractions investigated that the  $D_{90}$  was always much higher than the highest sieve value. Therefore for sand samples  $D_{90}$  is not recommended to be used. The origin of this discrepancy is unknown, but it could be related to the automatic "smoothing" of the data-set by the SLS software. As the particle size

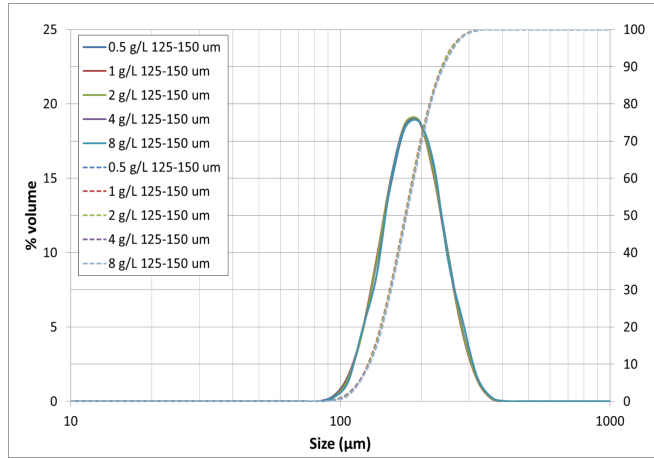


**Figure 2.4** – Effect of concentration of a sand sample of size range between 125 and 150  $\mu\text{m}$ . Full lines: PSD; dashes lines: cumulative PSD.

bins are logarithmically spaced "smoothing" of the highest bin sizes can lead to larger errors than "smoothing" of the lowest bin sizes.

For sand particles in the range 45 - 53  $\mu\text{m}$ , it was found that the PSD varied slightly with concentration. The particle size range (45 - 53  $\mu\text{m}$ ) was found by sieving. The  $D_{50}$  decreased from 62 to 59  $\mu\text{m}$  between 0.2 g/L and 4 g/L. The  $D_{10}$  is found to be (42 - 44  $\mu\text{m}$ ) in agreement with the lowest sieve value. The  $D_{90}$  is found to be (86 - 83  $\mu\text{m}$ ) which is higher than the highest sieve value.

In this chapter, a clay sample was used that is representative for the clay used throughout this thesis. We used both natural clay and kaolinite for these tests. The conclusion derived from the tests are all the same (not all tests are therefore shown).

The clay concentration used in the other chapters of the thesis is 0.7 g/L which gives the optimum laser obscuration value recommended by the manufacturer. Above 1 g/L clay, laser obscuration starts to be beyond the limit of validity of the equipment. At 1.5 g/L clay a peak in the PSD appears below 0.2  $\mu\text{m}$  that is related to a detection failure. These results are shown in figure 2.6.

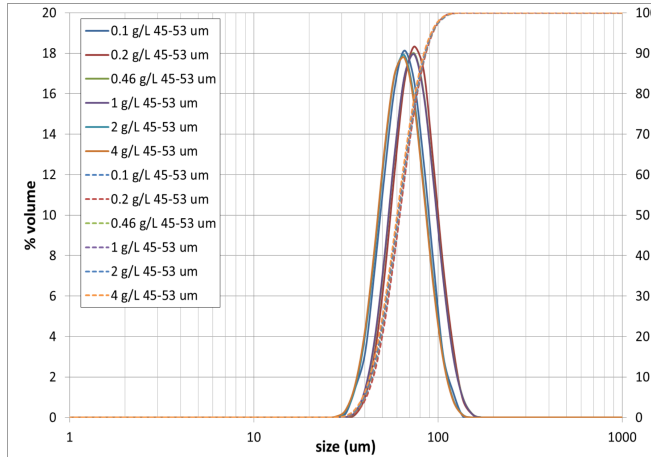


**Figure 2.5** – Effect of concentration of a sand sample of size range between 45 and 53  $\mu\text{m}$ . Full lines: PSD; dashes lines: cumulative PSD.

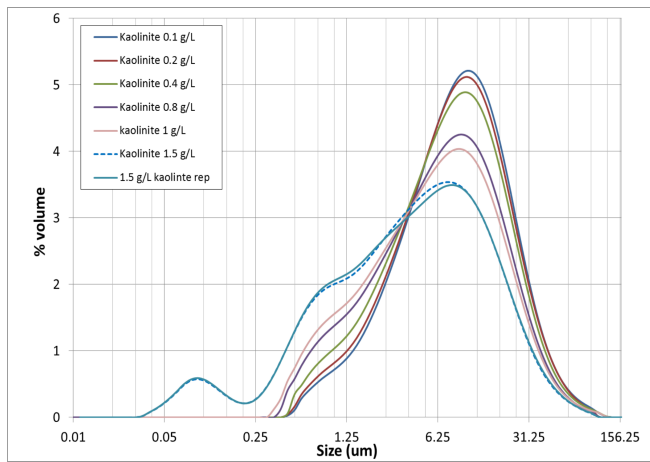


**Figure 2.6** – Effect of concentration of a kaolinite sample.

In the range of validity of the equipment, one observes two features. First of all, the PSD is bimodal, which is due to the asymmetry of the clay particles which have a platelet shape (see ESEM picture 2.1). As all particle orientations are assumed to be equally probable, the long edge of the platelet should correspond to an occurrence of  $2/3$  and the small edge to  $1/3$ , the ratio of the two being  $1/2$ . This roughly corresponds to what is observed for the sample of  $1.5 \text{ g/L}$  kaolinite concentration. Second, the PSD is observed to be quite dependent on concentration: the shoulder at  $0.09 \mu\text{m}$  increases in relative size with increasing concentration. This does however not affect much the  $D_{10}$ ,  $D_{50}$  and  $D_{90}$ . The  $D_{10}$  decreases from  $2$  to  $1 \mu\text{m}$  between  $0.1 \text{ g/L}$  clay and  $1 \text{ g/L}$  clay, whereas the  $D_{50}$  varies from  $8$  to  $6 \mu\text{m}$  and the  $D_{90}$  from  $25$  to  $29 \mu\text{m}$  in the same range of concentration.

### Effect of polydispersity

The mixtures studied in the previous subsection are fairly monodisperse. In the present subsection, the effect of polydispersity on the PSD is studied. In figure 2.7, the same mass of  $125\text{-}150 \mu\text{m}$  and  $45\text{-}53 \mu\text{m}$  particles is mixed in one liter of water. The mass per liter of each sand fraction is indicated in the legend. One can observe that the relative ratio of the two peaks changes with concentration. The largest peak becomes more and more apparent with increasing concentration. Assuming that the sand particles all have the same density, for the same mass of sand, the smallest fraction will have more suspended particles than the largest fraction. At low concentration, the number of largest particles will be at the limit of detection. As the relative ratio of the two peaks is concentration-dependent it would appear that the SLS technique is not suited to determine the relative concentration ratios between the two sand fractions.

When the smallest size sand ( $45\text{-}53 \mu\text{m}$ ) and clay are mixed (see figure 2.8a), one finds that a substantial amount of sand is required to observe the peak associated to sand. Moreover, the peaks shift with concentration. The same occurs for other sand fractions (see figure 2.8b). When sand is added to clay (figure 2.8c) one peak is observed for the sand fractions instead of multiple peaks. This confirms that



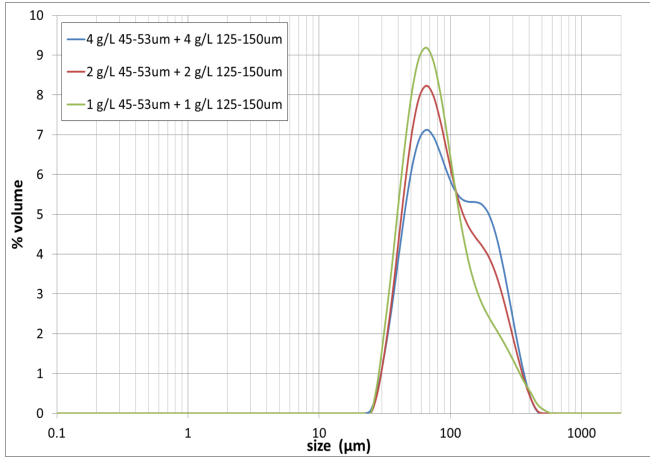
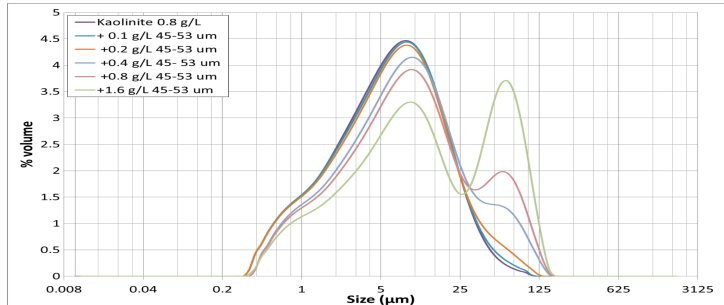


**Figure 2.7** – Effect of polydispersity. PSD of a sample composed of two sand samples.

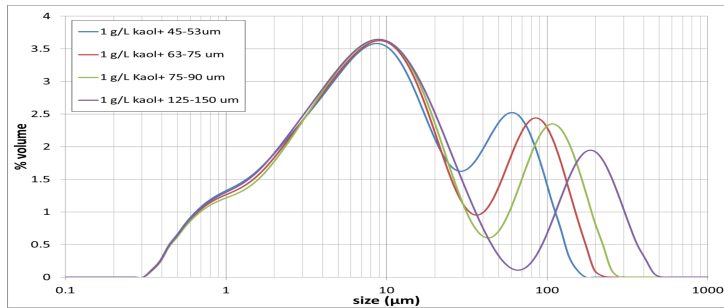
SLS is not appropriate for determining the PSD of sand mixed with fine particles and that sieving should be done ( $> 63 \mu\text{m}$ ) .

### **Influence of sediment treatment**

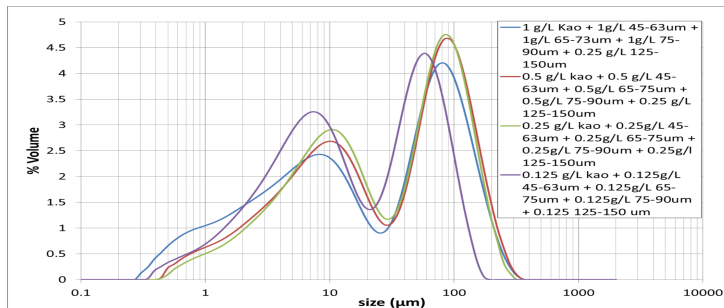
The particle size distribution of the clay sample was analyzed with the Malvern device by Static Light Scattering. The sample was analyzed with and without pre-treatment. The pre-treatment consists of dispersing the sample in a dispersant agent (Sodium Hexametaphosphate) for 16 hours to de-flocculate the sample. The difference in particle size distribution between the two samples is shown in figures 2.9. Figure 2.9a represents the cumulative PSD and 2.9b the non-cumulative PSD. The particle size distribution of the pre-treated sample (de-flocculated) contains a larger amount of fine sediments, as an increase of 13% in clay content ( $2 \mu\text{m}$ ) when the samples is de-flocculated is observed.



(a)

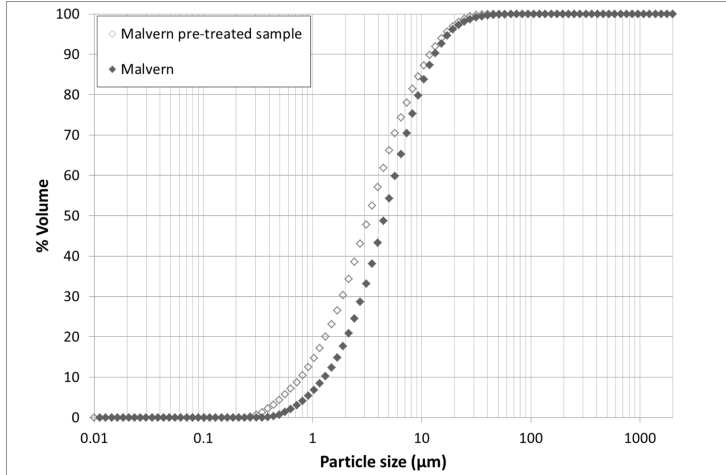


(b)

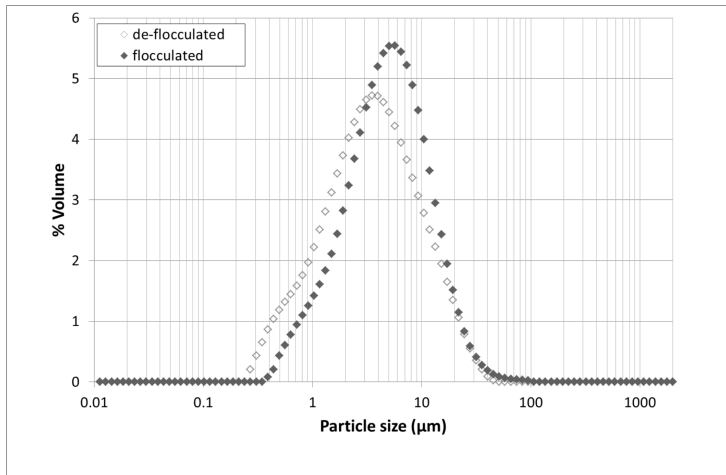


(c)

**Figure 2.8** – Effect of polydispersity. PSD of a sample composed of kaolinite and sand. a) kaolinite and sand of size 45-53 μm, combined with different concentrations of sand. b) kaolinite combined with different sand sizes, 45-53 μm, 63-75 μm, 75-90 μm and 125-150 μm. c) each curve represents a sample done by mixing kaolinite with sand at different concentrations, the concentrations are given in the legend.



(a)



(b)

**Figure 2.9** – PSD cumulative and noncumulative of clay sample with and without pretreatment, analyzed by Malvern.

### 2.4.2 Comparison between devices

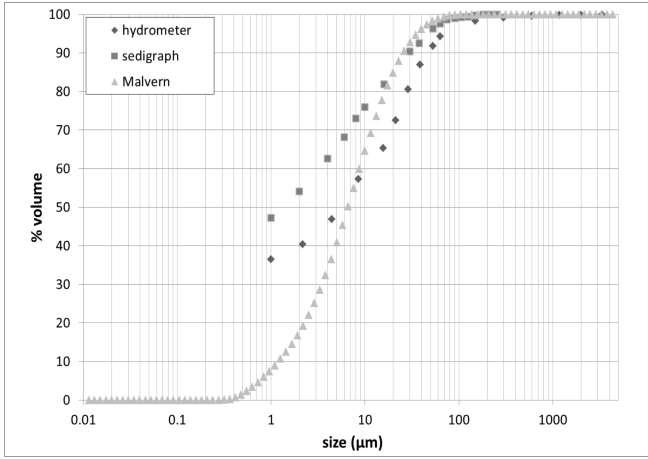
Figure 2.10 shows the particle size distribution for a clay sample analyzed by the 3 devices: Hydrometer, Sedigraph and SLS. The only difference between the samples analyzed is that the samples used for the Hydrometer and Sedigraph were ground after drying which was not the case for the SLS. The 23% (Hydrometer) and 37% (Sedigraph) difference in clay content ( $< 2 \mu\text{m}$ ) with SLS is therefore due to the grinding of the sample which fractures silt and sand particles in smaller particles. Another reason can be also the different devices.

Table 2.5 defines the range of sand, silt and clay following the standard ISO 14688-1:2002. The sand and silt range values by the three devices are in good agreement (see figure 2.10), although they do not show exactly the same values. In order to compensate for the difference in the clay range, some authors have proposed to increase the range defining the clay range. When one considers a clay range for SLS as the range for which particles are smaller than  $8 \mu\text{m}$ , there is a good overlap between the hydrometer and SLS [Konert and Vandenberghe, 1997].

As discussed in section 2.4., SLS gives access to the full PSD in the range [ $2 \text{ nm} - 2 \mu\text{m}$ ] whereas the other techniques are limited to sizes above  $2 \mu\text{m}$ . As particles smaller than  $2 \mu\text{m}$  do not settle and experience Brownian motion, sedimentation experiments give unrealistic values for particles of size of the order of  $1 \mu\text{m}$  [Di Stefano et al., 2010]. Even though, the total amount of particles  $< 2 \mu\text{m}$  are very different. One reason, is associated to sample preparation. Another reason, reported by many authors [Berlamont et al., 1993, Beuselinck et al., 1998, Loizeau et al., 1994, McCave et al., 1986, Singer et al., 1988, Vdović et al., 2010, Di Stefano et al., 2010] is the "shadowing" of fines by the larger particles where the SLS technique is used.

**Table 2.5** – Range sand, silt and clay by the standard ISO 14688-1:2002

Name	Size range
clay	$< 2 \mu\text{m}$
Silt	$2 \mu\text{m} - 63 \mu\text{m}$
Sand	$63 \mu\text{m} - 2 \text{ mm}$



**Figure 2.10** – PSD cumulative of clay sample with pre-treatment, analyzed with Sedigraph, hydrometer and Malvern.

A last reason for the discrepancy in the clay range is associated with the shape of the clay particles. In section 2.4.1 we discussed the influence of particle shape on the PSD found by SLS. Most clay particles will be detected when the platelet face faces the laser. The associated length is defined in figure 2.11. In sedimentation experiments, Stokes law given in equation 2.3.1, requires the mean (or characteristic) radius of the particle. The mean radius of a platelet is given by:

$$R = a \left( \frac{3d}{4a} \right)^{1/3} \quad (2.4.1)$$

where  $d$  is the thickness of the platelet and  $a$  the radius of the face of the platelet see figure 2.11. For any  $d < a$ , one finds  $R < a$ . For this reason, both sedigraph, hydrometer tests and pipette technique (also based on sedimentation) will always give smaller particles sizes than SLS [Lerman et al., 1974].

In the light of what is discussed above, a better protocol for measuring PSD with the Malvern device was sought.

This protocol is illustrated in figure 2.12 and is as follows:

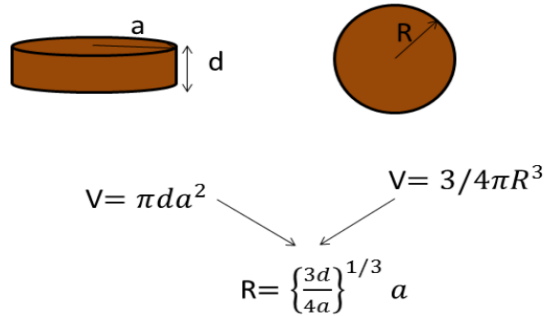


**Figure 2.11** – Left: platelet particle of size  $a \times d$ ; right: equivalent sphere of radius  $R$ .

- The PSD of a bulk sample is measured by SLS. This will indicate if sieving for  $\mu\text{m}$  sized particles is required. The bulk sample is defined as the fluid in which all particles are in suspension (by use of the proper stirring).
- A sub-sample (1) of the bulk sample (particles  $< 2 \text{ mm}$ ) of known volume is placed in the oven to dry. After drying, the mass of this sample is recorded. The concentration ( $C_{\text{bulk} > 63 \text{ microns}}$ ) of the bulk (1) sample is then calculated. This concentration is used to re-calculate the new PSD.
- If sand is detected, than the sample has to be sieved. After sieving particles smaller than  $63 \mu\text{m}$  are analyzed by SLS.
- A sub-sample of the clay (particles  $< 63 \mu\text{m}$ ) sample of known volume is placed in the oven to dry. After drying, the mass of this sample is recorded. The concentration ( $C_{\text{clay}}$ ) of the clay sample can be estimated, and is a parameter that will be used to re-calculate the new PSD.

- The clay sample (particles  $< 63 \mu\text{m}$ ) is left settling for at least one hour. After this hour, some supernatant is carefully pumped out and its PSD is measured by SLS.
- A sub-sample of the supernatant of known volume is placed in the oven to dry. After drying, the mass of this sample is recorded. The concentration ( $C_{supernatant}$ ) of the supernatant sample is known, and it is a parameter that will be used to re-calculate the new PSD.
- The full PSD curve which combines the supernatant and bulk results, can be obtained from the relation:

$$\%PSD_{total} = \left(\frac{C_{bulk>63}}{C_{totalbulk}}\right) \times PSD_{>63} + \left(\frac{C_{supernatant}}{C_{totalbulk}}\right) \times PSD_{<63} \quad (2.4.2)$$

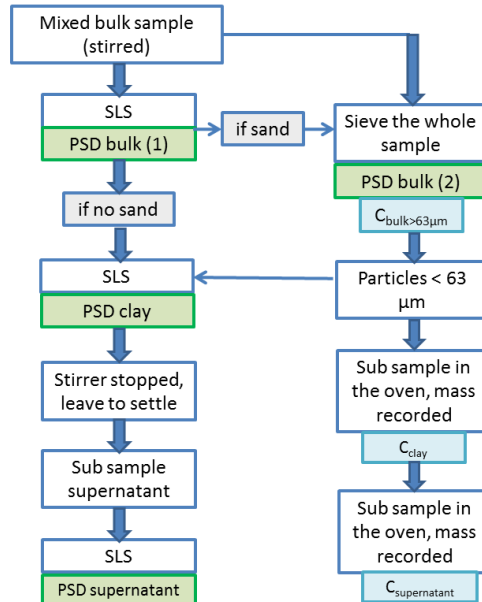


Figure 2.12 – Flow chart with the steps of the full protocol.

### 2.4.3 Application of the new protocol

The new protocol gives excellent results in the case that one type of clay is mixed with a variety of sand as clay and sand segregate very easily by decantation.

In order to analyze the discrepancies observed for the smallest clay fraction ( $< 10 \mu\text{m}$ ), a clay sample was used to test the protocol. In figure 2.13 the PSD of supernatant and corrected bulk samples (new PSD after obtained after the new protocol is used) are shown together with Sedigraph and Hydrometer in the range  $[0.01 - 10] \mu\text{m}$ . The clay content of the corrected PSD is 21% higher than in the PSD of the bulk sample. The clay content for the corrected sample is the same as the one obtained with the Hydrometer and the difference with the Sedigraph is smaller. In figure 2.14 the new PSD corrected with the new protocol is compared with the one analyzed by Sedigraph, Hydrometer and the Malvern without being corrected. The new PSD gives similar results to the Hydrometer for the clay content, although the amount of silt particles decreases as a result of the correction. The corrected PSD is very similar to the PSD obtained by the Sedigraph in all the range except for the clay content, there is still a difference of 10% in clay content.

In order to assess the limitations of the new protocol, we made a mixture of two types of clay particles. One clay is boehmite with a  $D_{50}$  of  $50 \mu\text{m}$  and the other is halloysite with a  $D_{50}$  of  $0.27 \mu\text{m}$ . We note that contrary to the clay presented in the previous sections (which has a platelet form), halloysite has a cylindrical shape, see figure 2.15. The PSD of halloysite is therefore bimodal with a second (smaller) peak at the right of the larger one. The boehmite particles are aggregates of primary particles, and from the PSD it can be deduced that they are fairly isotropic in shape. The full PSD of boehmite, halloysite and the mixture of both can be compared in figure 2.16. The exact concentrations of the original suspensions of boehmite and halloysite are not precisely known, however both concentrations were high enough to enable a good measurement by SLS (see "halloysite" and "boehmite" curves). The mixture of both clays ("halloysite + boehmite" curve) was made by mixing 50% of each clay suspension. In this curve the smallest fraction (below  $10 \mu\text{m}$ ) is not detected. The mixture was left to decant for one hour



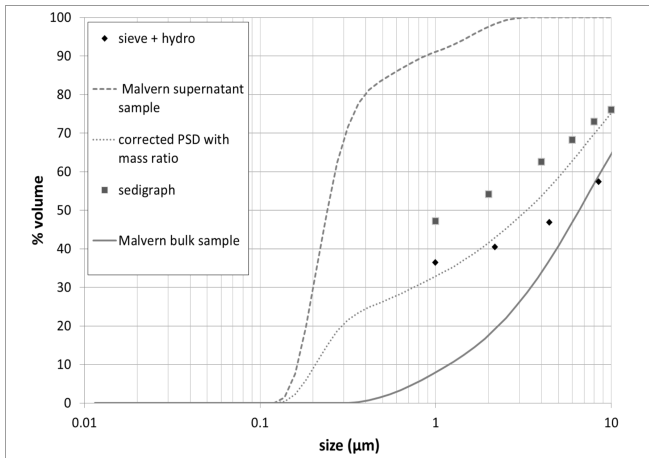


**Figure 2.13** – PSD cumulative of corrected and supernatant analyzed by Malvern, and PSD cumulative analyzed by Sedigraph and Hydrometer.

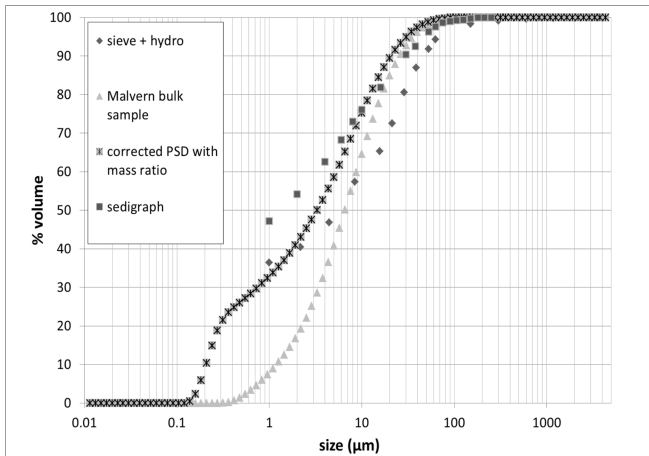


**Figure 2.14** – PSD cumulative of supernatant and the corrected PSD of clay after calculating the mass ratio analyzed Malvern. And PSD cumulative of the same sample analyzed by Sedigraph and Hydrometer.

and the particle size was again recorded. The results are given in figure 2.17. Contrary to sand particles, the boehmite particles do not deposit on the bottom of the jar, but a boehmite-rich layer (concentrated region of a few cms thick) above the bottom of the jar can be observed. Due to the polydispersity of the original samples it is quite likely that some boehmite particles remain in the upper part of the jar, while some halloysite particles settled on the bottom. The  $D_{50}$  of the PSD of the settled material is  $42 \mu\text{m}$ , whereas the  $D_{50}$  of the mixture was  $38 \mu\text{m}$ . Both values are lower than  $50 \mu\text{m}$  (the  $D_{50}$  of boehmite). The  $D_{50}$  of the supernatant is  $5 \mu\text{m}$ , higher than the  $D_{50}$  of halloysite (which is  $0.27 \mu\text{m}$ ). Nonetheless the decantation method enables to recover a large part of the fine fraction that was shadowed in the PSD of the mixture. In order to make even the smallest fraction apparent (below  $1 \mu\text{m}$ ), a larger decantation time (of the order of days) should be performed. Another, faster, option would be to filtrate the supernatant through a  $2 \mu\text{m}$  filter paper and measure the PSD of the water coming through the paper. Due to the limited volume of halloysite at our disposal this was not checked.

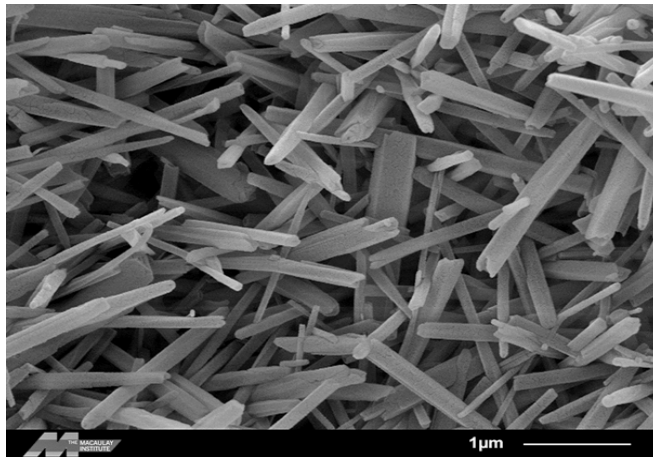


**Figure 2.15** – ESEM picture of Halloysite (picture taken from the mineralogical society [www.minsocam.org, 2017])

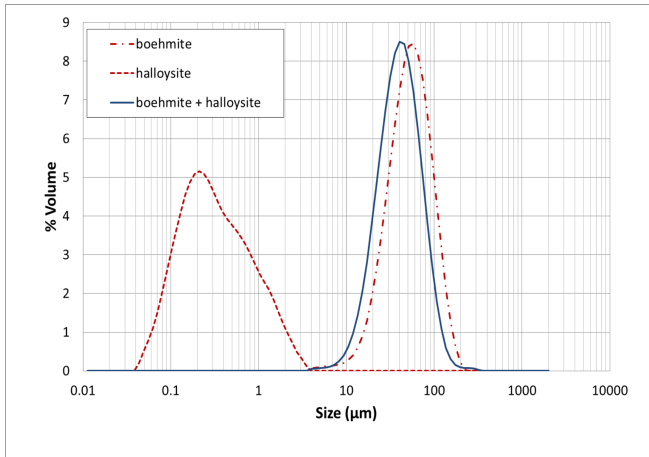


**Figure 2.16** – PSD's of suspensions of boehmite, halloysite and a 50% mixture of the two by SLS

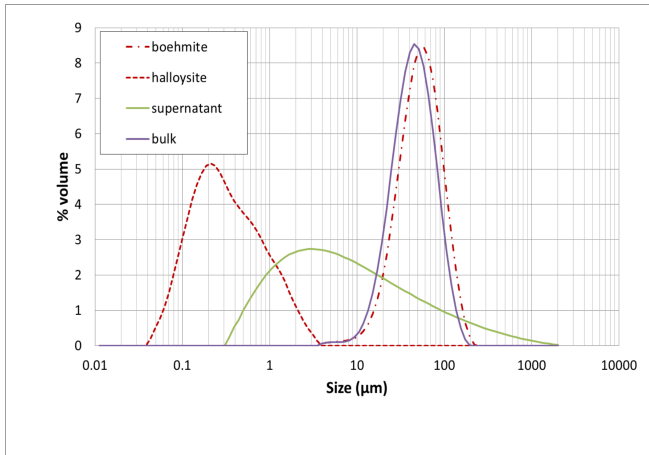


**Figure 2.17** – PSD's of suspensions of boehmite, halloysite and a decanted 50% mixture of the two by SLS. The supernatant corresponds to the top layer of the suspension that is carefully pumped out, while the settled part (at the bottom of the jar) remains undisturbed. The settled part corresponds to the liquid in the lowest part of the jar.

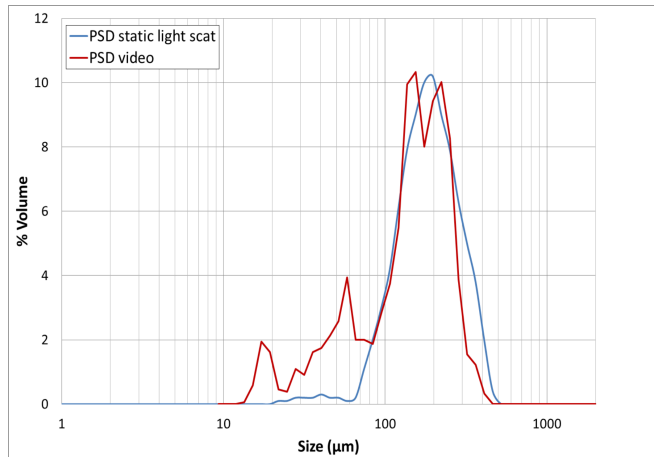


**Figure 2.18** – Comparison between the PSD found by SLS and by video microscopy. The sample consists of 0.7 g/L clay flocculated with 4.7 mg/L flocculant (zetag 7587). The (normalized) PSD by video microscopy is found by tracking a representative amount of settling particles ( $\approx 1500$ ), and estimating the volume of each particle from its equivalent radius. No “smoothing” function has been applied to the PSD. The PSD found by SLS is obtained from the output of the manufacturer’s software and is “smoothed”. We observe that the amount of finer particles ( $< 100$  microns) is underestimated by SLS whereas the amount of the largest particles is over-estimated.

Contrary to samples containing unflocculated sand and silt particles, samples containing large flocculated particles cannot be sieved as this would break the flocs. In that case, the SLS technique is useful to estimate the mean floc size in the  $\mu\text{m}$ -size range without much damage of the sample. In case fines are present in the sample, a decantation can be performed and the supernatant be measured as described in the protocol given above. We compared the PSD's of flocculated particles obtained by two different techniques in figure 2.18. The sample was prepared in a jar, following the procedure described in chapter 4. We waited till the PSD achieved its equilibrium value (this occurred after 30 min). The measurement of the PSD was then done by SLS. Meanwhile, a sub-sample was directly pipetted from the jar to a settling column and the size of particles was recorded by video microscopy. As the flocculant dose is close to optimum, the flocs formed were fairly isotropic. Incidentally, we noted that for under-dose flocculant the larger flocs have the tendency to "catch-up" and aggregate with the smaller ones. This results in elongated flocs. This does barely happen at optimal dose as all particles are well saturated with flocculant and aggregation between flocs is prevented.

The PSD found by video microscopy was normalized to correspond to the PSD found by SLS. This implies that PSD is expressed in % volume and that the class bins are the same as the ones used by SLS. The % volume of flocs is estimated from the mean equivalent radius of each floc. Contrary to the SLS data, the video microscopy data is not mathematically smoothed. The results are based on the observation of more than 1500 settling particles. This PSD obtained by the video microscopy data seems to be the correct one.

As can be seen in figure 2.18, the amount of finer particles ( $< 100$  microns) is underestimated by SLS whereas the amount of the largest particles is over-estimated. A decantation procedure (see the protocol given above) is therefore advised also in this case to better account for the fines. As the flocs observed are rather spherical shape anisotropy is not the reason to explain the deviations observed at large particle sizes. As discussed above, the discrepancy is most probably due to the mathematical smoothing of the SLS data. Due to lack of time,

this was not further investigated, as this would require re-fitting of the raw data obtained from SLS. Despite the over-estimation of the largest particle size and under-estimation of smallest particles volume, both video microscopy and SLS give the same bimodal  $D_{50s}$  (around 50 and 200 microns).

## 2.5 Conclusions

In this chapter the PSD of a clay sample was determined with three different devices (Malvern, Sedigraph, and Hydrometer). The  $D_{90}$  of the sand fractions by SLS is always higher than the highest sieving value. This is probably due to the mathematical adjustment ("smoothing") of the data-set by the equipment software. Moreover it was found that in a mixture of two types of sands, the relative ratio between the two peaks corresponding to each mean size is concentration dependent. In view of these results, it is advised to sieve the samples for the sand fraction, which clearly will give better sizes and relative concentration ratios than SLS. In accordance with previous studies it was found that the laser diffraction technique underestimates the fines content. A new protocol for estimating the full PSD by laser diffraction technique is presented. This PSD is in line with the PSD found by traditional methods (sieve, hydrometer and sedigraph).

Some discrepancies still exist between the methods. Some of these discrepancies are due to measurement errors, which were not analyzed in the present chapter. One of these errors, concerning the Malvern experiments, would be the limitation of the software as it is based on the assumption that all the particles are spherical, an hypothesis that can be questioned for natural sediments, see figure 2.1 for example. Another possible error, concerning the hydrometer, is the inaccuracy at the beginning of the test (bobbling up and down of the hydrometer rod until it is stable) as well as the inaccuracy in the reading of the meniscus.

It is concluded that SLS can be a useful tool to study the time evolution of the PSD of aggregating particles, as a full PSD can be recorded in 30 s. In case there is a monomodal PSD peak the % volume given by SLS will be realistic, but caution is required if multimodal

peaks are observed as their relative ratio is concentration-dependent. Overall it was observed that, if the silt and clay fraction is comparable or larger than the clay fraction in volume, the smallest clay fraction is usually underestimated by SLS. For a better estimation of this smallest fraction, the protocol given in this chapter can be followed.

## References

- [Berlamont et al., 1993] Berlamont, J., Ockenden, M., Toorman, E., and Winterwerp, J. (1993). The characterisation of cohesive sediment properties. *Coastal Engineering*, 21(1):105–128.
- [Beuselinck et al., 1998] Beuselinck, L., Govers, G., Poesen, J., Degraer, G., and Froyen, L. (1998). Grain-size analysis by laser diffractometry: comparison with the sieve-pipette method. *Catena*, 32(3):193–208.
- [Di Stefano et al., 2010] Di Stefano, C., Ferro, V., and Mirabile, S. (2010). Comparison between grain-size analyses using laser diffraction and sedimentation methods. *Biosystems Engineering*, 106(2):205–215.
- [Gee and Bauder, 1986] Gee, G. and Bauder, J. (1986). Particle-size analysis in: Klute, a.(ed) methods of soil analysis, part 1. american society of agronomy. *Inc., Ma.*
- [Konert and Vandenberghe, 1997] Konert, M. and Vandenberghe, J. (1997). Comparison of laser grain size analysis with pipette and sieve analysis: a solution for the underestimation of the clay fraction. *Sedimentology*, 44(3):523–535.
- [Lerman et al., 1974] Lerman, A., Lal, D., and Dacey, M. F. (1974). Stokesâ settling and chemical reactivity of suspended particles in natural waters. In *Suspended solids in water*, pages 17–47. Springer.
- [Loizeau et al., 1994] Loizeau, J.-L., Arbouille, D., Santiago, S., and VERNET, J.-P. (1994). Evaluation of a wide range laser diffraction grain size analyser for use with sediments. *Sedimentology*, 41(2):353–361.



- [McCave et al., 1986] McCave, I., Bryant, R., Cook, H., and Coughanowr, C. (1986). Evaluation of a laser-diffraction-size analyzer for use with natural sediments: research method paper. *Journal of Sedimentary Research*, 56(4).
- [Muggler et al., 1997] Muggler, C., Pape, T., and Buurman, P. (1997). Laser grain-size determination in soil genetic studies 2. clay content, clay formation, and aggregation in some brazilian oxisols. *Soil Science*, 162(3):219–228.
- [Singer et al., 1988] Singer, J., Anderson, J., Ledbetter, M., McCave, I., Jones, K., and Wright, R. (1988). An assessment of analytical techniques for the size analysis of fine-grained sediments. *Journal of Sedimentary Research*, 58(3).
- [Vdović et al., 2010] Vdović, N., Obhodaš, J., and Pikelj, K. (2010). Revisiting the particle-size distribution of soils: comparison of different methods and sample pre-treatments. *European journal of soil science*, 61(6):854–864.
- [www.malvern.com, 2015] www.malvern.com (2015). Malvern website. <http://www.malvern.com>. Accessed: 2015-04-30.
- [www.micromeritics.com, 2015] www.micromeritics.com (2015). micromeritics website. <http://www.micromeritics.com/Product-Showcase/SediGraph-III-Plus.aspx>. Accessed: 2015-04-30.
- [www.minsocam.org, 2017] www.minsocam.org (2017). Mineral website. <http://www.minsocam.org/>. Accessed: 2015-04-30.

## Chapter 3

# Experiments: Electrophoretic mobility.

### Abstract

$\zeta$ -potential measurements can be used to predict the salinity, pH or organic matter concentration range where flocculation (coagulation) is likely to occur. One of the most used equipments measure  $\zeta$ -potential is electrophoresis. The accuracy of  $\zeta$ -potential measurements is evaluated in the present chapter by comparing the results of two measuring devices, using a model suspension.

The electrophoretic mobility of sulfate latex nanospheres (radius  $300 \pm 10$  nm) was measured as a function of ionic strength for different salts. The results were obtained from two similar instruments (Malvern ZetaSizer 3000 HSA and Malvern ZetaSizer Nano) using the same dispersions, at the same conditions. The difference between the capillary cell used in the two devices is that the cell of the ZetaSizer 3000 HSA is made of quartz and platinum electrodes and for the ZetaSizer Nano is of polycarbonate with gold electrodes. Analysis of the Doppler shift in the ZetaSizer Nano is done by using phase analysis of light scattering and in the ZetaSizer 3000 HSA this is performed by Fourier transformation. The values predicted from the standard electrokinetic model for constant surface charge were in good agreement with the data over a

large range of ionic strength. The influence of the protocol used to fill the cells is of importance for 1 – 10 mM of added monovalent salt. In this range of ionic strength, the capillary wall properties seem to influence the electrophoretic measurements, even at fast field reversal (FFR), where electro-osmosis should be absent. We found that during a series of measurements with monovalent salts, it was best to fill the cell starting from high ionic strength and decreasing the ionic strength during the series. The measurements with divalent salts were not sensitive to the filling procedure.

Most of the content of this chapter have been published in:

- Chassagne, C., & Ibanez, M., 2012. Electrophoretic mobility of latex nanospheres in electrolytes: Experimental challenges. *Pure and Applied Chemistry*, 85(1), 41-51.

## 3.1 Introduction

As has been demonstrated in [Kobayashi, 2008, Lin et al., 2006, Borkovec et al., 2000], the mobility maximum often observed when plotting the mobility as a function of the ionic strength can be interpreted using the so-called standard electrokinetic equations, provided that the particle has a constant surface charge density (and not a constant surface potential). The sulfate latex nanoparticles studied here can be assumed to carry a constant negative charge irrespective of ionic strength or pH. We show that the standard theory describes well the measurements for both the monovalent (KCl) and divalent ( $\text{MgCl}_2$ ) salts used. Each measured data point is the average of at least 10 consecutive measurements, and the difference between the consecutive measurements is less than 5%. We noticed, however, that the difference between two data points for the same sample can display a much larger deviation when not measured consecutively. The electrophoretic mobility (expressed here in zeta potential units, see equation 3.4.1) can vary from -75 to -85 mV for 5 mM of added KCl, for example. This is a significant difference, considering the fact that the electrophoretic mobility (in zeta potential units) varies about 10 mV in the range 1 – 10 mM of added KCl. The aim of this chapter is to analyze these differences.

## 3.2 Materials

### 3.2.1 Particles

The particles used were obtained from Interfacial Dynamics Corporation. They consist of surfactant-free polystyrene sulfate latex. The radius of the particles was measured by dynamic light scattering and found to be  $300 \pm 10$  nm. The radius found by transmission electron microscopy (TEM) reported by the manufacturer is 265 nm. For the theoretical derivations, we used 300 nm, as obtained in the lab when the size was measured. The sulfate groups are considered to be strongly acid and hence the particle's surface charge should not vary as a function of pH or ionic strength. The manufacturer reports that the surface charge of the particles is  $3.9 \cdot 10^{-2}$  C/m<sup>2</sup>. This is the value used in the calculations.

The particle concentration was about 19 mg/L in all experiments. We checked that the values of the electrophoretic mobilities were insensitive to particle concentration changes in the range 10 – 30 mg/L. The temperature was set at 298 K (25 °C). The pH of all suspensions was about 7.5. The samples were made by adding the required amounts of particle stock solution and electrolyte solution. These electrolyte solutions were prepared from demi water (conductivity  $< 1 \mu\text{S}/\text{cm}$ , PureLab) and analytical grade salts ( $\text{MgCl}_2$  and  $\text{KCl}$ ).

### 3.3 Methods

#### 3.3.1 Apparatus

Two commercial devices were used to measure the electrophoretic mobility of the samples: the Malvern ZetaSizer 3000 HSa (ZetaSizer) and the Malvern ZetaNano ZS cell (ZetaNano). Both measuring devices use laser Doppler velocimetry to assess the particles' mobility. Details of the technique can be found in [Hunter, 2013, Hunter, 1993, Ohshima and Furusawa, 1998]. The main differences between the measuring devices are as follows:

- In the ZetaNano, only the scattering beam passes through the capillary cell and the reference beam is routed outside. Analysis of the Doppler shift in the ZetaNano is done by using phase analysis light scattering. In the ZetaSizer, the two laser beams cross in the capillary cell and Doppler shift analysis is performed by Fourier transformation.
- The capillary cell of the ZetaSizer is made of quartz and has platinum electrodes, whereas the U-shaped capillary cell used for the ZetaNano was the disposable polycarbonate "Size & Zeta potential" Folded Capillary cell DTS1060, which has gold electrodes.

In principle, these differences should not have an influence on the measurements. We noticed, however, that for all samples we have analyzed so far using both the ZetaSizer and the ZetaNano, we had to apply 50 V across the measurement cell DTS1060, instead of the 150 V advised

by Malvern in order to get results comparable to the ZetaSizer. For higher voltages convective effects due to heating (electrodes' reaction) were observed when the ZetaNano was used. We used an applied voltage of 150 V for the ZetaSizer. (For lower voltages, the signal-to-noise ratio deteriorates.) As the measurements should be independent of the applied voltage value, we also checked that the measured mobilities were insensitive to the applied voltage, around 50 V for the ZetaNano (around an applied voltage of 150 V, the measurements were voltage-sensitive) and around 150 V for the ZetaSizer.

### 3.3.2 Protocol

Before each series of measurements the cells were thoroughly cleaned with ethanol, and then extensively with pure water of conductivity  $< 1 \mu\text{S}/\text{cm}$  following the manufacturer protocol. For each measurement, 10 mL of the suspension to be measured was injected gently with a syringe in the cells. The minimum volume required for the build-in quartz capillary cell of the ZetaSizer is 2 mL, and it is 0.75 mL for the ZetaNano. The large volume injected into the cells was meant to insure that the cells are sufficiently washed with the desired suspensions. Except when stated otherwise, no extra cleaning was performed during a series of measurement. In order to test whether the cell wall properties are affected by the way the series of experiments were conducted, two types of experiments were performed:

- (high  $>$  low) series: the samples are injected starting from the sample with the highest ionic strength, and finishing with the sample with the lowest ionic strength.
- (low  $>$  high) series: the samples are injected starting from the sample with the lowest ionic strength, and finishing with the sample with the highest ionic strength.

For each series, the same samples were used, only the filling order was changed. We checked for all samples that the conductivity measured in the cells corresponds to the conductivity expected for the given salt

concentration. Below 0.05 mM of added salt (below 0.02  $\mu\text{S}/\text{cm}$ ), however, the conductivities displayed by the measuring devices were not reliable anymore. The measurements were run simultaneously with the ZetaSizer and the ZetaNano. The two series were done the same day. Each data point presented in the figures represents the average of more than 10 consecutive measurements. The difference between each value measured within these consecutive measurements is less than 5%.

### 3.4 Theory and Models

The measured mobilities are plotted as an "apparent" zeta potential obtained from the Smoluchowski formula, as is often done in the literature. This Smoluchowski zeta potential  $\zeta_{Smolu}$  (V) is linked to the particle mobility  $u$  through:

$$\zeta_{Smolu} = \frac{u\eta}{\varepsilon_0\varepsilon_1} \quad (3.4.1)$$

where  $\eta = 8.904 \cdot 10^4$  Pa.s is the viscosity of the solvent (water) and  $\varepsilon_0\varepsilon_1 = 80 \times 8.8542 \cdot 10^{12}$  (F/m) its dielectric permittivity.  $u$  ( $\text{m}^2/\text{Vs}$ ) is the particle electrophoretic mobility, which is related to the particle's velocity  $v$  ( $\text{m/s}$ ) by  $v = uE$  where  $E$  ( $\text{V/m}$ ) is the applied electric field.

#### 3.4.1 Relation between surface charge and surface potential

The relation between the particle's surface charge and surface potential is evaluated numerically using the following equations:

Poisson-Boltzmann equation:

$$\nabla^2 \left( \frac{e\Psi_{eq}}{kT} \right) = -\kappa^2 \sum_i z_i \nu_i \exp \left( \frac{-z_i e \Psi_{eq}}{kT} \right) / \sum_i z_i^2 \nu_i \quad (3.4.2)$$

where  $\Psi_{eq}$  is the electric potential around the particle in the absence of an external applied electric field for which we have defined  $\Psi_{eq}(\infty) = 0$  and  $\Psi_{eq} = \Psi_0$  at the surface of the particle. The relation between

surface potential and zeta potential is given by:

$$\zeta = \Psi_{eq}(x_s) \quad (3.4.3)$$

where  $x_s$  is a given distance from the particle's surface. The zeta potential is defined as the electric potential at the surface of shear. When not specified, we will use

$$\zeta = \Psi_{eq}(x_s = 0) = \Psi_0 \quad (3.4.4)$$

Furthermore,  $k = 1.38 \cdot 10^{-23}$  (J/K) is the Boltzmann constant,  $T = 298$  ( $^{\circ}$ K) is the temperature,  $e = 1.6 \cdot 10^{-19}$  (C) the absolute value of the electron charge,  $z_i$  the valence of ion  $i$  and  $\nu_i$  its stoichiometric coefficient.  $\kappa^2$  (where  $\kappa^{-1}$  is the Debye length) is given by

$$\kappa^2 = \frac{-e^2 N_A C_S}{\varepsilon_0 \varepsilon_1 k T} \sum_i z_i^2 \nu_i \quad (3.4.5)$$

where  $N_A = 6.02 \cdot 10^{23}$  ( $\text{mol}^{-1}$ ) is Avogadro's number and  $C_S$  the added salt concentration in mM (millimol/L). The relation between the particle surface charge  $\sigma$  ( $\text{C}/\text{m}^2$ ) and potential is given by Gauss' law

$$\sigma = -\varepsilon_0 \varepsilon_1 \left( \frac{d\Psi_{eq}}{dr} \right)_{\text{at the particle surface}} \quad (3.4.6)$$

where we neglect the contribution of the particle's internal field [Ohshima and Furusawa, 1998]. The potential  $\Psi_0$  corresponding to  $\sigma = 3.9 \cdot 10^{-2}$   $\text{C}/\text{m}^2$  (the value given by the manufacturer) is found for each ionic strength by the bisection method, starting from two values  $\Psi_0^1$  and  $\Psi_0^2$  for which  $\sigma(\Psi_0^1) < \sigma < \sigma(\Psi_0^2)$  until  $|\Psi_0^1 - \Psi_0^2| < 10^{-4}$ . The relation between the dimensionless surface potential  $e\Psi_0/kT$  and ionic strength is shown in figure 3.1 for the particles used in this study. For comparison, we included the formula derived for plate-like particles for symmetric electrolytes [Ohshima, 2006b]

$$\frac{e\Psi_0}{kT} = 2 \left( \frac{e\sigma}{2\varepsilon_0 \varepsilon_1 k T \kappa} \right) \quad (3.4.7)$$

Note that the plate-like particles and the numerical solution are in very good agreement, even for small  $\kappa a$  ( $\approx 10$ ) ( $[KCl] < 10^{-3}$  mM), where  $a$  is the radius of the particle.



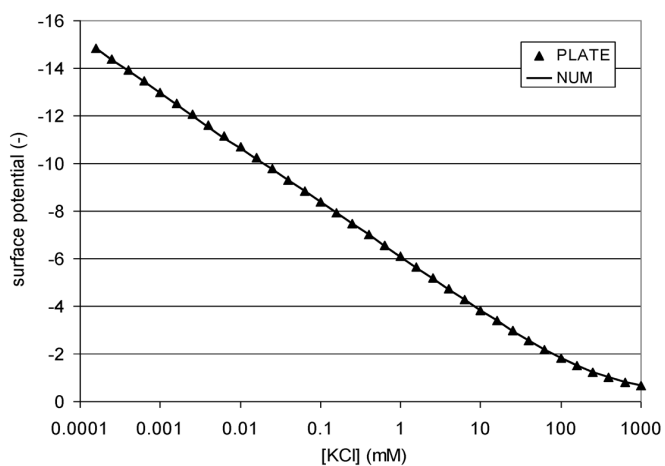


**Figure 3.1** – Variation of the dimensionless surface potential as a function of added KCl concentration (mM), for a constant surface charge of  $3.9 \times 10^{-2} \text{ C/m}^2$ . The numerical calculation (NUM) was done for a sphere of radius 300 nm. PLATE indicates the analytical formula for flat surfaces.

### 3.4.2 Relation between surface charge and mobility

For each ionic strength, a surface potential is found according to the procedure described in the preceding section. Using this surface potential, the mobility of the particle is obtained by solving numerically the standard set of electrokinetic equations (see, e.g., [Ohshima and Furusawa, 1998] for more details on the derivations and corresponding curves referred to as NUM in the figures' legend). The calculated mobility differs from the Smoluchowski formula by a parameter  $F$  that is called Henry's function [Ohshima and Furusawa, 1998]

$$\zeta = \frac{\zeta_{smolu}}{F} \quad (3.4.8)$$

In figure 3.2, the parameter  $F$  is displayed. The formula of Henry (valid for low zeta potentials, i.e.,  $|e\zeta/kT| < 1$ ) is included for comparison. From figure 3.1 it can be seen that  $|e\zeta/kT| < 1$  for  $[\text{KCl}] > 100$  mM, where Henry's function is in agreement with the numerically evaluated parameter  $F$ . We also included the parameter  $F$  evaluated from Ohshima's analytical solution [Ohshima and Furusawa, 1998], valid for  $\kappa a \geq 30$

$$F_{Ohshima} = 1 - 2 \frac{2G}{1+G} \ln \left( \frac{1 + \exp |e\zeta/2kT|}{2} \right) / |e\zeta/2kT| \quad (3.4.9)$$

$$G = \frac{2}{\kappa a} \left( 1 + \frac{2\varepsilon_0\varepsilon_1 kT N_A}{\eta \Lambda^0} \right) (\exp |e\zeta/2kT| - 1) \quad (3.4.10)$$

where  $\Lambda^0$  is the limiting conductance of the ion. We took  $\Lambda^0$  ( $\text{K}^+ \simeq \Lambda^0$  ( $\text{Cl}^- \simeq 75 \times 10^{-4}$  (S m<sup>2</sup> mol<sup>-1</sup>)). As can be seen in figure 3.2, Ohshima's formula indeed is valid for  $[\text{KCl}] > 1$  mM, where  $\kappa a = 31$ . Therefore we can use Ohshima's formula.

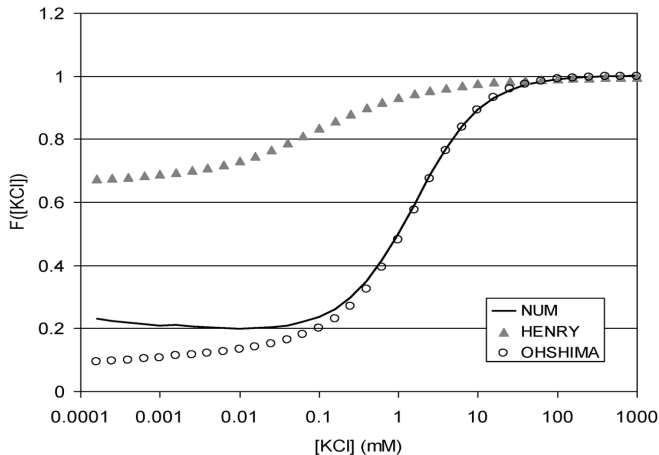


**Figure 3.2** – Variation of the dimensionless parameter  $F$  as function of added KCl concentration (mM) for the particle used in this study.

## 3.5 Results and discussion

### 3.5.1 Monovalent salt (KCl)

#### Influence of the measurement equipment

There are minor differences between the results found with the ZetaSizer and the ZetaNano for the optimal protocol used. In figure 3.3, we show the variation of the electrophoretic mobility found for the (high > low) series. The differences between the points measured with the ZetaNano and ZetaSizer are less than 5% (the same difference as between consecutive measurements). When we used a different cell for the ZetaNano, using the same sample, we also find differences of less than 5%.

#### Influence of the measurement protocol

We note a significant influence (both for the ZetaSizer and ZetaNano) of the measurement protocol. As can be observed in figures 3.4 and 3.5, the measured mobility expressed in zeta potential units (see equation 3.4.1) is about  $-75$  mV for the (low > high) series and about  $-85$  mV

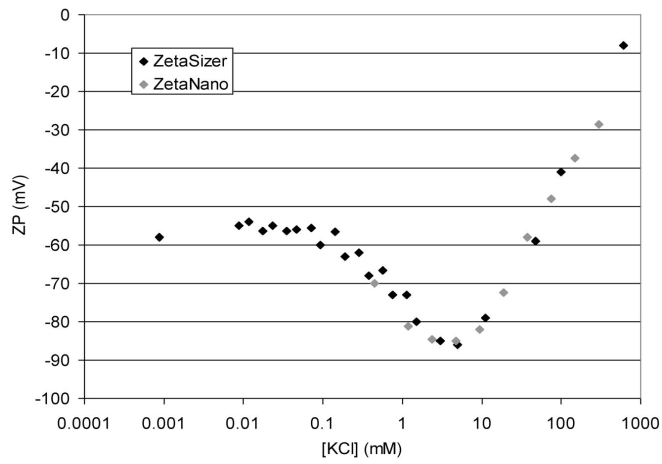


**Figure 3.3** – Electrophoretic mobility of the latex particles of radius 300 nm expressed as apparent zeta potentials (ZPs) (see equation 1), as function of added KCl concentration (mM) using the optimal protocol for the two measuring equipment used in this study (high > low series).

for the (high > low) series for 5 mM of added KCl. This is a significant difference, considering the fact that the electrophoretic mobility (in zeta potential units) varies about 10 mV in the range 1 – 10 mM of added KCl. In figures 3.4 and 3.5, the measured mobilities are compared to the mobilities evaluated from the numerical derivations and using Ohshima's relationship and the plate-like formula 3.4.7

$$\zeta_{Ohshima} (mV) = 2000 \frac{kT}{e} \arcsin h \left( \frac{e\sigma}{2\varepsilon_0\varepsilon_1 kT\kappa} \right) \frac{1}{F_{Ohshima}} \quad (3.5.1)$$

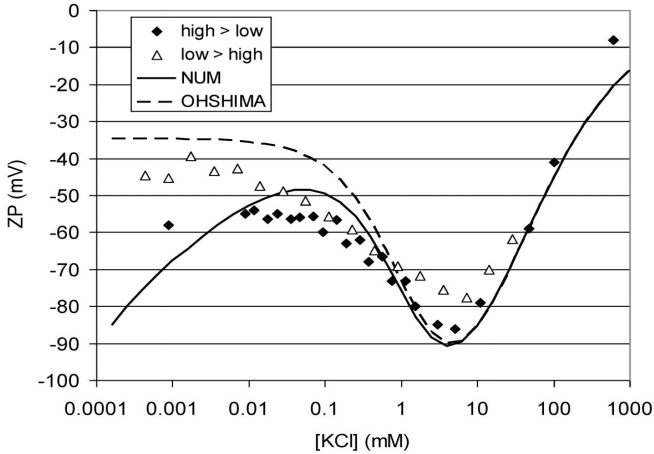


**Figure 3.4** – Mobilities measured with the Malvern ZetaSizer 3000 HSa. The mobilities are expressed as apparent zeta potentials (ZPs), using Smoluchowski's formula. Measurement series are performed filling the cell from high to low ionic strength (high > low) or from low to high ionic strength (low > high). The theoretical predictions are included, using no adjustable parameters. The full line is the mobility from the numerical derivations using the plate-like formula. The dashed line is the mobility from the numerical derivations using Ohshima's relationship.

We note first that without any adjustable parameter, the agreement between the measured and predicted mobilities is quite good. There

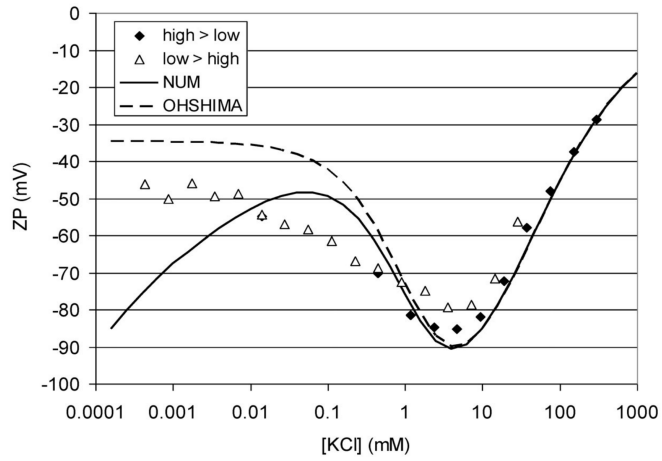


**Figure 3.5** – Mobilities measured with the Malvern ZetaNano ZS. The mobilities are expressed as apparent zeta potentials (ZPs), using Smoluchowski's formula. Measurement series are performed filling the cell from high to low ionic strength (high > low) or from low to high ionic strength (low > high). The theoretical predictions are included, using no adjustable parameters. The full line is the mobility from the numerical derivations using plate-like formula. The dashed line is the mobility from the numerical derivations using Ohshima's relationship.

are, however, deviations for low values of the ionic strength, and around the mobility maximum, where the measurements are quite sensitive to the filling protocol. Measurements at low ionic strength are difficult, as samples are very sensitive to contamination, and we found that the measurement accuracy is poor for monovalent salts (the deviations are  $\pm 10$  mV for the lowest concentrations). Moreover, at concentrations around  $10^{-4}$  mM, the double layer becomes very large ( $\kappa a = 0.31$ ), and in theory the surface potential has to become extremely large to ensure the same constant surface charge (see figure 3.1). This could be different in practice. We could improve the agreement between the measured and predicted mobilities for low ionic strength using either of the following hypotheses:

- by assuming a constant surface potential in which range of concentration, as shown in figure 3.7. In that figure, the dashed line was evaluated using a dimensionless constant surface potential of  $-11$  (corresponding to  $-275$  mV). This is the surface potential at approximately 0.005 mM of added KCl, assuming the constant charge behavior (see figure 3.1).
- From separate conductivity measurements, we found that below 0.005 mM of added KCl, the conductivity of the samples did not vary anymore and was about  $0.8 \mu\text{S}/\text{cm}$ . We may, therefore, also assume that below that concentration, the surface charge (as the surface potential) does not change anymore, as the amount of (monovalent) ions is constant. Subsequently, the electro-phoretic mobility would be constant and equal to the mobility at 0.005 mM of added KCl.

As the particles are assumed to have a constant surface charge, independent of ionic strength, we prefer the last hypothesis.

Finally, we note that for very low ionic strengths, the mobility evaluated from Ohshima's formula reaches a constant value, independent of the surface charge, equal to:

$$\zeta_{Ohshima} = -2 \ln(2) \frac{kT}{e} = -35 \text{ mV} \quad (3.5.2)$$

Around the mobility maximum (around 5 mM of added KCl), there are significant differences between the measurement series. They were observed systematically with the two measuring devices, and the mobility maximum was in both cases higher (in absolute value) for the (high > low) series. The (high > low) series is also the series that corresponds best to the model in both cases. As specified in the previous section, the same samples were used for each series. The conductivity was also the same for both measuring devices at each concentration of the series, and this conductivity corresponded to the expected theoretical value. We therefore conclude that the observed differences between protocols must lay in the properties of the capillary cells and the particle/wall interactions.

To investigate the sensitivity of the measurements dependency on cell filling history we did a series of experiments where the cell was cleaned with pure water prior to each filling during a series. We then observed that the measured zeta potentials were lower (in absolute values) than the (low > high) results. This occurs when the measurements are done right after filling the cell (which takes 1 or 2 min). When the cell is left to equilibrate for a longer period, from 15 min to 24 h, we observed large shifts in the values of the zeta potential, especially at low ionic strength. At moderate ionic strength, cells filled using the (high > low) protocol give in general time-independent results. Cells filled using the (low > high) protocol or which were cleaned prior to filling were in general time-sensitive. The filling history of the cell, and not only the equilibrium time, is therefore of importance for the capillary wall properties.

### 3.5.2 Wall zeta potential

The software of ZetaNano gives access to the so-called wall zeta potential, i.e., the zeta potential of the capillary tube in which the samples are injected [Malvern, 2015]. This wall zeta potential is derived from the two types of measurements performed within a measurement cycle: first, the particle mobility is evaluated at a slow field reversal (SFR), then at a fast field reversal (FFR). At SFR, the mobility of the particle is the sum of its electrophoretic mobility and the electro-osmotic velocity of the fluid (which is set in movement by the ions in the capillary



double layer). At FFR, the electroosmotic flow is assumed negligible and the measured mobility is the electrophoretic mobility alone. The zeta potential of the capillary walls is then evaluated by

$$\zeta_{wall}(mV) = -[u(SFR) - u(FFR)]1000\eta/(\varepsilon_0\varepsilon_1) \quad (3.5.3)$$

This wall zeta potential, therefore, gives an indication on the capillary cell wall properties: if particles adhere to this wall, the wall zeta potential values will be affected. The wall zeta potential corresponding to the measurements presented in figure 3.5 is given in figure 3.6. Now there was no significant deviation of the wall zeta potential values between the series. When we cleaned the cell with water prior to filling, the wall zeta potential was much lower (in absolute values) than these series. The capillary cell of the Malvern ZetaSizer is made of quartz, whereas the capillary cells of the ZetaNano (Size & Zeta potential Folded Capillary cell DTS1060) are made of polycarbonate. Studies have demonstrated that latex particles have an interaction with both quartz and polymers [Matsuoka et al., 1998, Faghihnejad and Zeng, 2012, Mishchuk, 2011] and may adhere to the capillary cell walls through hydrophobic forces in particular. We included the numerical predictions for the wall zeta potential using the Poisson-Boltzmann formulation for plates and assuming that the cell's surface charge was  $-2.0 \times 10^{-2}$  C/m<sup>2</sup> and that the shear plane was located at either 0.5 or 0.6 times the Debye length from the surface. Other values for the surface charge and shear plane location did not fit the experimental data. Further study is required to evaluate these values and their physical interpretation.

The mobility  $u(FFR)$  is used to evaluate the particle's mobility displayed in the figures. As  $u(FFR)$  is different for the different filling procedures, for the same ionic strength in the range 1 – 10 mM of added KCl, we assume that in that case, as in the SFR mode, electro-osmosis plays a role, despite the fact that the field reversal is assumed by the manufacturer to be high enough to minimize electro-osmosis.

### 3.5.3 Divalent salt (MgCl<sub>2</sub>)

The values measured with divalent salts are in general much more reproducible than the ones measured with monovalent salts. We also did

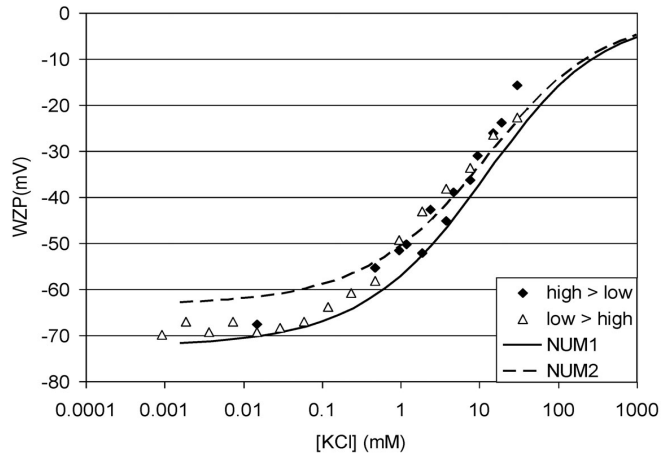


**Figure 3.6** – Wall zeta potential (WZP) corresponding to the measurements displayed in figure 3.4. NUM1 corresponds to numerical calculations using a WZP defined at a distance of  $0.5 \kappa^{-1}$  of the capillary surface and NUM2 calculations using a WZP defined at a distance of  $0.6 \kappa^{-1}$  of the capillary surface. For both a constant surface charge of  $-2.0 \times 10^{-2} \text{ C/m}^2$  is used.

not observe any differences between (low > high) or (high > low) filling protocols. The measured zeta potentials together with the numerical predictions are displayed in figure 3.7. We first tried to improve the fitting of the curve by shifting the plane of shear from the particle's surface and locate it at  $x_S = 0.25$  or  $0.5$  nm from the surface, using a surface charge of  $-3.9 \times 10^{-2}$  C/m<sup>2</sup>. We found that locating the shear plane at 0.25 nm improves the fitting. This was also found by Kobayashi, who used the same type of sulfate latex particles as we used, but of radius  $1.4 \mu\text{m}$  and surface charge  $-7.0 \times 10^{-2}$  C/m<sup>2</sup> [Kobayashi, 2008].

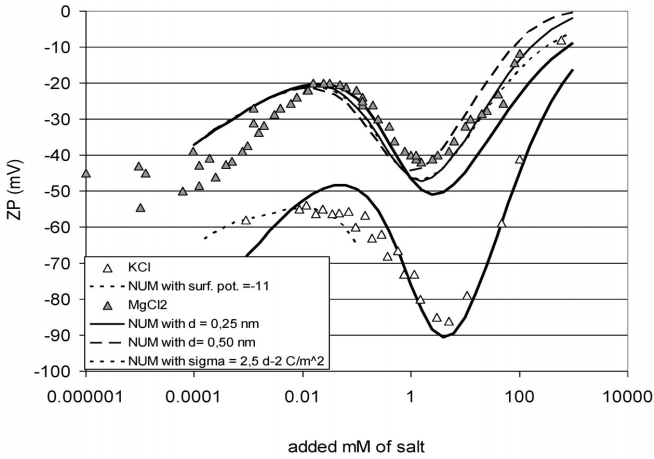


**Figure 3.7** – Mobilities measured with the Malvern ZetaSizer 3000HSa. The mobilities are expressed in apparent zeta potentials (ZPs), using Smoluchowski's formula. Measurement series are performed filling the cell from high to low ionic strength (high > low). The theoretical predictions are included, see text for details. The thick lines (not indicated in the figure's legend) were evaluated with  $d = 0$  and no adjustable parameter using NUM. Other lines are explained in the legend of the graph.

We then tried to fit the data by adjusting the surface charge and keeping  $x_S = 0$  and found that lowering the surface charge by a factor of 1.5 (using a surface charge of  $-2.5 \times 10^{-2}$  C/m<sup>2</sup>) lead to almost the same prediction as shifting the shear plane of 0.25 nm using a surface charge

of  $-3.9 \times 10^{-2}$  C/m<sup>2</sup>. This was also observed by Kobayashi [Kobayashi, 2008]. The surface potential is then nearly similar in both cases and starts to deviate slightly above 10 mM of added salt, which is reflected in the mobility differences observed above that concentration. (The factor  $1/F$  is identical in both cases.) The behavior at (very) low ionic strength is more in line with the numerical predictions for divalent salts. In that region, the surface potential is evaluated assuming constant charge of the particle is half the value of the surface potential for monovalent salts (e.g., the dimensionless surface potential  $e \psi_0 / kT$  is 12.9 for  $10^{-3}$  mM KCl and 6.3 for  $10^{-3}$  mM MgCl). As can be observed in the figure 3.7, the numerical predictions are also less dependent on the values of surface charge or shear plane distances in that range. The differences between measured and computed mobility values are difficult to explain as the theory should be adapted for low ionic strength [Ohshima, 2006a].

### 3.6 Conclusions

We have demonstrated that the standard electrokinetic model for constant surface charge can be used to predict the electrophoretic mobility values for 300 nm sulfate latex nanospheres. The agreement was good over a large range of ionic strength, for both monovalent and divalent salts. Measurements performed on the same type but micron-sized particles gave similar results [Kobayashi, 2008] in the range 0.1 – 1000 mM of added salt investigated by this author. The differences we found between measured values may be related to cell-filling procedures. There were nearly no differences between measurements performed by the two types of equipment used (ZetaNano and ZetaSizer, Malvern) provided a voltage of 50 V is applied with the ZetaNano (and not 150 V as advised by the manufacturer). The cell capillary wall properties seem to affect the particle mobility even at FFR where electroosmosis should, in principle, be absent, in the case of monovalent salts. In order to improve the accuracy of the measurement in the case of monovalent salts for this type of system, we recommend starting a series of measurement with injecting the sample with the highest ionic strength first and finishing with the sample with the lowest ionic strength. Measurements with divalent

salts are nearly independent of the cell-filling procedure.

We conclude that the (high > low) protocol is the most adapted to study the  $\zeta$ -potential of suspended particles. An application of how sediments are analyzed by the zeta potential and which information can be obtained from this measurements will be explained in chapter 7.

## References

- [Borkovec et al., 2000] Borkovec, M., Behrens, S. H., and Semmler, M. (2000). Observation of the mobility maximum predicted by the standard electrokinetic model for highly charged amidine latex particles. *Langmuir*, 16(11):5209–5212.
- [Faghihnejad and Zeng, 2012] Faghihnejad, A. and Zeng, H. (2012). Hydrophobic interactions between polymer surfaces: using polystyrene as a model system. *Soft Matter*, 8(9):2746–2759.
- [Hunter, 1993] Hunter, R. (1993). Introduction to modern colloid scienceoxford univ. Press, London.
- [Hunter, 2013] Hunter, R. J. (2013). *Zeta potential in colloid science: principles and applications*, volume 2. Academic press.
- [Kobayashi, 2008] Kobayashi, M. (2008). Electrophoretic mobility of latex spheres in the presence of divalent ions: experiments and modeling. *Colloid and polymer science*, 286(8-9):935–940.
- [Lin et al., 2006] Lin, W., Kobayashi, M., Skarba, M., Mu, C., Galletto, P., and Borkovec, M. (2006). Heteroaggregation in binary mixtures of oppositely charged colloidal particles. *Langmuir*, 22(3):1038–1047.
- [Malvern, 2015] Malvern (2015). Malvern website. <http://www.malvern.com>. Accessed: 2015-04-30.
- [Matsuoka et al., 1998] Matsuoka, H., Morikawa, H., Tanimoto, S., Kubota, A., Naito, Y., and Yamaoka, H. (1998). Evaluation of the dynamic properties of polymer latex particles interacting with quartz interface by evanescent wave dynamic light scattering. *Colloid and Polymer Science*, 276(4):349–355.

- [Mishchuk, 2011] Mishchuk, N. A. (2011). The model of hydrophobic attraction in the framework of classical dlvo forces. *Advances in colloid and interface science*, 168(1):149–166.
- [Ohshima, 2006a] Ohshima, H. (2006a). Electrophoresis of colloidal particles in a salt-free medium. *Chemical engineering science*, 61(7):2104–2107.
- [Ohshima, 2006b] Ohshima, H. (2006b). *Theory of colloid and interfacial electric phenomena*, volume 12. Academic Press.
- [Ohshima and Furusawa, 1998] Ohshima, H. and Furusawa, K. (1998). *Electrical Phenomena at Interfaces: Fundamentals: Measurements, and Applications*, volume 76. CRC Press.

## Chapter 4

# Effect of polyelectrolytes on the electrokinetic surface potential and flocculation behaviour of cohesive sediments

### Abstract

This chapter presents the flocculation behavior of a commercially available clay. The flocculation was induced by adding either an anionic or a cationic polyelectrolyte to a clay suspension of 0.7 g/L. The flocculation behavior was studied in terms of the evolution of floc size in time by means of Static Light Scattering. Different flocculation behaviors were found depending on the polyelectrolyte type. The reversibility upon shear stress of the mean floc size allowed analyzing the floc strength. The cationic polyelectrolyte induced faster flocculation and the flocs created were bigger than the ones created with the anionic polyelectrolyte. The anionic polyelectrolyte produced flocs that could regrow nearly to their initial size after a subsequent increase and decrease in shear rate, whereas



the flocs produced with cationic polyelectrolyte could not. The optimum dose of anionic polyelectrolyte (i.e. the dose at which flocs are formed the fastest) was related to the amount of cations in the system. These two findings are in line with other authors. The electrokinetic surface potential (zeta potential) measurements as function of polyelectrolyte and clay concentration allowed to find a good parameter to predict the polyelectrolyte dose for optimal flocculation in the case of cationic polyelectrolyte. This is due to the fact that in this case electrokinetic surface charge neutralization was linked to optimal flocculation. In the case of anionic polyelectrolyte the zeta potential indicated qualitatively the degree of flocculant coverage on a particle. For anionic flocculant, the zeta potential measurements also confirmed that the flocculant coverage onto particles was limited by the amount of cations present in the system.

## 4.1 Introduction

The influence of organic matter, pH and salinity on natural sediment flocculation has been studied from samples in situ [Manning et al., 2011, Kranck and Milligan, 1992, Liss et al., 2005] and also in the laboratory [Gregory, 1988, Tombacz and Szekeres, 2004, Tombácz and Szekeres, 2006, Mietta et al., 2009, Lee et al., 2012, Bergaya and Lagaly, 2013, Liss et al., 2004]. In estuarine systems, flocculation plays a predominant role, and leads to estuarine siltation. This is one of the main causes for the dredging activities in harbors. Organic matter in particular plays a major role in sediment flocculation, because it can easily adhere to the clay particles of the sediment and induce bridging flocculation between the clay particles [Bergaya and Lagaly, 2013]. Organic matter can be composed of various substances like polysaccharides, lipides, hydrocarbons, and humic acids [Winterwerp and Van Kesteren, 2004]. The cohesive behavior of sediments is mainly related to the presence of polyelectrolytes like polysaccharides. Polysaccharides come in various shapes (linear or branched polymers) with different molecular weight and different charges. Dissolved salts i.e. ions also contribute to clay flocculation [Mietta et al., 2009, Bergaya and Lagaly, 2013]. Most studies are therefore about the flocculation behavior of sediment in the presence of both salt and polyelectrolytes.

In this chapter our study is limited to the flocculation of clay suspensions by polyelectrolytes in demi-water (deionized) without any added salt. In order to study the effect of different charges and molecular weight on the flocculation behavior of sediment, we used synthetic polyelectrolytes. Synthetic polyelectrolytes (flocculant) are derived from petrochemical raw materials [Mortimer, 1991]. They consist of polymers with repeating units of ionized groups that can be negatively or positively charged depending on the specific functional groups present [Sperling, 2005]. Even though the effect of flocculants has been studied extensively in disciplines like sanitary engineering, process industry, contaminated sediments management, mineral processing, and oil drilling and recovering [Ackroyd et al., 1986, Mortimer, 1991, Stewart and Thompson, 1997, McLaughlin and Bartholomew, 2007, Sojka et al., 2007], few sys-

tematic studies have been published on the flocculation behavior of clay as function of flocculant type, charge and shear stresses applied to the system [Barany et al., 2009, Barany et al., 2011].

The electrokinetic surface potential is known to be a good measure for the flocculation ability of a suspension [Hunter, 1993, Hunter, 2001]. Some authors have already studied the link between zeta potential, measured by electrophoresis, and flocculation [Hunter, 2001, Mietta, 2010, Gregory and Barany, 2011, Yu and Somasundaran, 1996, Narkis et al., 1991], but systematic studies are lacking. For instance, no electrophoretic mobility study has been performed varying systematically the flocculant dose and the (clay) particle concentration, as done in the present study. We will demonstrate that doing so, important information is gained about the binding of polyelectrolyte to the clay, and that in the case of cationic polyelectrolyte, electrophoretic mobility (zeta potential) measurements allow to predict the optimal flocculant dose for fastest flocculation.

## 4.2 Materials

All studies in this chapter are performed for each of two polyacrylamide-based polyelectrolytes (anionic and cationic) which have different charge and different molecular weight. All experiments are performed in demi-water, with no added salt and the pH for all experiments was about 8.

### 4.2.1 Clay

The clay used in the experiments is the same river clay used in chapter 2. The clay was always dispersed in demi-water, the obtained suspension having conductivity less than 0.005 mS/cm. The original clay lump has a water content of 35.7% defined as the mass of water per total mass (solids and water) and a sand content of 21%.

### 4.2.2 Flocculant

Two different commercially available flocculants from the company BASF were used in the experiments. These flocculants are from the product line Zetag, which are dry powder flocculants. Cationic flocculant is principally used for conditioning municipal and industrial substrates prior to mechanical or static solid/liquid separation. Anionic flocculant is mainly used for industrial effluent applications. The flocculants used were:

- Zetag 4110 which is an anionic co-polymer of polyacrylamide and sodium acrylate. Its apparent viscosity is 1.7 mPa s at 1% concentration (10 g/L) in water.

- Zetag 7587 which is a cationic co-polymer of polyacrylamide and quaternized cationic monomer. Its apparent viscosity is 2.2 mPa s at 1% concentration (10 g/L) in water.

More specifications, as given by the manufacturer, are shown in table 4.1.

**Table 4.1** – Specifications of the polymers used in the experiments.

Product	Charge [mol %]	Type of charge	Molecular weight [g/mol]
Zetag 4110	Medium (25)	Anionic	High ( $>10^6$ )
Zetag 7587	High (50-100)	Cationic	Medium ( $10^5$ - $10^6$ )

The dry powder polyelectrolyte was dissolved in demi-water to prepare two stock solutions. The stock is the reference solution used in the experiments. The concentration of stock solutions used were 0.25 g/L and 0.5 g/L.

## 4.3 Methods

### 4.3.1 Particle Size Distribution

The Particle Size Distribution of the samples was measured by Static Light Scattering by means of a Malvern Mastersizer 2000. The software

evaluates the volume particle size distribution based on Mie theory of light scattering, assuming spherical and solid particles [Malvern, 2015]. In particular, this theory does not account for the porosity and irregularity in shape of flocs. The Malvern particle size distribution always gave an average value of  $6\ \mu\text{m}$  for the  $D_{50}$  of the clay suspensions (no added flocculant).

In order to characterize the Particle Size Distribution of the clay suspension (no added flocculant), we also performed hydrometer and sieve tests, evaluating the Particle Size Distribution following British Standards (BS 1377: Part 2: 1990). The hydrometer test links the settling velocity of particles to their diameter, using Stokes law, hereby assuming that the particles are spherical and their density uniform and known. The  $D_{50}$  of the clay found by the hydrometer and sieve tests is also around  $6\ \mu\text{m}$ .

All the other particle size measurements in the remaining of this chapter are done by Static Light Scattering using the Malvern. The presence of fines (smaller than 2 microns) might therefore be underestimated or undetected. In this chapter however, we focus on the particles larger than  $2\ \mu\text{m}$ .

### **Floc size distribution measurements**

The flocculation experiments were performed in a JLT6 jar test set-up from VELP scientifica. The dimensions of the jar are 95 mm for the inner diameter and 110 mm for the height of the fluid. The suspension is stirred using a single rectangular paddle. The paddle is 25 mm high and 75 mm in diameter. It is placed centrally 10 mm above the bottom of the jar.

The suspensions were pumped through the Malvern Mastersizer 2000 with the help of a peristaltic pump from the mixing-jar to the Malvern and back again to the mixing-jar. A sketch of the set-up is shown in figure 4.1. This set-up allows to control independently the speed of the pump and of the mixing-jar. The internal diameter of the connecting tubes is 5 mm and the total length as shortest as allowed by the geometry of the set-up (2400 mm from the jar to the pump, to the cell and back to the jar). The discharge for pumping the sample into the Malvern was

1.92 mL/s (98 mm/s), the lowest possible to prevent particles settling in the tubes. The average shear rate in the jar was the lowest shear rate possible for preventing particles settling in the jar. We used 75 rpm, which, for our set-up was estimated to correspond to a shear rate less than  $50 \text{ s}^{-1}$  [Bouyer et al., 2005]. Using these shears, we try to minimize floc break-up in the jar. With this set-up it is possible to record a full Particle Size Distribution every 30 seconds. The residence time in the tube is 25 s and in the jar is 520 s.

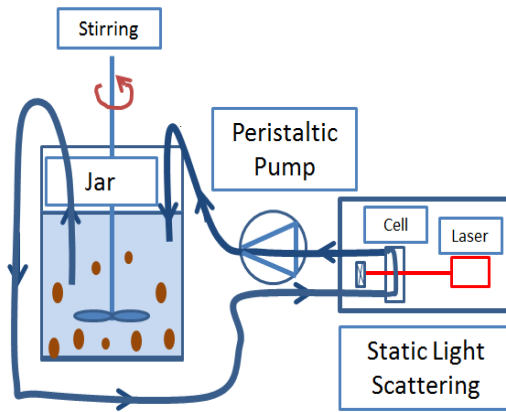


Figure 4.1 – Sketch of the experimental set-up.

### Shear stress

The same set-up described above for the floc size measurements is used during the shear stress experiments. The strength of the flocs was studied as function of the shear rate. The discharge of the pump was increased in four steps from 1.92 mL/s ( $150 \text{ s}^{-1}$ ) to 15 mL/s ( $1200 \text{ s}^{-1}$ ) and then decreased again, to study if the flocculation was reversible. For each step we waited until the mean floc size reached steady-state. This took about 30 minutes for all experiments. The shear rate in the tubes for each discharge was calculated with the formula:  $G = 4Q/\pi r^3$ , where

$Q$  is the discharge,  $r$  is the radius of the tube ( $r = 2.5$  mm).

### 4.3.2 $\zeta$ - Potential

The electrophoretic mobility of the suspensions was measured using a Malvern ZetaNano ZS device. The mobilities were related to the zeta potential values ( $\zeta$ ) using the Smoluchowski formula [Hunter, 2013]. Explanation about device and theory used are given in chapter 3. The zeta potential was measured at different clay concentrations and as function of flocculant dose. The flocculant was added to the clay suspension, gently stirred for 10 seconds in a 50 mL beaker and injected immediately into the measuring cell. The flocculant used was always fresh, less than 4 days old. After four days, degradation in the flocculant solution occurred in our stock solutions of 0.5 g/L or 0.25 g/L. With aged flocculant, flocculation still happened but higher doses were required to obtain the same results as for fresh flocculant. In the case of anionic polyelectrolyte, which has a higher molecular weight than the cationic, the degradation was faster than in the case of cationic polyelectrolyte. After 4 days the cationic flocculant was not yet aged, whereas the anionic was.

## 4.4 Particle size evolution as function of time

The flocculation behavior of clay as function of time was studied with the two types of polyelectrolytes. The flocculant concentration was changed in each experiment. The clay concentration was always 0.7 g/L. This clay concentration was the highest at which detection was possible by the laser of the Malvern (obscuration of 30%). The shear rate in the jar was less than  $50 \text{ s}^{-1}$  during all experiment and the discharge of the pump was 1.92 mL/s. The flocculant was added in all experiments at a time defined arbitrarily to be  $t = 1$  s. The time  $t = 0$  s corresponds to the particle size distribution of the clay before addition of flocculant. In figures 4.2 and 4.3 an example of the changes of the particle size distribution as function of time for cationic flocculant is given and in figures 4.8, 4.9 and 4.10 an example of the changes of the particle

size distribution as function of time for anionic flocculant is given. The optimal dose of flocculant can be deduced from these experiments. We define the optimal dose as the dose for which the initial slope  $dD_{50}/dt$  is the highest and the supernatant turbidity is the lowest. This definition is line with other authors, definition [Gregory, 1973].

#### 4.4.1 Cationic flocculant (Zetag 7587)

In figures 4.2 and 4.3 we show two examples of the time evolution of the Particle Size Distribution of clay in the presence of the cationic flocculant. For concentration 0.35 mg/L we are below the optimal flocculant dose, whereas for 1.8 mg/L we are close to the optimal dose. During flocculation the amount of small particles ( $< 10 \mu\text{m}$ ) is considerably reduced, indicating that they are taken up in the flocs of larger size. This is reflected in the clarity of the suspension: in time, large flocs are observed in clear water. The size of the largest particles obtained with 1.8 mg/L added flocculant becomes smaller after reaching maximum size, as the peak of the distribution shifts towards lower sizes (figures 4.2, 4.3) in time. This is also reflected in the decrease of the  $D_{50}$  in time (figure 4.4). The decrease in size of macro-flocs was also observed during salt induced flocculation experiments on kaolinite [Mietta, 2010].

The residence time for the formation of the flocs is around 400 s and it is defined by time that the samples stays in the jar. In figure 4.4 we display some of the results obtained from the evolution of  $D_{50}$  as function of time. We present four typical curves for concentrations below the optimal flocculant dose, the curve obtained for the optimal dose (3.5 mg/L), and four typical curves for concentrations above the optimal flocculant dose. The decrease in size of the macro-flocs was visible from a flocculant dose larger or equal to 1 mg/L.

We estimated the change in particle size according to (% size):

$$\%size = ((D_{50max} - D_{50(t=750s)}) / (D_{50max} + D_{50(t=750s)})) \times 100 \quad (4.4.1)$$

where  $D_{50max}$  is the largest size for a given flocculant concentration. This largest size is reached at about 200 s for concentrations between 1 mg/L and 18 mg/L. For flocculant concentration below 1 mg/L and



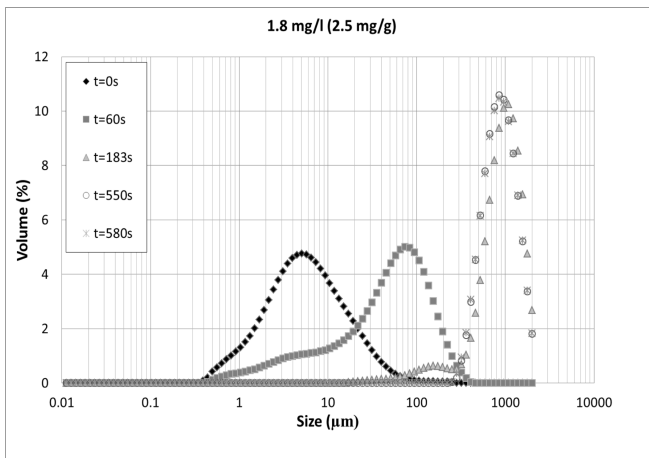


**Figure 4.2** – Evolution in time of the Particle Size Distribution for 0.7 g/L clay with cationic 7587 flocculant. Shear rate ( $G$ ) in the jar  $50 \text{ s}^{-1}$  and discharge in the pump is  $1.92 \text{ mL/s}$  ( $150 \text{ s}^{-1}$ ). The amount of flocculant is given in the title and times in the legend,  $t = 1 \text{ s}$  corresponds to the addition of polyelectrolyte.

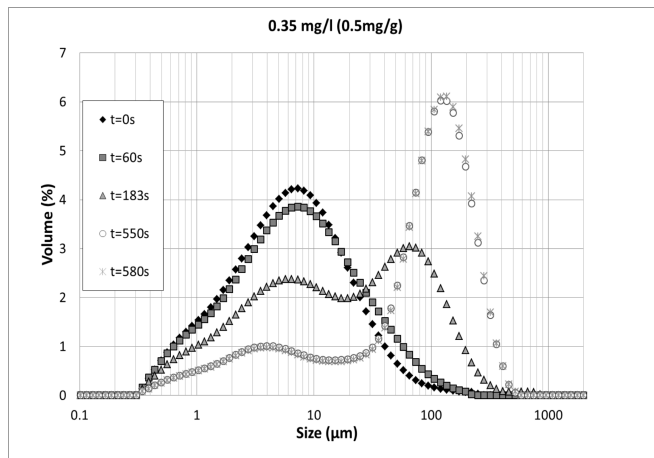


**Figure 4.3** – Evolution in time of the Particle Size Distribution for 0.7 g/L clay with cationic 7587 flocculant. Shear rate ( $G$ ) in the jar  $50 \text{ s}^{-1}$  and discharge in the pump is  $1.92 \text{ mL/s}$  ( $150 \text{ s}^{-1}$ ). The amount of flocculant is given in the title and times in the legend,  $t = 1 \text{ s}$  corresponds to the addition of polyelectrolyte.

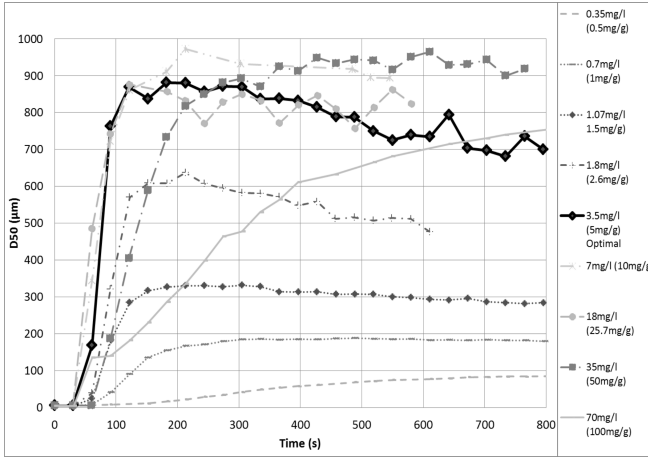


**Figure 4.4** – Evolution of the  $D_{50}$  in time. The clay concentration is 0.7 g/L and the different concentrations of cationic flocculant, Zetag 7587, are indicated in the legend. The optimal dose corresponds to a value between 1.8 mg/L and 3.5 mg/L.

above 18 mg/L the largest size is reached at times much larger (800 s or larger, when the equilibrium is reached). The change in size and  $D_{50max}$  are plotted in figure 4.5.

Both the  $D_{50}$  and the  $dD_{50}/dt$  display a peak around 5 mg/g (3.5 mg/L) at the beginning of the flocculation ( $t < 200$  s), see figures 4.6 and 4.7. From our definition, the optimal dose is for 3.5 mg/L (5 mg of flocculant per g of clay). For concentrations below the optimal dose the change in  $D_{50max}$  increases with increasing flocculant concentration and the time to reach  $D_{50max}$  decreases with increasing flocculant concentration. This is expected: at these concentrations aggregation is limited by the amount of flocculant available. The repulsion between particles decreases with the addition of flocculant, leading to the formation of large open flocs. These large flocs are more erodible or can re-conform better as their size is larger than the flocs formed by lower flocculant concentration as discussed in [Lekkerkerker and Tuinier, 2011]. For concentrations above the optimal dose, the time to reach  $D_{50max}$  increases

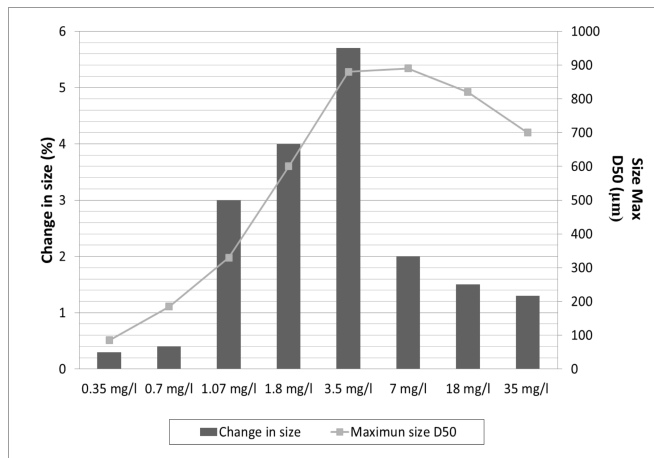


**Figure 4.5** – Bars: Change in floc size in percentage according to eq. 4.4.1 during the particle size distribution experiments. The line with symbols represents the maximum  $D_{50}$  obtained for each flocculant dose. The optimum dose for 3.5 mg/L corresponds to 5 mg/g cationic flocculant (Zetag 7587)/clay.

with increasing flocculant concentration as can be seen in figure 4.6, and the flocculation times are larger. Above the optimal flocculant dose there is a substantial amount of flocculant in suspension which is not bound to the clay. The individual particles are probably first coated by large amounts of flocculant and the creation of flocs is then prevented by electrostatic repulsion between the polyelectrolyte tails of these coated particles and the electrostatic repulsion of the loose polyelectrolyte in solution. Above the optimal dose, the change in particle size decreases with increasing flocculant concentration by more than half between 3.5 mg/L (the optimal dose) and 7 mg/L. Above the optimal dose, the flocs reach  $D_{50max}$  similar to the  $D_{50max}$  at optimal dose. This is most probably due to the fact that the flocs above optimal dose are fully saturated by polyelectrolytes that are not erodible or/and cannot re-conform easily due the strong steric repulsion between their tails. These flocs also have a more open structure than the flocs obtained at lower dose as discussed in 5.

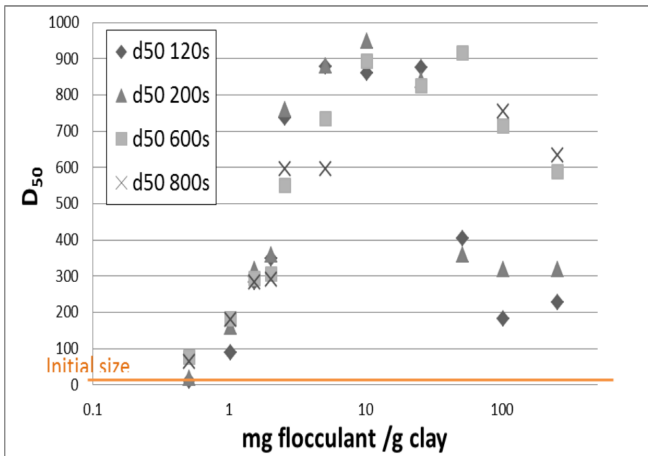
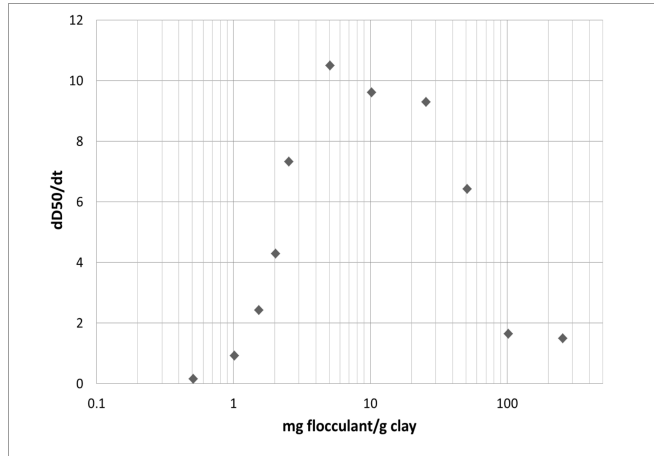


Figure 4.6 – Evolution of  $D_{50}$  as function of mg cationic flocculant Zetag 7587 per g clay.



**Figure 4.7** –  $dD_{50}/dt$  as function of mg cationic flocculant zetag 7587 per g clay. The slope is calculated for  $t < 120$  s.

#### 4.4.2 Anionic flocculant (Zetag 4110)

In figures 4.8, 4.9 and 4.10 we show three examples of the time evolution of the Particle Size Distribution of clay in presence of the anionic flocculant below, at and above the optimal dose. For a concentration of 0.18 mg/L we are close to the optimal dose, through this is difficult to determine with this flocculant, as can be seen in figure 4.11: the error is large when estimating the slope  $dD_{50}/dt$ . From figures 4.12 and 4.13 it is not easy to identify the optimal dose. We can only give a range for this optimal dose: between 0.1 mg/g (0.035 mg/L) and 0.25 mg/g (0.18 mg/L). In this case the optimal dose is not only based on the  $dD_{50}/dt$ , but we also took into account the fact that the largest flocs are obtained for these concentrations. The largest  $D_{50}$  is less than 20  $\mu\text{m}$  for all the experiments for experimental times less than 800 s. We did not observe changes in particles size (as with cationic) at these low particle sizes as the  $D_{50}$  is only increasing in time (figure 4.11). We note that during flocculation the amount of small particles ( $< 10 \mu\text{m}$ ) is still substantial, indicating that these particles are not taken up in the flocs of larger size.

This is reflected in the turbidity of the suspension: with anionic flocculant, the suspension was never as clear as with cationic flocculant. Some samples were left overnight, stirred in the jar, and re-measured the next morning. The distribution then obtained is given in figure 4.8. Some particles have grown up to 1 mm, but 55% (in volume) is still below 200  $\mu\text{m}$ . The fact that some particles become so large overnight is due to the fact that the sample was only stirred, and hence the particles growth was not limited by continuous pumping through the system.

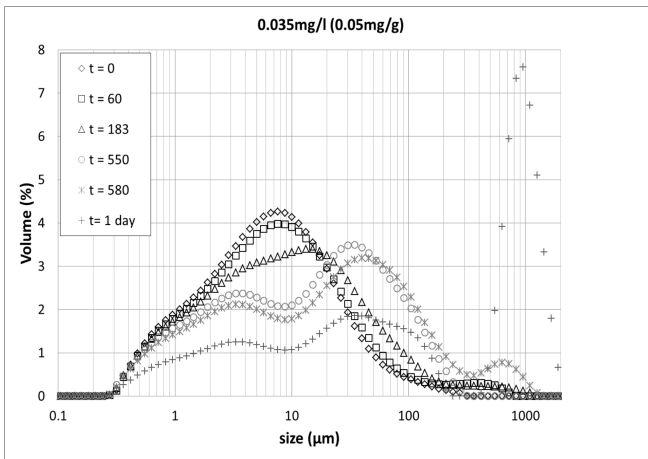


**Figure 4.8** – The evolution of particle size distribution during three flocculation experiments, with anionic flocculant concentrations of 0.035 mg/L. The flocculation is slower than with cationic polyelectrolytes and not all particles flocculate. ( $G$  in the jar is  $50 \text{ s}^{-1}$ )

Though the surface charge of the polyelectrolytes is negative, the flocculant can still bind to the clay. Mpofu *et al.* [Mpofu et al., 2003, Mpofu et al., 2004] explain this behavior by the hydrogen bonding between the silanol and aluminol at their smectite clay particles surface and the amide groups of the polymer. We note that the aggregation between flocculant and clay is in principle strongly weakened due to the electrostatic repulsion between the polyelectrolyte and the negatively charged clay. Several authors [Goodwin, 2009, Sworska et al., 2000a, Sworska et al.,

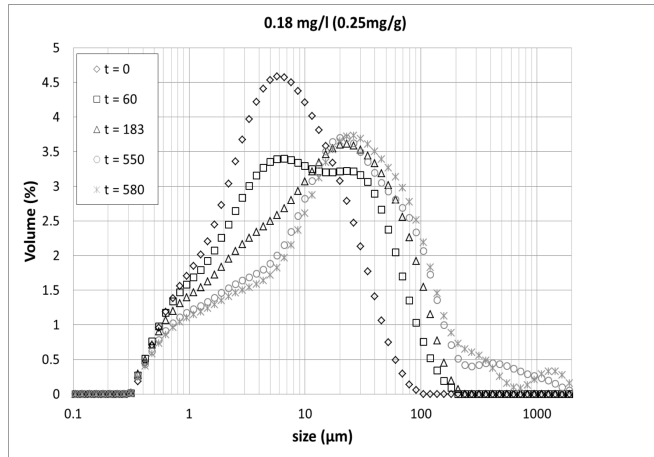


**Figure 4.9** – The evolution of particle size distribution during three flocculation experiments, with anionic flocculant concentrations of 0.18 mg/L. The flocculation is slower than with cationic polyelectrolytes and not all particles flocculate. ( $G$  in the jar is  $50 \text{ s}^{-1}$ )

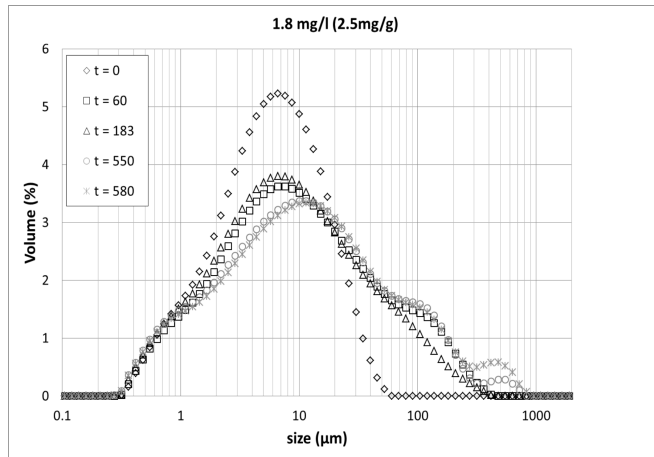


**Figure 4.10** – The evolution of particle size distribution during three flocculation experiments, with anionic flocculant concentrations of 1.8 mg/L. The flocculation is slower than with cationic polyelectrolytes and not all particles flocculate. ( $G$  in the jar is  $50 \text{ s}^{-1}$ )



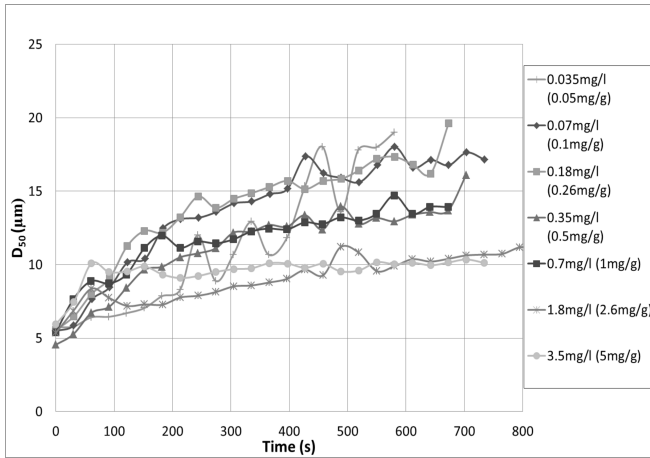


**Figure 4.11** – Evolution of  $D_{50}$  in time. The clay concentration is 0.7 g/L and the different concentrations of anionic flocculant Zetag 4110 are indicated in the figure.

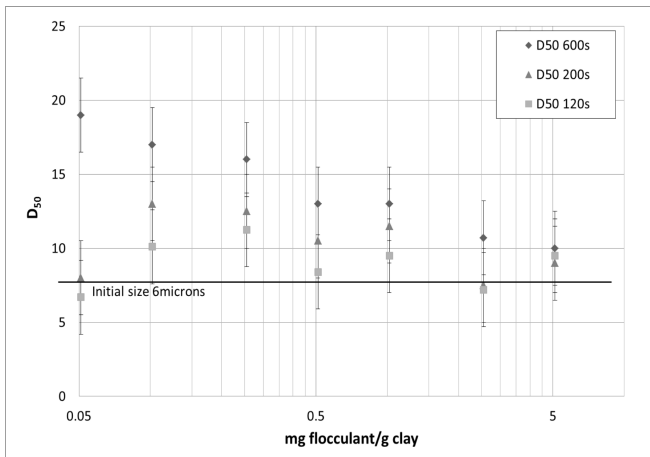


**Figure 4.12** – Evolution of  $D_{50}$  as function of added mg Zetag 4110 flocculant per g clay. The clay concentration is 0.7 g/L.

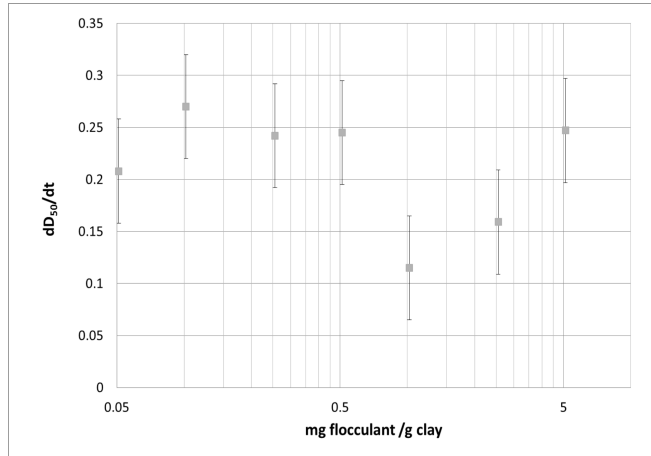


**Figure 4.13** –  $dD_{50}/dt$  as function of mg Zetag 4110 flocculant per g clay. The clay concentration is 0.7 g/l.

2000b, Lee et al., 2012] have therefore suggested a "cationic bridging" mechanism to explain how the negative clay binds to the negative polyelectrolyte. According to this hypothesis, divalent cations would link the negatively charged clay to the negatively charged polymer. Note that, at the same time, in the presence of salt, the Coulombic repulsions between particles and flocculant would reduce dramatically as compared to a (nearly) salt-free situation, favoring van der Waals attraction. We have verified that the presence of divalent cations indeed changes the flocculation behavior. When, as in the experiments of Lee *et al.* [Lee et al., 2012], divalent salt is added to the clay suspension and then flocculant is added, flocculation is improved. The supernatant becomes extremely clear in a situation where it would remain turbid with tap water or demi-water.

From the experiments, as reflected in the figures, increasing flocculant concentration beyond the optimal dose does not promote flocculation. Small amounts of salt ions in the water at small amounts of flocculant seem to favor the flocculation. This probably occurs until doses at which all cation links that could be formed are formed and the

remaining flocculant stays in suspension. The electrostatic (steric) repulsion between the negatively charged clay and the negatively charged flocculant then prevents the binding between clay and flocculant.

## 4.5 The reversibility of growth and break-up of flocs under applied shear stress.

The strength of the flocs was studied as function of the shear rate generated in the tubes. The size of the flocs, expressed as  $D_{50}$ , was analyzed as function of this shear rate. To characterize the flow regime in the tube, the Reynolds number was estimated for all the discharges used during the experiment. The Reynolds number in a tube (or pipe) is equal to:

$$Re = \frac{\rho u d_h}{\mu} \quad (4.5.1)$$

where  $\rho$  is density,  $u$  is velocity,  $d_h$  is hydraulic diameter (diameter of the pipe) and  $\mu$  dynamic viscosity. The Reynolds number is larger than 2000 (turbulent regime) for discharges higher than 7.34 mL/s. The clay concentration was always 0.7 g/L and two different flocculant concentrations were studied for each flocculant. We did two types of experiments. First we started with a low shear rate  $150 \text{ s}^{-1}$  (1.92 mL/s) and increased it stepwise up to  $1200 \text{ s}^{-1}$  (15 mL/s). Then we decreased stepwise the shear rate until  $150 \text{ s}^{-1}$  (1.92 mL/s). The pump speed from the set-up was changed to the next discharge when  $D_{50}$  reached equilibrium (we define equilibrium at time in which  $D_{50}$  does not vary any more). This residence time is approximately 30 minutes for all measurements. The arrows in the figures indicate the direction of the steps. The size of the flocs was compared with the Kolmogorov length scale. The shear rates analyzed are extremely large to compare with shears in natural systems. However these results can be used for industrial purposes.

### 4.5.1 Cationic flocculant (Zetag 7587)

Figure 4.14 shows the floc size evolution as function of shear rate for two different concentrations, i.e. 0.71 mg/L under optimal flocculant

dose and 7.14 mg/L above optimal flocculant dose for cationic flocculant. For 0.71 mg/L flocculant concentration, the size of the flocs under turbulent flow conditions is a factor 3 smaller than the Kolmogorov length. For 7.14 mg/L flocculant concentration the size of flocs is much larger (10 times at low shear) than the Kolmogorov length. This is because polymers-induced flocs produce stronger flocs than salt-induced flocs [Gregory, 1988]. Salt-induced flocs have a size which scales with the Kolmogorov length [Mietta et al., 2009]. All size flocs scale with Kolmogorov length.

The reversibility of the growth/break-up processes was studied in this section as function of shear rate. When the pump speed is increased, the size of flocs decreases due to the increased shear stresses. When the pump speed decreases to the first discharge value, the equilibrium flocs size reached is always lower than the ones found at the beginning of the experiment. This experiment demonstrates that flocculation is irreversible upon increasing/decreasing shear stress in our experiments. This irreversibility can be due to break of the polymers under the high shears. Quite some literature is available on shear stress dependence of floc sizes (see for instance [Jarvis et al., 2005, Barany et al., 2009, Barany et al., 2010, Barany et al., 2011] for a review) however it is very difficult to make a comparison between studies, as for instance impeller type, sample volume, shear rates and shear times are often different and sometimes unknown.

Yoon *et al.* [Yoon and Deng, 2004] performed jar test experiments with an unspecified clay (from Dry Branch) in the presence of cationic polyacrylamide and found irreversible floc breakage after the shear level was adjusted by changing the impeller speed between 300 and 900 rpm every 60 s. The total test duration was 12 minutes. They used a 500 mL beaker containing 300 mL of 0.2% clay suspension. The suspension was stirred by using a four-blade propeller stirrer. The clay suspension was stirred for 30 s at 300 rpm before initiating the test. They do not give any conversion for their rpm into shear rates, but their highest rpm would roughly correspond to  $500 \text{ s}^{-1}$  if we use a standard conversion formula [Nagata, 1975]. Yukselen *et al.* [Yukselen et al., 2006] studied the reversibility of floc breakage with kaolin samples flocculated with

anionic and cationic flocculant in London tap water. The kaolin was dispersed in London tap water with small amounts of humic acid to prevent the coagulation of kaolin by the divalent calcium cations  $Ca^{2+}$  present in the London tap water. The maximum shear rate used in their experiments was  $520\text{ s}^{-1}$ . They used 800 mL of suspension in 1 L jar, with an impeller different from ours. Another difference between their experiments and ours is that they change the shear rate in the jar test and we did it in the tube (changing the pump speed). Contrary to what we find, they found that flocs grow with cationic flocculant at low shear, then, exposed to their high shear and again at low shear, do almost regrow to their full original size. The main difference between their experiments and ours is that we allow the floc sizes to reach equilibrium (30 minutes) before changing the shear. They only keep the highest shear during maximum 300 seconds, before decreasing it. After 5 minutes the mean floc size in our experiment would similarly not be too different.

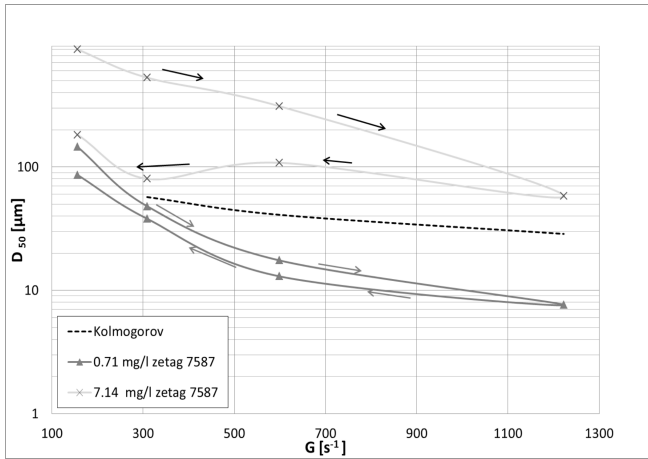


**Figure 4.14** – The growth and break-up of flocs processes for cationic flocculant (Zetag 7587). Variation of flocs  $D_{50}$  as function of shear rate. The value of  $D_{50}$  is the steady-state flocs size reached after 30 minutes under the shear applied. The arrows indicate the order of increase and decrease of shear rates.

### 4.5.2 Anionic flocculant (Zetag 4110)

Figure 4.15 shows the floc size as function of shear rate for two different concentrations 0.35 mg/L and 0.71 mg/L of anionic flocculant, both above optimal dose. For 0.35 mg/L flocculant concentration, the size of the flocs under turbulent flow condition follows the Kolmogorov micro-scale as it did with ion-induced flocculation [Mietta et al., 2009]. The floc size evolution is reversible upon pump speed increase or decrease for 0.35 mg/L flocculant concentration. For 0.71 mg/L flocculant concentration the size of flocs is somewhat larger than the Kolmogorov length under the same turbulent flow conditions. As for cationic polymers we expect that the flocs thus obtained are stronger and bigger than flocs obtained by salt-induced flocculation. When the pump speed is decreased, the flocs size follows roughly the Kolmogorov micro-scale until the shear rate reaches  $500 \text{ s}^{-1}$ . As for cationic flocs, the ratio between the smallest floc size (at highest shear) and largest floc size (at lowest shear) is of the order of 1 : 8. However, the anionic flocs re-grow to nearly their original (low-shear) sizes. This could be due to the fact that the anionic flocculant produces stronger flocs than the cationic flocculant flocs, because the flocculant itself may be stronger. As flocs are assumed to be fractal in structure [Kranenburg, 1994] smaller flocs like the anionic ones, are able to support larger strength, therefore they are stronger (or re-conform less) than the cationic ones upon increasing shear. Another explanation is that the anionic flocs may be weaker than the cationic ones owing to the cationic links between clay and polyanion, but regrow easily to their original size upon decreasing shear. It is possible that by shearing, the link between the particles and anionic flocculant will be severed at the position of the cation (which does not bind strongly to either clay or flocculant), and the flocculant will simply detach from the cation without damage, and be able to re-attach upon decreasing shear.

In favor of this second hypothesis, it was observed that salt-induced flocs are weak (they follow the Kolmogorov microscale) and are able to regrow to their full original size upon decreasing the shear rate [Mietta, 2010]. Some authors found similar results, using kaolin clay in tap water with anionic flocculant, with a different set-up though [Yukselen et al., 2006, Owen et al., 2008, Zhu et al., 2009]. Yukselen *et al.* [Yukselen

et al., 2006] used kaolin clay and anionic polyacramide in their experiments (their set-up was discussed in the previous section), keeping the highest shear rate for the breakage of flocs only during 10 s, they observed near reversibility of floc size upon shear. Even with these short break-up times, the recovery factor (= a measure for the regrowth of particles to their original sizes) for anionic flocs was in their case higher (93%) than the one obtained for cationic (87%). Similar to what we have found in our experiments, where the recovery factor for anionic flocs is much larger than for cationic flocs.

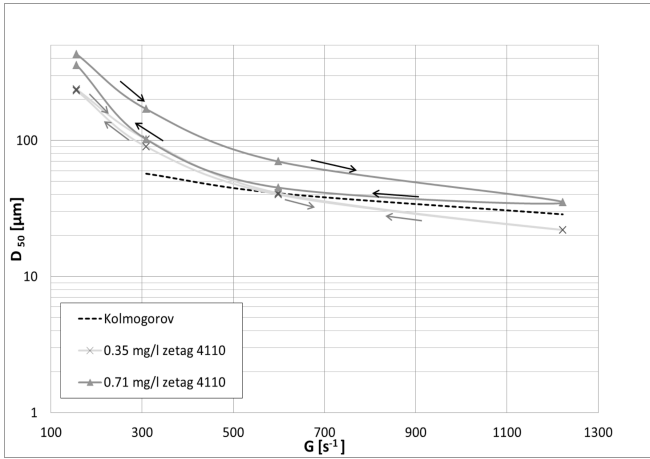


**Figure 4.15** – The growth and break-up of flocs for anionic flocculant (Zetag 4110). Variation of flocs  $D_{50}$  as function of shear rate. The value of  $D_{50}$  is the flocs size after 30 minutes under the shear applied when steady-state is reached. The arrows indicate the order of increase and decrease of shear rates.

The dependence of the floc size upon shear rate is often given in terms of the empirical relation [Jarvis et al., 2005]:

$$d = C \times G^{-\gamma} \tag{4.5.2}$$

where  $d$  is the floc diameter,  $C$  and  $\gamma$  are empirical parameters to be determined from fitting the data. Usually the exponent  $\gamma$  is found to be

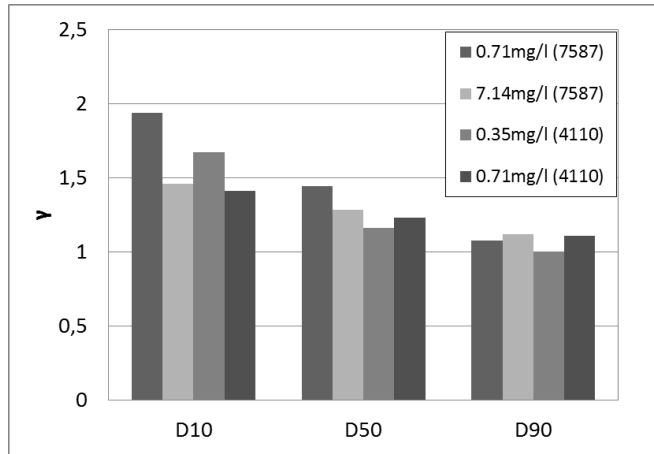


**Figure 4.16** – Values of  $\gamma$  for  $D_{10}$ ,  $D_{50}$  and  $D_{90}$  of 0.71 mg/L zetag 7587, 7.14 mg/L zetag 7587, 0.35 mg/L zetag 4110 and 0.71 mg/L zetag 4110.

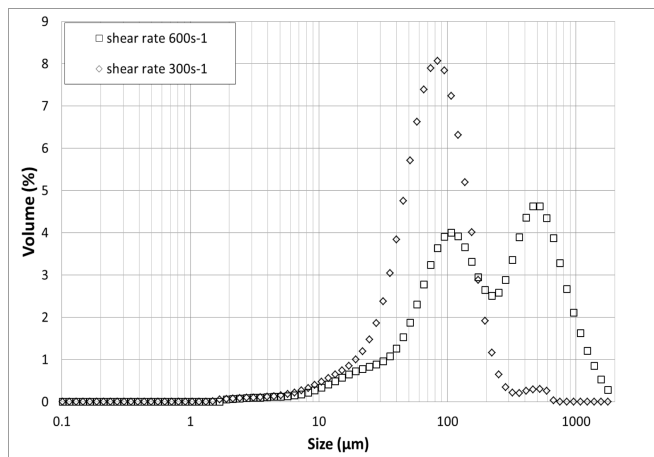


**Figure 4.17** – Particle size distribution at steady-state for  $G = 600 \text{ s}^{-1}$  ( $t = 9000 \text{ s}$ ) and  $300 \text{ s}^{-1}$  ( $t = 3000 \text{ s}$ ) during the re-grow phase.



close to 0.5, which is to be related to the Kolmogorov microscale  $L$ , i.e.

$$L = (\nu/G)^{-1/2} \quad (4.5.3)$$

where  $\nu$  is the kinematic viscosity. The Kolmogorov microscale therefore would appear to be good measure for the characteristic size of flocs. This is true for salt-induced flocs [Jarvis et al., 2005, Bouyer et al., 2005, Mietta et al., 2009]. For flocs produced in the presence of polyelectrolytes we could not find any data to compare our results with. It is however generally found that polyelectrolyte-induced flocs are stronger than salt-induced flocs [Gregory and Barany, 2011] and therefore their size is larger than the Kolmogorov microscale. For low shear the sizes are between 3 and 5 times larger than Kolmogorov microscale. Bubakova *et al.* [Bubakova et al., 2013] studied the shear rate dependency, at steady state, of aggregates from a water reservoir. They addressed the influence of the mixing tank type (Taylor-Couette or pilot plant) on the average and maximum diameter of their aggregates as function of a shear rate between 50 and 350 s<sup>-1</sup>. They fitted their results with the following relation:

$$d = B/(1 + kG^\gamma) \quad (4.5.4)$$

where  $B$ ,  $k$  and  $\gamma$  are empirical parameters to be determined from fitting the data. Note that for high  $G$ , equation (4.5.4) reduces to equation (4.5.2), and  $C = B/k$ . Following the debate in the literature [Jarvis et al., 2005] about whether the maximum or the average aggregate size should be used in the equation, they tested both. They found that for the average size  $\gamma = 1.351$  (Taylor-Couette) and  $\gamma = 1.61$  (pilot plant) and for the maximum size  $\gamma = 1.585$  (Taylor-Couette) and  $\gamma = 1.808$  (pilot plant). We have fitted our data (curves from low shear to high shear rates) according to equation (4.5.2) and the results are presented in figure 4.16. Like Bubakova *et al.* [Bubakova et al., 2013] we obtain values for  $\gamma$  between 1 and 2, even though in our case  $\gamma$  decreases with particle size.

We also investigated the dependence of  $\gamma$  as function of time. We found that when equilibrium (steady-state) was not reached equation (4.5.2) or equation (4.5.4) could in most cases not be applied (figures 4.2, 4.3, 4.8, 4.9 and 4.10), as the particle size distribution is then

bimodal. The average aggregate size has then no proper meaning. The same problem arises when the shear rate is decreased, see in particular figure 4.14: during the "regrow" phase between 600 and 300  $\text{s}^{-1}$ ,  $D_{50}$  decreases upon decreasing shear rate, whereas the opposite would be expected. The reason for this behavior can be understood from the Particle Size Distribution at equilibrium, given in figure 4.17. The equilibrium (steady-state) was reached for both shear rates. In the case of 600  $\text{s}^{-1}$ , the distribution shown in the figure was taken 9000 s after the change of shear rate, and this distribution was already observed at 2000 s. Clearly, the equilibrium distribution is bimodal, since two peaks can be observed in the figure. Therefore the corresponding  $D_{50}$  is unfit to be compared to monomodal  $D_{50}$ 's. Because of the complexity of the influence of aggregation and break-up on the dependence of the size upon shear rate, it is very difficult to comment on the values found for  $\gamma$  for each particle size ( $D_{10}$ ,  $D_{50}$  and  $D_{90}$ ). But we can confirm that smaller particles are more sensitive to shear ( $G$ ) than larger particles. It seems logic because one large particle is formed by more smaller particles.

## 4.6 The electrophoretic mobility.

The interaction between polyelectrolytes and the surface of colloidal particles has been studied extensively [Lafuma et al., 1991, Mpofo et al., 2003, Bonet Avalos et al., 2006, Goodwin, 2009, Gregory and Barany, 2011], both experimentally and theoretically. The configuration of the polyelectrolyte onto a (curved) surface has been shown to depend on the amount of polyelectrolyte adsorbed. Under the maximum particle coverage, the polymer layers can collapse onto the surface under specific conditions. These conditions depend on the ratio of the polyelectrolyte size to the particle size, their charge, the presence of ions, and the reaction time. For low molecular weight polyelectrolyte and large particles, this collapse is more likely to occur, and the aggregation between particles is then due to the attraction between oppositely charged regions of the coated particles ("patching" mechanism). Instead of collapsing onto the particle surface, if the polyelectrolyte has a large molecular weight, it may extend into the solution and be able to bridge two particles to-

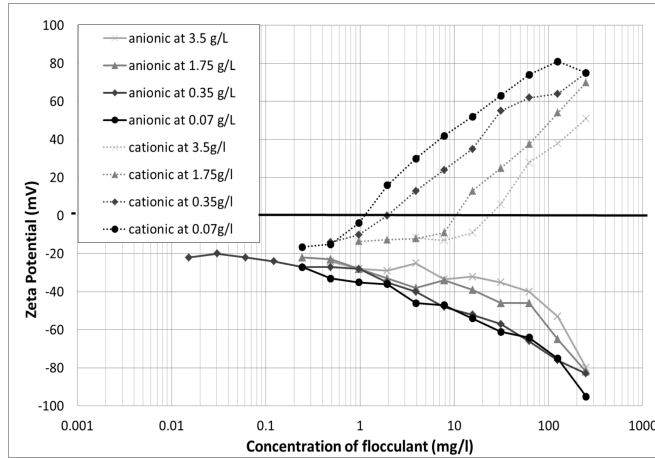
gether ("bridging" mechanism). This also happens in the case where the polyelectrolyte coverage onto the particle is large, as then loops and tails are extending further into the solution.

The simplest relation between zeta potential and flocculation is given in textbooks [Hunter, 2013]: in principle flocculation is optimal when the zeta potential is lowest in absolute value. When the zeta potential is close to zero, the electrokinetic charge is also close to zero and van der Waals interactions will allow aggregation, according to DLVO theory (it is named after Derjaguin, Landau, Verwey, and Overbeek). In the case of polymer-coated particles, two intertwined facts can render the interpretation of the electrophoretic mobility measurements difficult: aggregation can occur because of (Coulombic) attraction between the negative parts of the clay and the positive loops and tails of the polyelectrolyte. The zeta potential of a particle coated with polyelectrolyte should therefore not necessarily be small in order to induce (fast) aggregation. The extension of the polymer layer, coated onto a clay particle, into the solution is able to happen beyond the shear plane (where the zeta potential is defined). Therefore, from electrophoretic mobility measurements no precise information can be gained about this extension of the polymer beyond the shear plane. The electrophoretic mobility (zeta potential) is consequently not necessarily an indicator for flocculation.

The objective of the electrophoretic mobility (zeta potential) study is to find a possible link between the electrokinetic surface charge of coated clay particles and the flocculation behavior described in the previous section. The zeta potential of the clay diluted in demi water was  $-17$  mV at pH 8. Figure 4.18 shows the zeta potential for four different concentrations of clay as function of cationic flocculant (Zetag 7587) and anionic flocculant (Zetag 4110). Explanations over this figure are given below.

#### 4.6.1 Cationic flocculant (Zetag 7587)

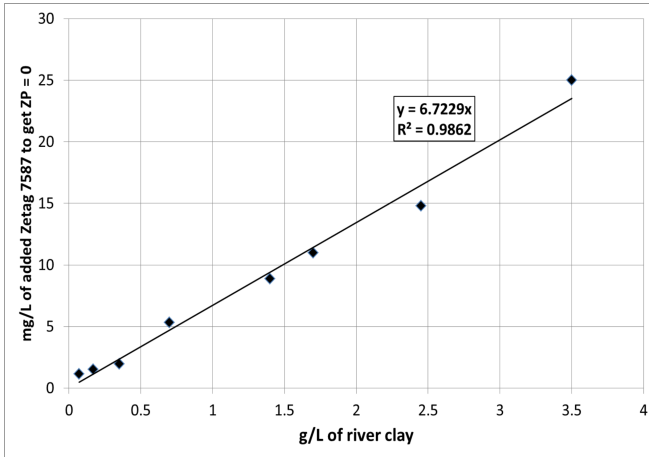
For a given concentration of flocculant, the zeta potential depends on particle concentration as shown in figure 4.18. The binding of flocculant to the clay is therefore limited by the amount of flocculant available for each clay particle. When larger amounts of polymers are added, the



**Figure 4.18** – Zeta Potential of four different concentrations of clay (0.07 g/L; 0.35 g/L; 1.75 g/L; 3.5 g/L) as function of cationic (Zetag 7587) and anionic (Zetag 4110) flocculant concentration.

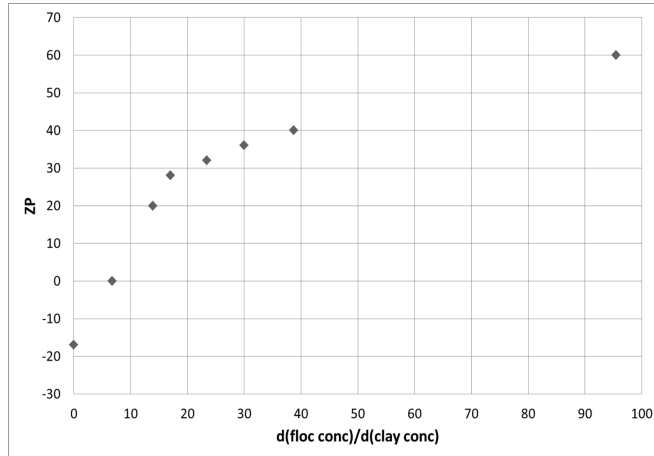
zeta potential for a given clay concentration increases, implying that more flocculant is bound to the clay. The addition of flocculant also increases the viscosity although not enough to make a significant change in the measured mobility. Petzold *et al.* [Petzold et al., 1998, Petzold et al., 2003] also found an electrokinetic charge reversal (change in sign of the zeta potential) with cationic polyelectrolytes. In their study with kaolin clay in the presence of cationic polyelectrolyte, the point of zero zeta potential is reached through addition of cationic flocculant, and when the polyelectrolytes concentration increases the zeta potential increases as well. However their relative optimal flocculant dose is lower than ours, because the cationic flocculant used in their experiment has a higher charge. Petzold *et al.* [Petzold et al., 1998, Petzold et al., 2003] did additional measurements, as they measured the amount of free polycation in the supernatant by polyelectrolyte titration. They found that the supernatant is free of polycation at the point of optimum flocculation, and that the turbidity is then lowest. At that point, they also found that the zeta potential of their "residual particles" (non-

flocculated particles) is close to zero. The concentration of flocculant needed to reach zeta potential equal to zero is plotted as function of clay concentration giving a linear relation, see figure 4.19. This is a good indication that flocculation with cationic flocculant is linked to electrokinetic charge neutralization. Figure 4.19 is in agreement with the results of the flocculation experiments given in the previous section: for 0.7 g/L of clay a zero zeta potential value is expected for 4.7 mg/L of flocculant concentration. This value is very close to the found optimal dose value (3.5 mg/L) from the flocculation experiments.



**Figure 4.19** – Flocculant concentration for which the zeta potential equals zero as function of clay concentration.





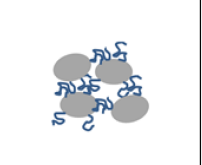
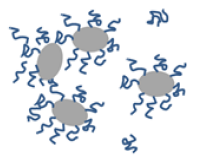
Figure 4.20 shows the relation between the variation in cationic flocculant concentration and clay concentration as function of the zeta potential. Each zeta potential in figure 4.20 is given as function of the slope of the curve representing the flocculant dose as function of clay concentration. This curve is assumed to be a linear function for every zeta potential value. At low flocculant concentrations, for a given clay concentration, the zeta potential increases fast as function of flocculant dose until a value of about 30 mV for 20 mg/g. In this range, flocculation should therefore be fast. This is in line with the flocculation experiments,



**Figure 4.20** – Relation between zeta potential (mV) and the slope (calculated from data shown in figure 4.18) of the cationic flocculant against clay concentration function.

where a fast increases in  $D_{50}$  is observed around the optimum flocculant dose. For zeta potential values larger than 30 mV, the slope of the relation is smaller. This may indicate that the adsorption of flocculant onto a particle is slower. This is in agreement with the results of Petzold *et al.* [Petzold et al., 1998], who found the same change in slope in their linear relation between the amount of polycation adsorbed (measured by titration) and the amount of polycation added. In our case, we presume that adsorption still occurs at the same rate, but the velocity of the particles decrease. In line with this second possibility, Ohshima [Ohshima, 1997] has demonstrated that polyelectrolyte-coated particles have their electrophoretic mobility reduced at a polymer layer to particle size ratio above 1 : 10. At high flocculant concentrations, flocculation is observed to be slower, probably because the particles are first coated by large amounts of flocculant and the creation of flocs is prevented by electrostatic repulsion between the polyelectrolyte tails of these coated particles. A sketch of the flocculant adsorption on the particles is given in figure 4.21. Figure 4.21 represents in the upper row the situation

during which electrophoretic mobility measurements have been done for clay particles as function of cationic flocculant concentration. The left column represents flocculant under dose thus zeta potential values between  $-17\text{mV}$  and  $-10\text{mV}$ . Optimal dose where zeta potential is between  $-10\text{mV}$  and  $10\text{mV}$  is the middle range and flocculant over dose where zeta potential is between  $10\text{mV}$  and  $80\text{mV}$  is given in the right column. The flocculation experiments are shown in the lower row. At low amount of flocculant (left column) small flocs are formed almost immediately due to attraction between flocculant and clay particles. Larger amount of flocculant induces more particles aggregation (middle column). When there is an overdose of flocculant. Flocs cannot grow more, both flocs and clay particles are completely covered by the cationic flocculant and steric repulsion plays a large role.

0 mg/L < flocculant concentration < 1 mg/L (under dose)	1 mg/L < flocculant concentration < 20 mg/L (optimal dose)	20 mg/L < flocculant concentration < 200 mg/L (over dose)
Electrophoretic mobility measurements: low clay concentration, no applied shear (no aggregation)		
		
$-17\text{mV} < \text{Zeta Potential} < -10\text{mV}$	$-10\text{mV} < \text{Zeta Potential} < 10\text{mV}$	$10\text{mV} < \text{Zeta Potential} < 80\text{mV}$
Flocculation experiments: low clay concentration with applied shear (aggregation)		
		

**Figure 4.21** – Sketch of cationic flocculant binding to negatively charged clay particles. Note that the flocculant size is completely out of scale compared to the clay particle size.

### 4.6.2 Anionic flocculant (Zetag 4110)

For anionic flocculant, the zeta potential is always negative and increases in absolute value with flocculant concentration for all clay concentration

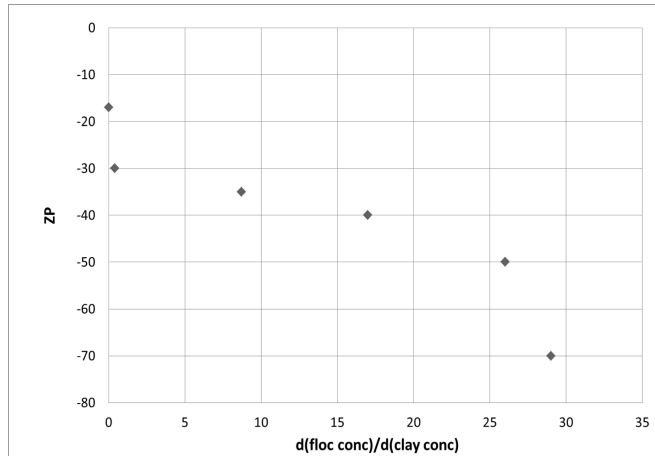


**Figure 4.22** – Relation between zeta potential and variation of anionic flocculant concentration as function of clay concentration.

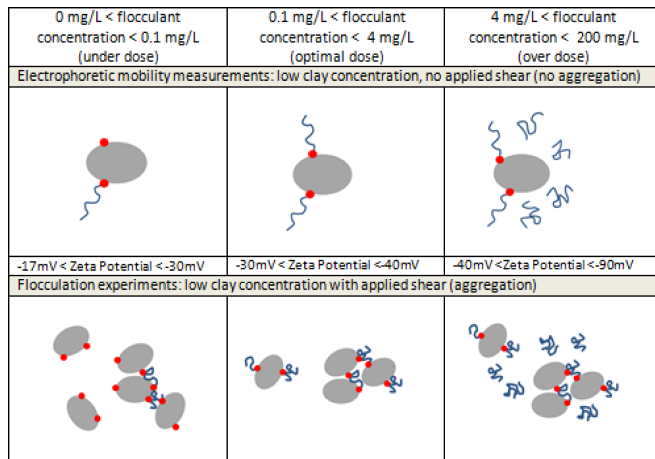


**Figure 4.23** – Sketch of cations (red balls) linking the anionic flocculant (blue) with negatively charged clay particles. Note that the flocculant size is completely out of scale compared to the clay particle size.



as depicted in figure 4.18. The zeta potential in this case, like for the cationic polyelectrolyte, represents the binding of the polyelectrolyte to the clay. The effective charge of the coated particle increases and leads to a higher electrophoretic mobility. In principle Coulombic repulsion forces between particles and polyelectrolytes are predominant when the two are mixed. In a previous section, we have already discussed that the presence of cations in the water will adhere the polyelectrolyte onto clay particles. Although the experiments were done with demi-water, for which the cation concentration is very low, there is always a small amount of cations present. From figure 4.18 it can be observed that the zeta potential depends on particle concentration only when the clay concentration is above 0.35 g/L. Therefore, below 0.35 g/L of clay, full coating of the clay by polyelectrolyte can be achieved due to the presence of the solution cations. Above 0.35 g/L the binding of flocculant to the clay is limited by the amount of cations available for each clay particle. Figure 4.22 shows the relation between the zeta potential and the slope of flocculant as function of clay concentration curves. Three different regions can be distinguished. The first is at extremely low flocculant-clay ratio (1 mg/g). It represents the region where the binding of flocculant to clay and flocculation is optimum, due to cation bridging. A second region is found between 1 mg/g and 25 mg/g, where the electrophoretic mobility (zeta potential) decreases linearly. In the third region (above 25 mg/g), the zeta potential decreases even more strongly. This decrease is difficult to interpret, and does not correspond to the adsorption of polyelectrolyte to clay. At high polyelectrolyte concentrations, it is expected that a lot of polyelectrolyte remains in solution and hereby increases the suspension's viscosity. This would lead to a decrease (in absolute values) of the electrophoretic mobility and not an increase as observed here. Since little polyelectrolyte is adsorbed onto the particles, we observed that for high doses, the suspension was more viscous than a suspension with cationic polyelectrolyte at the same doses, and even started to form a gel. The electrophoretic mobility of particles in gels has been investigated theoretically [Li et al., 2014]. It has been shown that in this case, the gel electroosmotic flow mobility has to be accounted for in the evaluation of the particle's mobility. Depending on the polyelec-

trolyte charge, this can change the value of the electrophoretic mobility substantially, which then is not anymore an indicator for the polyelectrolyte adsorption onto the particle's surface. In figure 4.23 a summary of the adsorption of polyelectrolyte onto clay is given. Figure 4.23 represents in the upper row the situation during which the electrophoretic mobility measurements have been done for clay particles as function of anionic flocculant concentration. The left column represents flocculant under dose thus zeta potential values between -17mV and -30 mV. Optimal dose where zeta potential is between -30 mV and -40 mV is the middle range, and flocculant over dose where zeta potential is between -40 mV and -90 mV is given in the right column. The flocculation experiments are shown in the lower row. At low amount of flocculant (left column) small flocs are formed after mixing a bit the sample. These flocs are formed due to the presence of cations in the system that make the bridge between flocculant and clay particles. Larger amount of flocculant results in a re-conformation of flocs and more particles can attach to the flocculant thanks to the cations in the system. When there is an overdose of flocculant in the system, flocs cannot grow larger, because there are not enough cations to make the bridge between clay particles and flocculant to create more flocs (right column).

## 4.7 Conclusions

This chapter shows how the aggregation processes can be understood by the use of the zeta potential measurements together with flocculation experiments. The optimal flocculant dose for each type of flocculant could be determined either from flocculation experiments or from zeta potential measurements. For the cationic flocculant the optimal dose corresponds to a maximum coverage of a clay particle, as was confirmed by the electrophoretic mobility (zeta potential) study. For the anionic flocculant, the optimal dose was linked to the cations available in the water, as was shown in the electrophoretic mobility (zeta potential) study. These findings are in line with work of other authors. For concentrations below the optimal dose, the cationic flocs are shown to be erodible or to be able to reform as a function of time for a given shear rate.

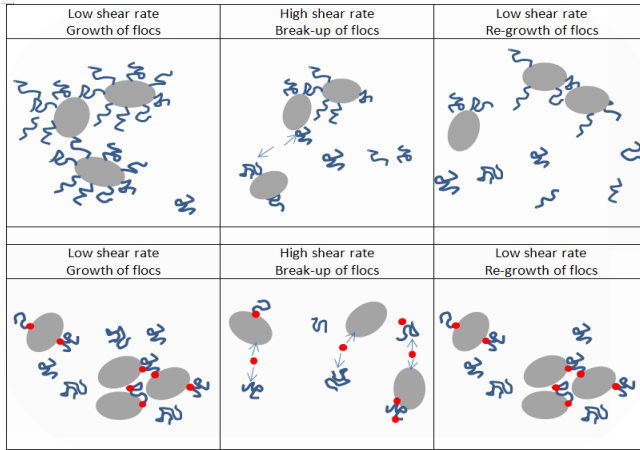


**Figure 4.24** – Sketch of break-up and re-growth of flocs with cationic flocculants (upper panel) and anionic flocculants (lower panel). Note that the flocculant size is not to scale compared to the clay particle size.

Above the optimal dose, the flocs are saturated by the polyelectrolyte, and their size does not vary much in time. It was demonstrated that when the cationic flocs experienced a cycle of low > high > low shear rates they did not regrow to their original low-shear rate value, whereas anionic flocs did. This led us to speculate that in the last case the polyelectrolytes were detached without damage from the clay at the cation anchoring, and that the clay-cation-anionic flocculant bridge could easily be reformed at lower shear. A sketch with the break-up and re-growth of flocs after a cycle of low > high > low shear rates is given in figure 4.24 for cationic and anionic flocculants. The shear rate dependence of the various sizes ( $D_{10}$ ,  $D_{50}$  and  $D_{90}$ ) was mentioned. It was found that, due to the complexity of the flocculation/break-up processes the values found for the coefficient  $\gamma$  given in equation ( 4.5.2) and ( 4.5.4) was difficult to interpret. Far from steady-state, when the particle size distribution is still varying in time, the data cannot be fitted with the simple equation ( 4.4.1) or ( 4.5.3), and Population Balance Equations

(PBE) should be used [Mietta, 2010]. The values of  $\gamma$  at steady-state were found in between 1 and 2, in agreement with other studies.

Besides giving an indication of the flocculant coverage onto a clay particle, the zeta potential study also enabled us to derive a linear relationship between the amount of clay and the amount of cationic flocculant at optimal flocculation. The flocculation results presented in this chapter were done for one clay concentration only (varying the flocculant dose), but the validity of the found relation is studied in chapter 5, where both clay and flocculant concentration are varied.



## References

- [Ackroyd et al., 1986] Ackroyd, D., Bale, A., Howland, R., Knox, S., Millward, G., and Morris, A. (1986). Distributions and behaviour of dissolved cu, zn and mn in the tamar estuary. *Estuarine, Coastal and Shelf Science*, 23(5):621–640.
- [Barany et al., 2010] Barany, S., Kozakova, I., Marcinova, L., and Skvarla, J. (2010). Electrokinetic potential of bentonite and kaolin particles in the presence of polymer mixtures. *Colloid journal*, 72(5):595–601.
- [Barany et al., 2009] Barany, S., Meszaros, R., Kozakova, I., and Skvarla, I. (2009). Kinetics and mechanism of flocculation of bentonite and kaolin suspensions with polyelectrolytes and the strength of floccs. *Colloid journal*, 71(3):285–292.
- [Barany et al., 2011] Barany, S., Meszaros, R., Marcinova, L., and Skvarla, J. (2011). Effect of polyelectrolyte mixtures on the electrokinetic potential and kinetics of flocculation of clay mineral particles. *Colloids and Surfaces A: Physicochemical and Engineering Aspects*, 383(1):48–55.
- [Bergaya and Lagaly, 2013] Bergaya, F. and Lagaly, G. (2013). *Handbook of clay science*, volume 5. Newnes.
- [Bonet Avalos et al., 2006] Bonet Avalos, J., Johner, A., and Diez-Orrite, S. (2006). Analysis of polymer adsorption onto colloidal particles. *The European Physical Journal E: Soft Matter and Biological Physics*, 21(4):305–317.
- [Bouyer et al., 2005] Bouyer, D., Coufort, C., Liné, A., and Do-Quang, Z. (2005). Experimental analysis of floc size distributions in a 1-l

- jar under different hydrodynamics and physicochemical conditions. *Journal of colloid and interface science*, 292(2):413–428.
- [Bubakova et al., 2013] Bubakova, P., Pivokonsky, M., and Filip, P. (2013). Effect of shear rate on aggregate size and structure in the process of aggregation and at steady state. *Powder Technology*, 235:540–549.
- [Goodwin, 2009] Goodwin, J. (2009). *Colloids and interfaces with surfactants and polymers*. John Wiley & Sons.
- [Gregory, 1973] Gregory, J. (1973). Rates of flocculation of latex particles by cationic polymers. *Journal of Colloid and Interface Science*, 42(2):448–456.
- [Gregory, 1988] Gregory, J. (1988). Polymer adsorption and flocculation in sheared suspensions. *Colloids and Surfaces*, 31:231–253.
- [Gregory and Barany, 2011] Gregory, J. and Barany, S. (2011). Adsorption and flocculation by polymers and polymer mixtures. *Advances in colloid and interface science*, 169(1):1–12.
- [Hunter, 1993] Hunter, R. J. (1993). Introduction to modern colloid science.
- [Hunter, 2001] Hunter, R. J. (2001). Foundations of colloid science.
- [Hunter, 2013] Hunter, R. J. (2013). *Zeta potential in colloid science: principles and applications*. Academic press.
- [Jarvis et al., 2005] Jarvis, P., Jefferson, B., and Parsons, S. A. (2005). Breakage, regrowth, and fractal nature of natural organic matter flocs. *Environmental science & technology*, 39(7):2307–2314.
- [Kranck and Milligan, 1992] Kranck, K. and Milligan, T. (1992). Characteristics of suspended particles at an 11-hour anchor station in san francisco bay, california. *Journal of Geophysical Research: Oceans (1978–2012)*, 97(C7):11373–11382.

- [Kranenburg, 1994] Kranenburg, C. (1994). The fractal structure of cohesive sediment aggregates. *Estuarine, Coastal and Shelf Science*, 39(5):451–460.
- [Lafuma et al., 1991] Lafuma, F., Wong, K., and Cabane, B. (1991). Bridging of colloidal particles through adsorbed polymers. *Journal of colloid and interface science*, 143(1):9–21.
- [Lee et al., 2012] Lee, B. J., Schlautman, M. A., Toorman, E., and Fetweis, M. (2012). Competition between kaolinite flocculation and stabilization in divalent cation solutions dosed with anionic polyacrylamides. *Water research*, 46(17):5696–5706.
- [Lekkerkerker and Tuinier, 2011] Lekkerkerker, H. N. and Tuinier, R. (2011). *Colloids and the depletion interaction*, volume 833. Springer Science& Business Media.
- [Li et al., 2014] Li, F., Allison, S. A., and Hill, R. J. (2014). Nanoparticle gel electrophoresis: Soft spheres in polyelectrolyte hydrogels under the debye–hückel approximation. *Journal of colloid and interface science*, 423:129–142.
- [Liss et al., 2004] Liss, S. N., Droppo, I. G., Leppard, G. G., and Milligan, T. G. (2004). *Flocculation in natural and engineered environmental systems*. CRC Press.
- [Liss et al., 2005] Liss, S. N., Milligan, T. G., Droppo, I. G., and Leppard, G. G. (2005). Methods for analyzing floc properties. *Flocculation in natural and engineered environmental systems*, pages 1–21.
- [Malvern, 2015] Malvern (2015). Malvern website. <http://www.malvern.com>. Accessed: 2015-04-30.
- [Manning et al., 2011] Manning, A., Spearman, J., Baugh, J., Whitehouse, R., and Soulsby, R. (2011). *Cohesive sediment flocculation and the application to settling flux modelling*. INTECH Open Access Publisher.



- [McLaughlin and Bartholomew, 2007] McLaughlin, R. A. and Bartholomew, N. (2007). Soil factors influencing suspended sediment flocculation by polyacrylamide. *Soil Science Society of America Journal*, 71(2):537–544.
- [Mietta, 2010] Mietta, F. (2010). *Evolution of the floc size distribution of cohesive sediments*. TU Delft, Delft University of Technology.
- [Mietta et al., 2009] Mietta, F., Chassagne, C., and Winterwerp, J. (2009). Shear-induced flocculation of a suspension of kaolinite as function of pH and salt concentration. *Journal of colloid and interface science*, 336(1):134–141.
- [Mortimer, 1991] Mortimer, D. A. (1991). Synthetic polyelectrolytes—a review. *Polymer International*, 25(1):29–41.
- [Mpfung et al., 2003] Mpfung, P., Addai-Mensah, J., and Ralston, J. (2003). Investigation of the effect of polymer structure type on flocculation, rheology and dewatering behaviour of kaolinite dispersions. *International Journal of Mineral Processing*, 71(1):247–268.
- [Mpfung et al., 2004] Mpfung, P., Addai-Mensah, J., and Ralston, J. (2004). Flocculation and dewatering behaviour of smectite dispersions: effect of polymer structure type. *Minerals Engineering*, 17(3):411–423.
- [Nagata, 1975] Nagata, S. (1975). *Mixing: principles and applications*. Halsted Press.
- [Narkis et al., 1991] Narkis, N., Ghattas, B., Rebhun, M., and Rubin, A. (1991). Mechanism of flocculation with aluminium salts in combination with polymeric flocculants as flocculant aids. *Water supply*, 9(1):37–44.
- [Ohshima, 1997] Ohshima, H. (1997). Electrophoretic mobility of a polyelectrolyte-adsorbed particle: effect of segment density distribution. *Journal of colloid and interface science*, 185(1):269–273.

- [Owen et al., 2008] Owen, A., Fawell, P., Swift, J., Labbett, D., Benn, F., and Farrow, J. (2008). Using turbulent pipe flow to study the factors affecting polymer-bridging flocculation of mineral systems. *International Journal of Mineral Processing*, 87(3):90–99.
- [Petzold et al., 2003] Petzold, G., Mende, M., Lunkwitz, K., Schwarz, S., and Buchhammer, H.-M. (2003). Higher efficiency in the flocculation of clay suspensions by using combinations of oppositely charged polyelectrolytes. *Colloids and Surfaces A: Physicochemical and Engineering Aspects*, 218(1):47–57.
- [Petzold et al., 1998] Petzold, G., Nebel, A., Buchhammer, H.-M., and Lunkwitz, K. (1998). Preparation and characterization of different polyelectrolyte complexes and their application as flocculants. *Colloid and Polymer Science*, 276(2):125–130.
- [Sojka et al., 2007] Sojka, R., Bjorneberg, D., Entry, J., Lentz, R., and Orts, W. (2007). Polyacrylamide in agriculture and environmental land management. *Advances in Agronomy*, 92:75–162.
- [Sperling, 2005] Sperling, L. H. (2005). *Introduction to physical polymer science*. John Wiley & Sons.
- [Stewart and Thompson, 1997] Stewart, C. and Thompson, J. (1997). Vertical distribution of butyltin residues in sediments of british columbia harbours. *Environmental Technology*, 18(12):1195–1202.
- [Sworska et al., 2000a] Sworska, A., Laskowski, J., and Cymerman, G. (2000a). Flocculation of the syncrude fine tailings: Part i. effect of ph, polymer dosage and mg<sup>2+</sup> and ca<sup>2+</sup> cations. *International journal of mineral processing*, 60(2):143–152.
- [Sworska et al., 2000b] Sworska, A., Laskowski, J., and Cymerman, G. (2000b). Flocculation of the syncrude fine tailings: Part ii. effect of hydrodynamic conditions. *International journal of mineral processing*, 60(2):153–161.

- [Tombacz and Szekeres, 2004] Tombacz, E. and Szekeres, M. (2004). Colloidal behavior of aqueous montmorillonite suspensions: the specific role of pH in the presence of indifferent electrolytes. *Applied Clay Science*, 27(1):75–94.
- [Tombác and Szekeres, 2006] Tombác, E. and Szekeres, M. (2006). Surface charge heterogeneity of kaolinite in aqueous suspension in comparison with montmorillonite. *Applied Clay Science*, 34(1):105–124.
- [Winterwerp and Van Kesteren, 2004] Winterwerp, J. C. and Van Kesteren, W. G. (2004). *Introduction to the physics of cohesive sediment dynamics in the marine environment*. Elsevier.
- [Yoon and Deng, 2004] Yoon, S.-Y. and Deng, Y. (2004). Flocculation and reflocculation of clay suspension by different polymer systems under turbulent conditions. *Journal of colloid and interface science*, 278(1):139–145.
- [Yu and Somasundaran, 1996] Yu, X. and Somasundaran, P. (1996). Role of polymer conformation in interparticle-bridging dominated flocculation. *Journal of Colloid and Interface Science*, 177(2):283–287.
- [Yukselen et al., 2006] Yukselen, M., Gregory, J., and Soyer, E. (2006). Formation and breakage of flocs using dual polymers. *Water Science & Technology*, 53(7):217–223.
- [Zhu et al., 2009] Zhu, Z., Li, T., Lu, J., Wang, D., and Yao, C. (2009). Characterization of kaolin flocs formed by polyacrylamide as flocculation aids. *International Journal of mineral processing*, 91(3):94–99.

## Chapter 5

# Study of flocculated clay settling rates as function of polyelectrolyte charge, concentration and shear history

### Abstract

In this study the settling behavior of commercially available clay with either anionic or cationic polyacrilamide polyelectrolyte (flocculant) is systematically investigated. The optimum flocculant to clay ratio is estimated to be 7 mg/g for the cationic flocculant at low clay concentrations in line with chapter 4 for both demineralised and tap water even though the shear rate and mixing method were different. For higher flocculant doses the ratio was found to increase non-linearly with clay concentration. For the anionic flocculant, a flocculant to clay ratio of 2.2 mg/g was found for all clay concentrations. This optimum value corresponds to the fastest settling rates observed, though not always to the most clear supernatant. However these values are not absolute and

depend on environmental factor governing the systems. For instance in the case of anionic flocculant, the amount of cations available in the system is the limiting factor as cations link the anionic flocculant to the negatively charged clay particles. This leads also to a delayed settling at high flocculant doses in the first 10-15 s of an experiment when most of the bridging between clay and flocculant takes place. Different mixing methods and times have large impact on flocculation efficiency and settling rate for both flocculant types. The width of the settling column is also found to have great influence on the flocculation process and hindered settling is found to be different for each flocculant types.

## 5.1 Introduction

Flocculation is the process whereby colloidal particles aggregate to form flocs of (primary) particles that are (ir)reversibly bound to each other. Depending on the flocculation mechanism, flocs can be irregular in shape, have an open or more compact structure, and be more or less resistant to shear [Fargues and Turchiuli, 2003, Jarvis et al., 2005, Tripathy and De, 2006]. Flocs can be formed by addition of flocculating agents which are classified in general in two categories: inorganic and organic. Organic flocculants are quite common in nature [Tripathy and De, 2006, Tan et al., 2012, Bolto and Gregory, 2007] where synthetic organic flocculants are widely used in industry for solid-liquid separation [Tripathy and De, 2006, Bolto and Gregory, 2007]. Polyacrylamides are the most widely used polyelectrolytes in industry and are used in this study. The choice of the flocculants is determined in the case of clay particles by chemical factors such as the mineral composition of the particles and solution chemistry [Concha Arcil, 2009].

We showed that the efficiency and type of flocculation (bridging or electrostatic patch mechanism) depend on the flocculant structure, molecular weight, charge and dose ( chapter 4). For instance for a system where bridging is the predominant flocculation mechanism, a high polyelectrolyte molecular weight improves the flocculation nearly irrespective of charge. Conversely high charge densities are needed for a system where particles and flocculant have an opposite charge. In that case flocculation can be induced by charge neutralization (patch mechanism) and electrostatic attraction between the polyelectrolyte coated particles [Tripathy and De, 2006, Goodwin, 2009]. The settling rate of the formed flocs and the turbidity of the water after settling are the parameters to determine the solid recovery and the efficiency of flocculation process for each flocculant type [Tripathy and De, 2006, Latif et al., 2005]. In principle, a larger aggregate will result in a higher settling rate, even though the settling strongly depends on the density of the flocs. The settling rate can be strongly influenced by hindered settling in case where the solid concentrations is high [Owen et al., 2008, Sutherland et al., 2014, Winterwerp and Van Kesteren, 2004, Dankers and Winter-

werp, 2007].

In order to get insight into the flocculation process, it is necessary to distinguish between the different parameters influencing either flocculation and/or settling. The rate of flocculation, collision efficiency, mixing time and mixing method are then important parameters to consider. In chapter 4 the relationship between polymer type (different molecular weight and charge density), dose and particle surface charge and flocculation behavior for the same clay as used in the present study was investigated. This usually also coincides with the lowest turbidity in the remaining water [Latif et al., 2005, Narkis et al., 1991], but not always as discussed in this chapter. It was not possible, due to the experimental set-up to investigate the floc formation at shear rates smaller than  $200 \text{ s}^{-1}$  in chapter 4. In the present study, the investigation is extended to smaller shear stresses ( $45\text{-}90 \text{ s}^{-1}$ ).

## 5.2 Materials

### 5.2.1 Clay

The clay used in the experiments is the same river clay used in chapter 2. The clay was always dispersed in demi-water (except one additional analysis in tap water), the obtained suspension having conductivity of  $69\text{-}70 \mu\text{S}/\text{cm}$ . The prepared clay stock solution ( $35 \text{ g}/\text{L}$ ) was prepared by suspending  $48.5 \text{ gram}$  of dry clay in one liter of demineralized water.

### 5.2.2 Flocculant

Flocculants used were anionic and cationic polyacrylamide-based polyelectrolytes. These flocculants are the same as the flocculants used in chapter 4. The specifications of both flocculants are given in chapter 4 in section 4.2.2. The monomers are copolymerized with acrylamide to yield water soluble polymers, and the charged acrylate groups determine the polymer surface charge. Low, medium and high charge densities refer to charge percentages (in mol %) of about 10 % (low), 25 % (medium) and 50-100 % (high). The qualification of low, medium or high molecular weight (MW) corresponds roughly to MW values in the range  $<$

$10^5$ ,  $10^5$ - $10^6$  and  $> 10^6$  [Bolto and Gregory, 2007]. The flocculant stock solutions were prepared in demineralized water and the concentration was 0.5 mg/L.

### 5.2.3 Water

The suspensions made of clay and flocculant at the desired concentrations were prepared with tap water with a conductivity of 0.5 mS/cm. The relevant tap water specifications are listed in table 2.3 in chapter 2.

## 5.3 Methods

### 5.3.1 Settling columns

The experiments were carried out in 250 mL columns with a diameter of 4 cm. The influence of the column volume (particularly the column width) was investigated for the optimum flocculant dose in different columns ranging in volume from 50 to 1000 mL. The diameter and the length of used columns are summarized in table 5.1.

**Table 5.1** – Column sizes and shear rates for the different mixing methods

V [mL]	DIAM [mm]	H [cm]	$G$ [ $s^{-1}$ ] (by hand)	$G$ [ $s^{-1}$ ] (by rod)	$G$ [ $s^{-1}$ ] (in jar)
50	22	18.5	90		
100	25	31	80		
250	33	24.6	70	2.2-3.6	156-387
500	45	25.3	60		
1000	55	36.5	45		

### 5.3.2 Mixing methods and mixing times

Studies were performed to compare the flocculation behavior and the settling rate for three different mixing methods and mixing times. Inversion 10 times by hand, a procedure that is defined in this work as the



standard procedure, was performed as the mixing method which provides the minimum shear. The corresponding shear rate ( $du/dz$ ) was estimated according to Eq. 5.3.1:

$$du/dz = \sqrt{2g\Delta H}/R \quad (5.3.1)$$

Where  $g$  is the gravity acceleration,  $R$  is the radius of the column and  $\Delta H$  is the distance between the liquid/air interface of the suspension and the top of the column.

The rod mixing procedure consists of inserting a plastic rod into the column which is moved up and down slowly. The shear rate corresponding to mixing with a plastic rod was estimated according to Eq. 5.3.2:

$$du/dz = (\Delta H r^2)/(\Delta t(R - r)(R^2 - r^2)) \quad (5.3.2)$$

Where  $r$  is the radius of the rod,  $\Delta H$  is the height of the suspension in the column and  $\Delta t$  is the time needed to push the rod from the suspension surface to the bottom of the column.

Jar stirring and jar stirring with pump procedures have been already described in chapter 4. Jar stirring experiments were performed at  $25 \text{ s}^{-1}$  for about 5 minutes. In some cases the suspension was pumped from the jar and back to the jar with a pump shear rate in the range  $156\text{-}387 \text{ s}^{-1}$ . The values for the shear rates in the jar and the pump and the jar characteristics are similar to the ones used in chapter 4.

### 5.3.3 Standard procedure to determine the optimum flocculant dose

The settling experiments were performed for different clay concentrations, from  $0.8 \text{ g/L}$  up to  $15 \text{ g/L}$ . In this chapter larger concentrations than in chapter 4 are used. The flocculants were added to each clay concentration in different doses ( $\text{mg/L}$ ), to determine the optimum flocculant dose per clay concentration ( $\text{mg/g}$ ). After adding the flocculant to the clay suspension, the settling column was inverted 10 times by hand (standard procedure) figure 5.1. Immediately after the end of inversions, when the column was placed on a table, pictures were taken

every 5 seconds during the whole time of the settling until the consolidation phase was reached. The settling rate was determined by reading the interface versus time (mm/s).

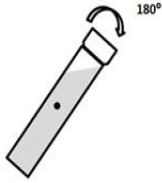


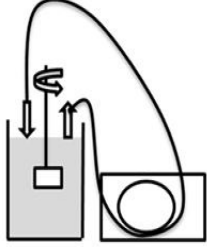
Hand mixing (standard procedure)	Rod mixing	Jar stirring	Jar stirring with pump
			
10 times	(n) inversions	33 rpm ( $25 \text{ s}^{-1}$ ) 5 min	with pump ( $156\text{-}387 \text{ s}^{-1}$ )

Figure 5.1 – Schematic view of the mixing methods

## 5.4 Settling rate

Each flocculant type, the cationic and the anionic, showed different flocculation behavior and produced different floc sizes and different settling rates depending on the mixing methods and flocculant to clay ratio. This is because different mechanisms like charge neutralization and electrostatic patch mechanism or bridging mechanism govern the flocculation in these different cases. The anionic flocculant used in the present study had a high molecular weight. High molecular weight anionic polyelectrolytes are known to be effective for bridging flocculation, the most typical mode of flocculation for anionic polyelectrolyte [Bergaya and Lagaly, 2013, Petzold et al., 2003, Mierczynska-Vasilev et al., 2013]. In contrast, the influence of the molecular weight of cationic polyelectrolyte on the flocculation is very small. In this case a high charge is required to get optimal flocculation. Therefore a highly charged cationic polyelectrolyte was chosen in this study. The adsorption of anionic polyelectrolyte onto

the clay is significantly affected by the ionic strength of the suspension and this in turn affects the flocculation [Tripathy and De, 2006].

### 5.4.1 Cationic flocculant

An example of the settling rate of a cationic flocculant suspension (i.e. a clay suspension flocculated by addition of a cationic flocculant) is shown in figures 5.2 and 5.3. From the initial slope of the interface against time curve the settling rate is estimated. It can be observed that the settling rate increases with increasing flocculants dose until 70 mg/L, where the highest settling rate is reached. The dose 70 mg/L is defined as the optimum flocculant dose, as it has the fastest settling rate. For higher flocculant dosages and overdose of flocculant is reached and the settling is delayed. In figure 5.4 the settling rate for different clay concentration is plotted as function of polyelectrolyte doses. The optimum flocculant dose is between 2.4 and 14.2 mg/g for the clay concentrations used. This wide range is due to lack of mixing and/or collision efficiency between the flocculant molecules and clay particles. Depending on the clay concentrations the optimum flocculant dose however does not always correspond to the lowest turbidity of the supernatant. This fact is verified for all clay concentrations. In figure 5.3, the 8.7 g/L clay suspension interface is plotted as function of flocculant dose. In this case, for flocculant concentrations between 40 mg/L and 70 mg/L the settling rate is fastest, however the supernatant clarity is decreasing from 50 mg/L to larger flocculant concentrations. For doses larger than 80 mg/L the settling rate decreases again indicating that the optimum flocculant dose has been exceeded, or that there is hindered settling. For these flocculant doses, the suspending fluid becomes more viscous and hence the settling rate of the flocs is reduced.

Above the optimum dose it was observed that flocs have a tendency to adhere to the column walls, as can be seen in figure 5.26 displayed in the Conclusion section. This behavior is consistent with our previous study (chapter 4) where it was found that above the optimum flocculant dose the zeta potential of the polyelectrolyte coated particles was largely positive. Positively charged flocs can therefore adhere easily to the negatively charged glass wall of the column. This was also found in the

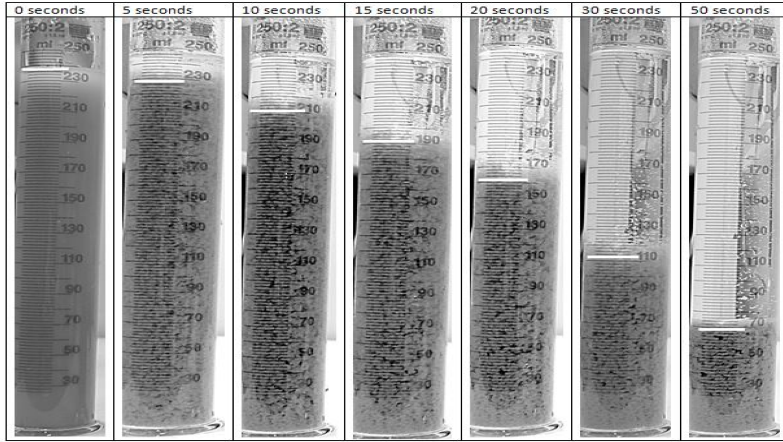


**Figure 5.2** – An example of clay suspension (8.7 g/L) with under-dose cationic flocculant (20 mg/L). The settling phase was completed within 50 seconds

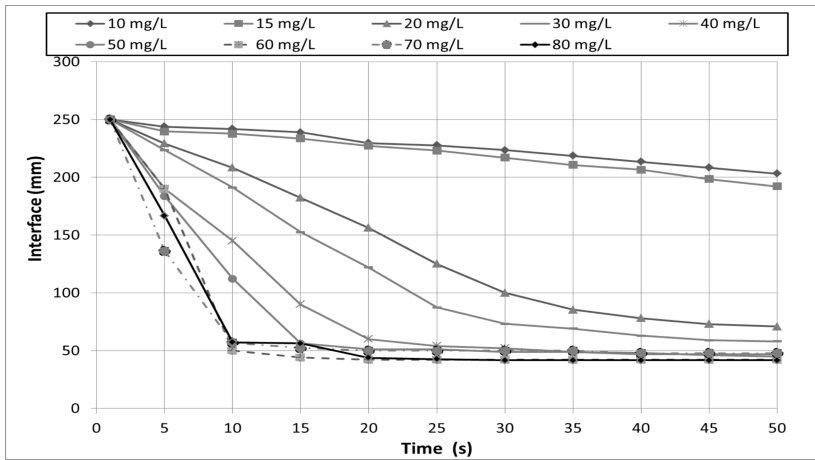


**Figure 5.3** – Settling rate of 8.7 g/L clay suspension in presence of different concentrations cationic flocculant (mg/L). For this clay concentration 70 mg/L flocculant is considered to be the optimum flocculant dose as it gives the fastest settling rate.

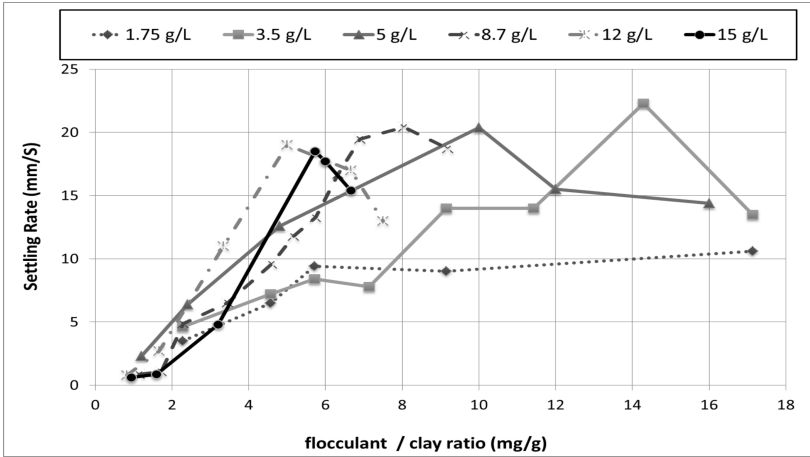


**Figure 5.4** – Settling rates of the different clay suspensions in presence of cationic flocculant. The different clay concentrations are given in the figure. The peaks indicate the optimum flocculant to clay ratio (mg/g) for each clay concentration

study of Narkis *et al.* who studied flocculation of montmorillonite clay suspensions in the presence of a linear polyquaternary Amine [Narkis et al., 1991]. Small clay particles were also seen to be imbedded in large suspended polyelectrolyte structures that due to their lower density did not settle.

The decrease in settling rate with increasing flocculant concentration is in agreement with other studies [Fargues and Turchiuli, 2003, Owen et al., 2008]. As shown in [Petzold et al., 2003] the flocs obtained at or above the optimum flocculant doses have a roughly similar size. This is in agreement with the study of H.J. Wen *et al.* [Wen et al., 1997] who measured both floc sizes and densities of cationic polymer flocculated clay sludge. They found that the flocs obtained at optimum dose have the same size but are denser than the flocs obtained at higher doses. In the present study it was observed by eye that the flocs obtained at overdose have a more open structure than the flocs formed at optimal dose. This is one reason that can explain why flocs formed at overdose

have a lower settling rate. An other reason that explains the decrease in settling can be hindered settling, also due to the presence of unbound cationic flocculant in suspension.

#### 5.4.2 Anionic flocculant

An example of the settling rate of an anionic flocculant suspension (i.e. a clay suspension flocculated with anionic flocculant) is shown in figure 5.5. The 7 g/L clay sequence (figure 5.6) is an example that represents the settling behavior of a suspension in presence of different doses of anionic polyelectrolyte. Figure 5.7 shows the settling rate of different clay concentrations with different flocculants doses. As shown in this graph, the settling rate increases with increasing flocculants dose until 16 mg/L, at which the highest settling rate is reached. This concentration corresponds to the optimum flocculant dose. This dose does correspond to the lowest turbidity of the supernatant, even though the supernatant clarity was never as high as for the optimum dose of cationic flocculant. The reason is that in the case of flocculation by anionic polyelectrolyte, the amount of cations available in the water is the limiting factor [Ji et al., 2013], see chapter 4. The cations act as a link between the negatively charged clay and the negatively charged polyelectrolyte. The stock clay suspension was made in demi-water. The desired suspensions were made by mixing clay from the stock, flocculant and tap water. It is the tap water which provides the majority of the cations. The amount of tap water for each clay concentration was different, especially for 15 g/L clay as indicated in table 5.2.

The  $C_{opt}$  (flocculant to clay ratio in mg/g) values are estimated according to equation 5.4.1.  $C_{opt}$  is calculated using the fastest rate ( $C_{opt}^{1.75}$  for 1.75 g/L clay) as reference, assuming that the amount of cations available for each experiment is proportional to the added tap water volume  $V$ . The  $C_{opt}$  values obtained are listed in the last column of table 5.2 :

$$C_{opt} = VC_{opt}^{1.75}/V_0 = V(2.28(mg/L)/233(mL)) \quad (5.4.1)$$

From the values obtained, it is clear that the estimated  $C_{opt}$  are in agreement with the experimental ones. As shown in figure 5.7,  $C_{opt}$  for

15 g/L is shifted to the position of the other maxima when the amount of tap water added to the column is the same as for the other clay concentrations. For this particular experiment a clay stock solution in tap water was used instead of the standard stock (clay in demi water).

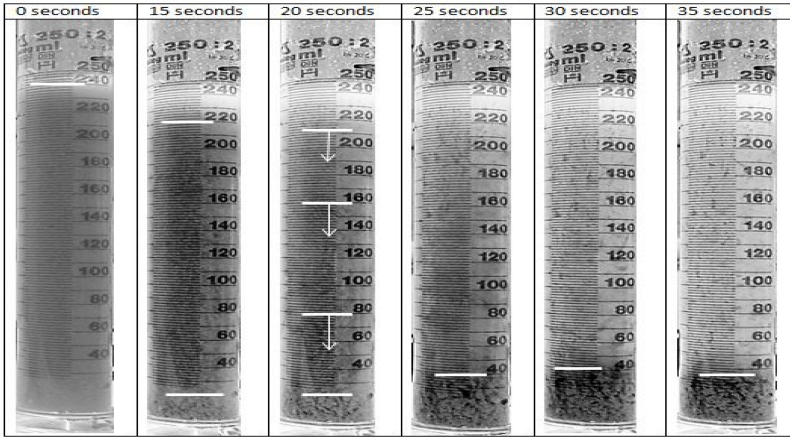


**Figure 5.5** – An example of clay suspension (7 g/L) with over-dose anionic flocculant (64 mg/L). The settling phase was completed within 35 s. The white line shows the interface. Times 0 s: right after mixing; 15 s: delayed settling is taking place; 20 s: settling rate is the highest; 25 and 30 s: the settling is almost finished. The picture taken at 20 seconds shows three white lines because the interface is not clear at this point. Although the interface is not clear it does not matter which interface ( white line) is the one selected because all of them give the same settling interface.

As shown in figure 5.6, for concentrations larger than the optimum dose  $C_{opt}$  (1.90 mg/g, 16 mg/L flocculant per 7 g/L clay), two rates can be observed. Other authors find similarly different settling rates when studying settling rates of activated sludge in the presence of anionic polyelectrolytes [Zhao, 2004, Chen et al., 1996]. The change of rate (that they define as "speed up" process) is the flocculation occurring during/prior to the settling. This change of rate was not observed for cationic flocculant as in this case, the flocculation occurred mainly

during the mixing.

**Table 5.2** – Amounts of clay and water used for the preparation of the suspensions of anionic flocculant. The final volume in all columns is 250 mL. The water used in the preparations was demi-water unless stated otherwise.

Stock (g/L)	stock (mL)	water (mL)	floc (mL)	clay conc (g/L)	$C_{opt}$ (mg/g)
35	12.5	233	2	1.75	2.28
35	25	221	4	3.5	2.16
35	35	209	6	5	2.04
35	50	192	8	7	1.9
35	107	133	10	15	1.30
100 (tap)	220	15	220	15	2.15

## 5.5 Settling time

For all clay concentrations it was found that:

- For  $C \leq C_{opt}$  only one settling rate was observed. The polyelectrolyte binding to the clay occurs during mixing. When the column is placed on a table, settling occurs immediately as the flocs are large and heavy. The flocs do not grow after the column is placed on a table. In this case there are sufficient cations available to bridge all the polyelectrolyte to the clay particles. The settling rate increases with increasing flocculant dose until  $C_{opt}$  where the optimum coverage of polyelectrolyte to clay is reached. This optimum coverage is limited by the amount of cations present as discussed in the settling rate section. The first settling rate decreases with increasing flocculant dose, being minimal at  $C = C_{opt}$ .

By mixing the sample in the column, the particles flocculate until a certain size which is limited by the shear rate created by the



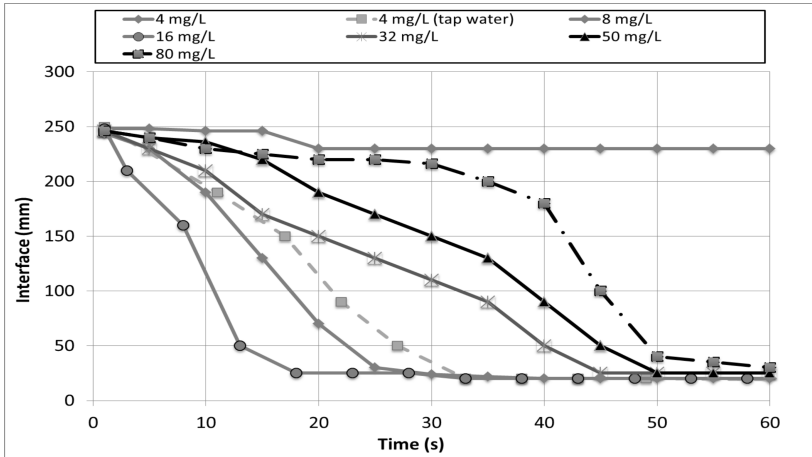


**Figure 5.6** – Settling rate of 7 g/L clay suspension in presence of different concentrations anionic flocculant (mg/L). For this clay concentration 16 mg/L flocculant is considered to be the optimum flocculant dose as it gives the fastest settling rate. Above flocculant optimum dose a delayed settling is observed.

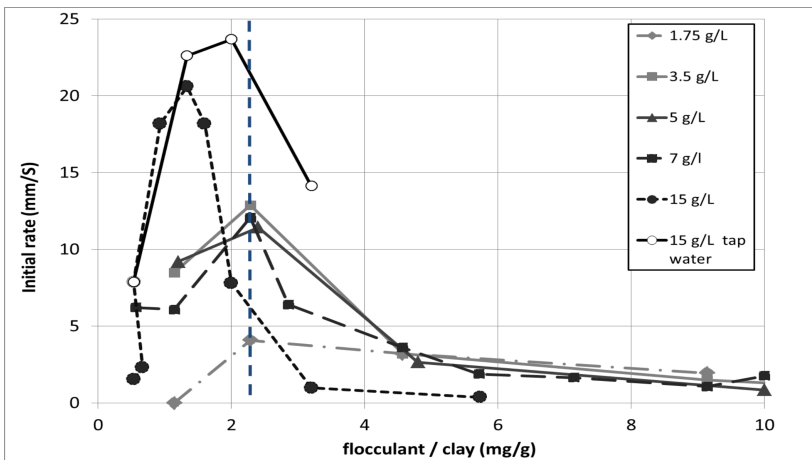


**Figure 5.7** – Settling rate of the different clay suspensions in presence of anionic flocculant. The dotted line indicates the optimum flocculant dose.

mixing ( $60 \text{ s}^{-1}$ ). It was found that the anionic flocculation is very sensitive to shear rate. This is probably the case in the experiments of Zhao [Zhao, 2004], who found a delayed settling for  $C \leq C_{opt}$ . In the present study a delayed settling was found only for  $C > C_{opt}$  using the standard mixing procedure.

- For  $C > C_{opt}$ , the first settling rate still decreases with increasing flocculant dose. The second settling rate appears and is higher than the initial rate (figure 5.8). There is a competition between the electrostatic repulsion between particles which keeps the suspension homogenous and prevent settling and the increasing gravity force caused by the growth that is responsible for the initial (slower) settling rate. When the column is set on a table, the flocs keep growing. The flocs are growing because the flocculation time is smaller than the settling time. The flocculation time in this case is the time needed for the cation links to form between the negatively charged clay and the anionic flocculant. When the floc size has exceeded a critical value, gravity dominates the system and the second (faster) settling rate is observed.

### 5.5.1 Influence of mixing method

#### Cationic flocculant

The rate of polyelectrolyte adsorption on clay is governed by the polyelectrolyte transport process, as collision and adherence are fast in the case of cationic flocculant. Therefore the primary mechanism for transport is linked to orthokinetic flocculation (turbulent mixing flocculation) where bulk fluid and turbulent motions are responsible for the transport. The other transport mechanisms are perikinetic flocculation (Brownian motion driven flocculation) induced by thermal forces and differential settling due to larger particles overtaking smaller particles. Orthokinetic flocculation is the dominant mechanism in polyelectrolyte-aided flocculation with mixing input [Young and Smith, 2000]. The rate of particle transport depends on the mixing intensity. The optimum mixing rate required in polyelectrolyte-aided flocculation is  $70\text{-}100 \text{ s}^{-1}$  [Young and

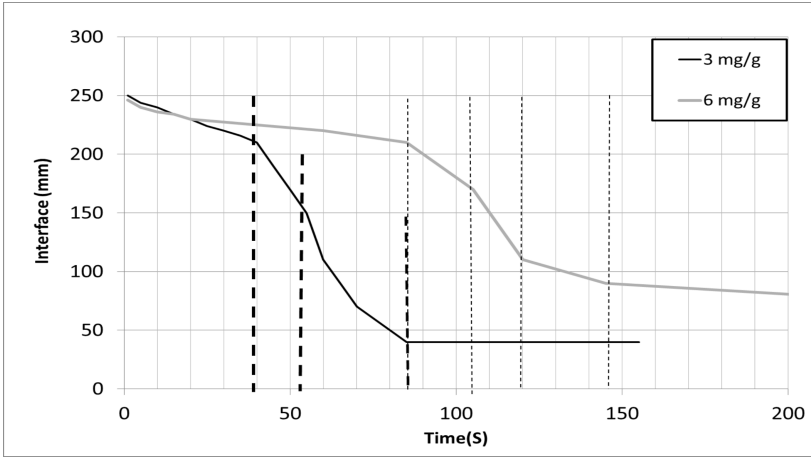


**Figure 5.8** – Influence of the flocculant dose on settling as function of time for a high clay concentration (15 g/L). For higher flocculant dose, the delayed settling is longer in time.

Smith, 2000]. Although cationic flocculation is driven by electrostatic attraction between oppositely charged particles, the mixing method plays an important role in the process. On the one hand, efficient mixing enables orthokinetic flocculation by increasing the amount of collisions between particles. On the other hand high shear rates can break the formed flocs. Poor mixing of the suspension can lead a non-homogenous distribution of the polyelectrolyte on the clay particles. Efficient flocculation then will take place in areas where the highest concentrations of both clay and polyelectrolytes are located [Owen et al., 2008].

Comparison between three mixing methods (Jar, Rod, Hand), for 8.7 g/L clay and 10 mg/L (1.15 mg/g) flocculant dose, shown in figure 5.9, indicates that stirring in the jar for 60 s results in the highest settling rate, while the difference between 10 times mixing by hand and 20 times mixing by rod is not significant. For 1.75 g/L clay and 4 mg/L flocculant (2.28 mg/g) it was found (figure 5.10) that the difference in settling rate between jar (shear rate  $25 \text{ s}^{-1}$ ) and hand mixing (shear rate  $70 \text{ s}^{-1}$ ) increases with flocculant dose. The reason is that with increas-

ing flocculant dose, larger flocs are formed in the jar which subsequently settle faster. In figure 5.11, the influence of pumping ( $156\text{--}387\text{ s}^{-1}$ ) the suspension while it is stirred within the jar is shown. In this case again, for the lowest flocculant dose, no significant influence of the method of mixing was observed. The differences increase with flocculant concentration, confirming the break-up of the formed flocs within the tube as was observed in chapter 4. Cationic flocculation is indeed found to be sensitive to breaking, since the polyelectrolyte strongly binds to the oppositely charged clay. The flocs thus obtained are therefore fragile [Yoon and Deng, 2004]. Owing to the clay concentration used, particle size distributions measurements could be performed on the samples by the Malvern. For  $2.28\text{ mg/g}$ , the  $D_{50}$  of the suspension was about  $95\text{ }\mu\text{m}$ , whereas for the higher flocculant concentrations, the mean particle size was about  $1\text{ mm}$ .

The influence of the mixing times using the rod was also investigated (figure 5.9). All the flocculant concentrations used were below the optimum flocculant dose, to study if increasing the mixing times would increase the orthokinetic flocculation. This is indeed the case for  $0.6\text{ mg/g}$ , the lowest flocculant concentration used. As can best be seen in figure 5.12, 40 times of mixing resulted in the optimal settling rate, while 50 and 60 times caused break-up of the flocs. For higher doses flocculant, increasing the mixing times resulted only in breaking the (large) flocs that are produced at the onset of mixing. Orthokinetic flocculation was also observed for larger flocculant concentration and lower clay concentrations in this case by mixing by hand as can be seen in figure 5.14. In that case the optimal mixing times was found to be between 30 and 40 inversion times.

### **Anionic flocculant**

It is clear that the way of mixing of the suspension has an impact on the flocculation process, especially when anionic flocculant is used; electrostatic repulsion forces then govern the suspension. In this case the cations present in the tap water play an important role inducing flocculation by adhering negatively charged clay particles to the anionic flocculant. Proper mixing promotes this binding mechanism resulting in

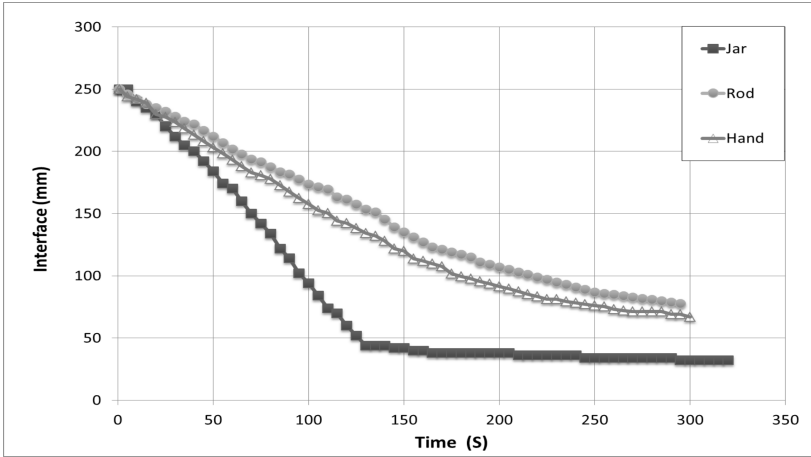


**Figure 5.9** – 8.7 g/L clay in presence of 10 mg/L cationic flocculant. Comparison between settling rates obtained using three different mixing methods. The shear rates are: Jar:  $25\text{ s}^{-1}$ , Hand:  $70\text{ s}^{-1}$  and Rod:  $3.6\text{ s}^{-1}$ .

more efficient flocculation.

Comparison between the inversions by hand, up-and-down mixing with rod and jar stirring shows that inversion by hand and jar stirring result in the highest settling rate (figure 5.15). Through mixing by rod, the flocculation time is larger and the settling rate is slower, as the shear in this case was estimated to be  $3.6\text{ s}^{-1}$ . In figure 5.16, the difference between the settling rates found by mixing with jar and hand are analyzed further. As can be seen from these graphs, there is a significant difference for the lowest clay concentration. This difference however is not a difference in settling rate but in the delay in settling. The regrowth of the flocs that were transferred from the jar to the settling column was longer than for the flocs mixed by hand. This resulted in a longer settling time in the case of jar mixing.

The influence of the number of consecutive up-and-down mixing by rod on the settling rate was investigated (figure 5.17). For the clay and flocculant chosen it was found that the optimum number of up-and-

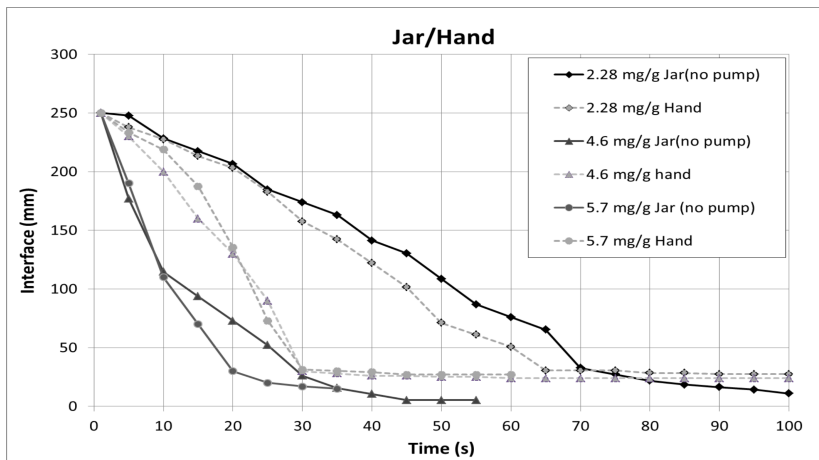


**Figure 5.10** – 8.7 g/L clay in presence of cationic flocculant. Comparison between hand mixing and jar mixing for three flocculant to clay ratios; at low concentration ratio (2.28 mg/g) the settling rates do not show significant differences but as the concentration ratio increases the influence of the mixing method become significant.

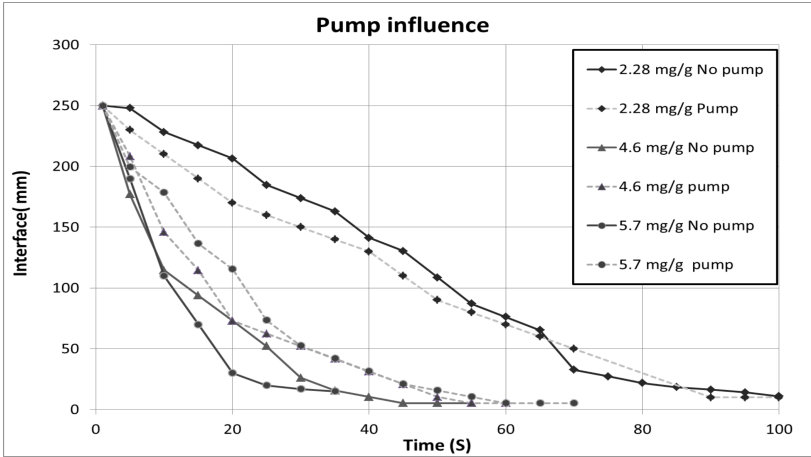


**Figure 5.11** – 8.7 g/L clay in presence of cationic flocculant. Influence of pumping (shear rate:  $156\text{ s}^{-1}$ ) during jar mixing for three flocculant to clay ratios. The higher the concentration ratio, the largest the flocs, the more flocs are broken by pumping.

down by rod mixing was reached at 40. For 40 up-and-downs by rod mixing the total settling time was the shortest. For more up-and-downs a longer delayed settling appear, as the regrowth of flocs takes longer, indicating that above 40 up-and-downs by rod mixing a large amount of flocs are broken by the shear.

In the experiment depicted in figure 5.18, the influence of the number of inversions by hand on the settling rate was investigated. The columns were inverted 10 times by hand and the suspension left to settle as in the standard procedure (inversion step 1). After complete settling, the suspensions were left 5 minutes without being disturbed. The columns were then inverted by hand again 10 times and left to settle (inversion step 2). This was repeated once more for the inversion step 3. In this experiment the flocculant concentration was chosen to represent the under-dose, optimum dose and over-dose flocculation situation. For under-dose, increasing the inversion steps led to a slight decrease in the initial settling rate. After the first inversion step, the flocs are

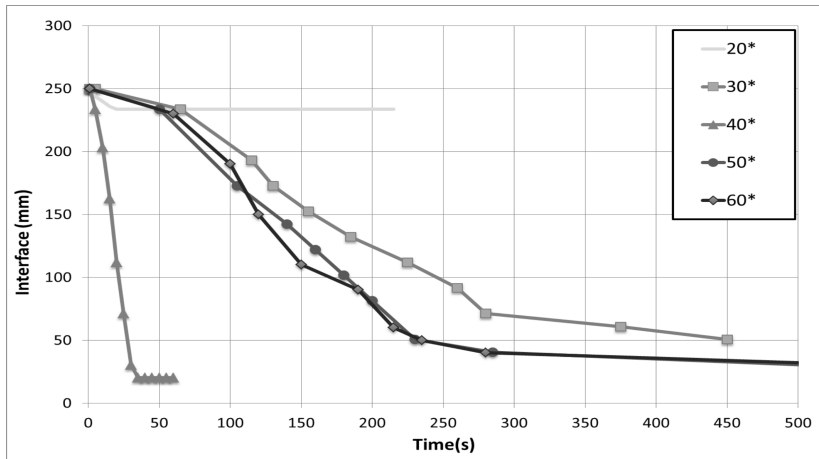


**Figure 5.12** – 8.7 g/L clay in presence of 5 mg/L cationic flocculant (0.6 mg/g flocculant to clay ratio). Settling behavior with different up-and-down times using rod mixing. Too few inversions results in no settling because the flocculant and clay particles are then not homogeneously mixed. Too many inversions results in the breaking of the formed flocs.



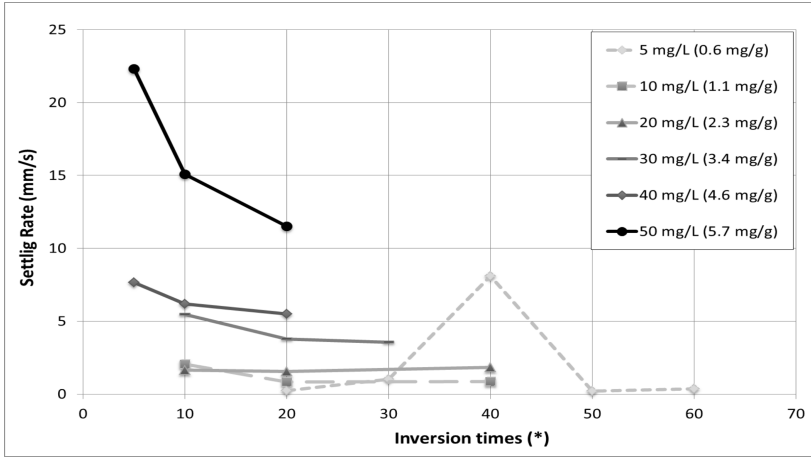


**Figure 5.13** – The influence of the inversion times on the different flocculant doses with 8.7 g/L clay: the higher flocculant concentration the less inversions are needed to perform efficient flocculation and avoid breaking.

re-growing and settling from the initial suspension, which was defined as un-flocculated clay in the presence of polyelectrolytes. At the second (and third) inversion step, the flocs only settle and barely re-grow from the flocs already formed in the previous step. These flocs settle less rapidly than the flocs from the first inversion step for under-dose flocculant as probably the flocs are broken during the extra shearing. For the optimum and over-dose flocculant concentration, the settling rate increases in step 2 compared to step 1, as the large flocs obtained in step 1 settle rapidly. At overdose flocculant the flocs in the step 3 are broken compared the flocs in step 2, leading to a decrease in the settling rate, therefore a possible hindered settling effect appears.

These results were also found for clay minerals (smectite and kaolinite): their settling rates showed a clear dependence on shear rate. Similarly to what was found in this study, Mc Farlane *et al.* found an optimum settling rate for a given shear rate and anionic polyelectrolyte dose [McFarlane et al., 2006].

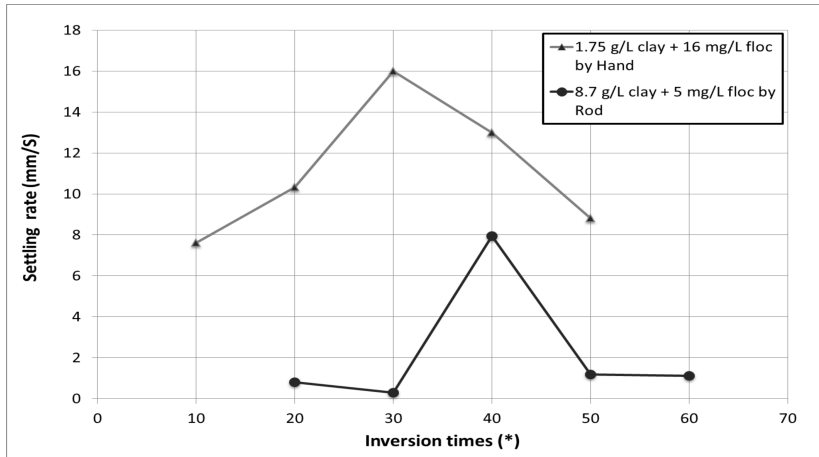


Figure 5.14 – Comparison between different inversion times with hand and rod for low and high clay concentrations. The optimum inversion times, for both methods are between 30 and 40 times. Every time a new sample is prepared, the final inversion times are not cumulative.

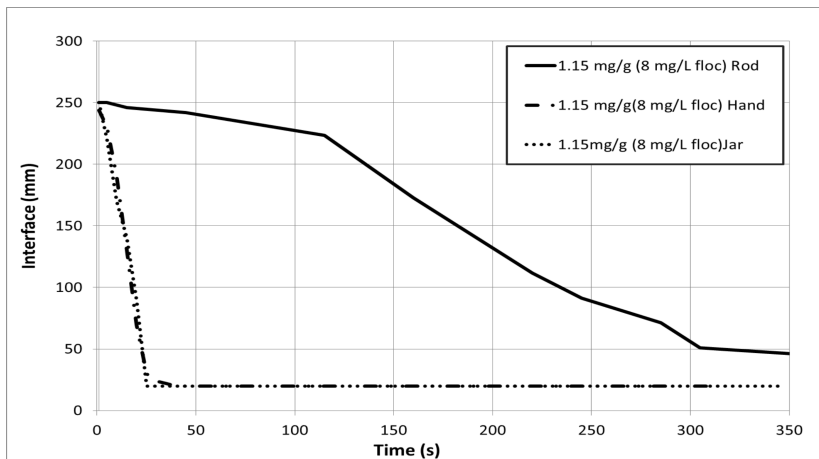
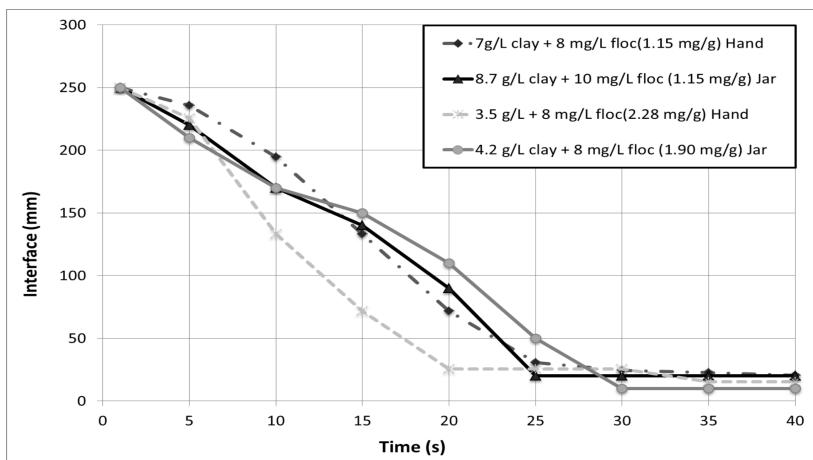
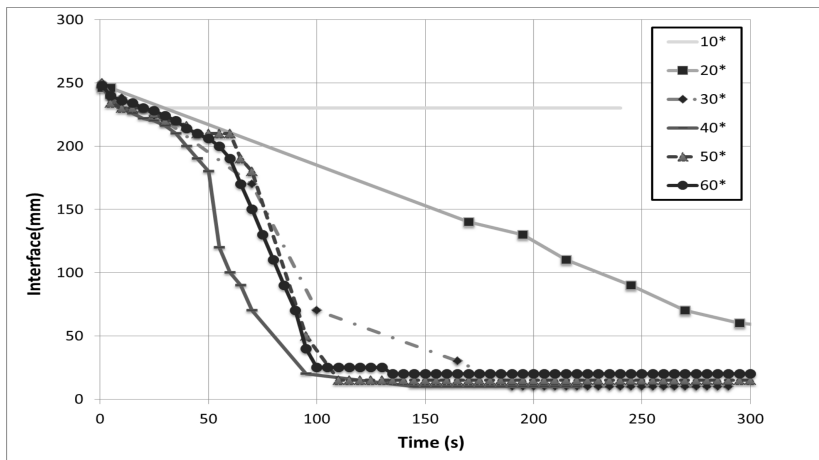


Figure 5.15 – Influence of three different mixing methods on the settling of the clay suspension with anionic flocculant. Mixing by Hand and Jar resulted in similar rates.



**Figure 5.16** – Comparison between mixing by Hand or Jar for different anionic flocculant to clay ratios. For low ratios (1.15 mg/g) there is no significant difference between the mixing methods. For higher ratios (2.28 mg/g) the influence of the mixing method becomes more significant.



**Figure 5.17** – Clay concentration is 7g/L and anionic flocculant dose is 4 mg/L (0.6 mg/g). Influence of the number of up-and-down times on the settling behavior using the rod mixing method. The number of up-and-down times is given in the figure. For 40 up-and-downs the optimum settling rate was obtained.

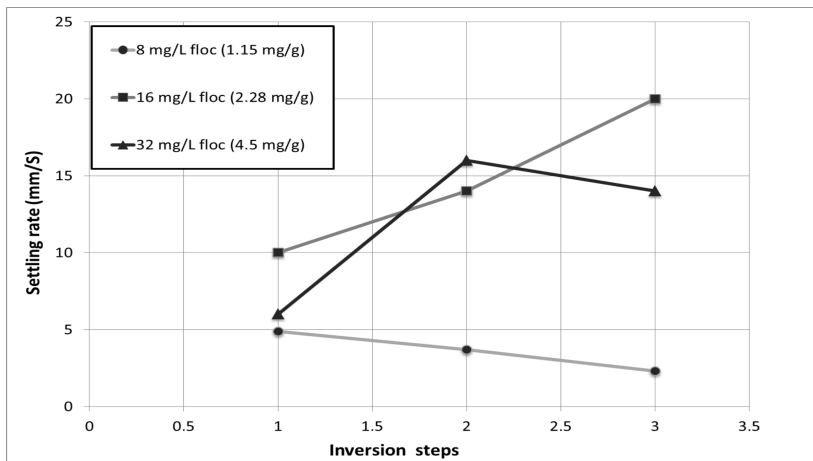


**Figure 5.18** – Settling rate as function of inversion steps for the mixing by Hand method. The columns were mixed by 10 times inversions (inversion step 1). After complete settling, the suspensions were left 5 minutes without being disturbed. The columns were then inverted again 10 times (inversion step 2). This was repeated once more for the inversion step 3.

## 5.5.2 Influence settling column size

### Cationic flocculant

The influence of the settling column diameter and volume is presented in figure 5.19. Figure 5.20 shows a picture of the different column sizes used. As can be seen, the dependence of the settling rate on column size is complex. Two different clay concentrations, a low clay concentration (1.75 g/L) and a very high clay concentration (25 g/L), both at optimum flocculant to clay ratio are studied. For the lowest concentration, the settling rate is high for smaller volume column, as the mixing of the suspension is efficient in smaller columns (50, 100 mL). The settling rate decreases with increasing column size because for larger column sizes the mixing is not efficient any more (as standard procedure is used), and from the 250 mL column on, it becomes roughly constant.

For high clay concentration (25 g/L), the settling rate is low for smaller columns (50-100 mL), because large flocs experience an interaction with the column wall and settling is hindered. The flocs obtained at high clay concentration were much larger than at low clay concentration, as expected. For larger column (250-500 mL), the bulk collective settling of the flocs is dominant and the settling is higher. For these column sizes, flocs were observed to (re-)grow during the settling phase. For the 1000 mL column, there is a stronger return water flow in the column which is delaying the settling bulk and leads to a slightly smaller settling velocity.

The hindered settling effect is studied more in detail in chapter 6. In this chapter the hindered settling effect on the settling rate at different clay concentrations for the same flocculant to clay ratio was studied. In figure 5.21, it was found that below 8.7 g/L clay hindered settling effects were negligible. Above this clay concentration, hindered settling effects cause a decrease in settling rate for increasing clay concentrations [Winterwerp and Van Kesteren, 2004]. This explains that the settling rate for 5 g/L is always higher than for 25 g/L. Therefore for the results shown through this section, the hindered settling effect appears when the supernatant in the column is clean.

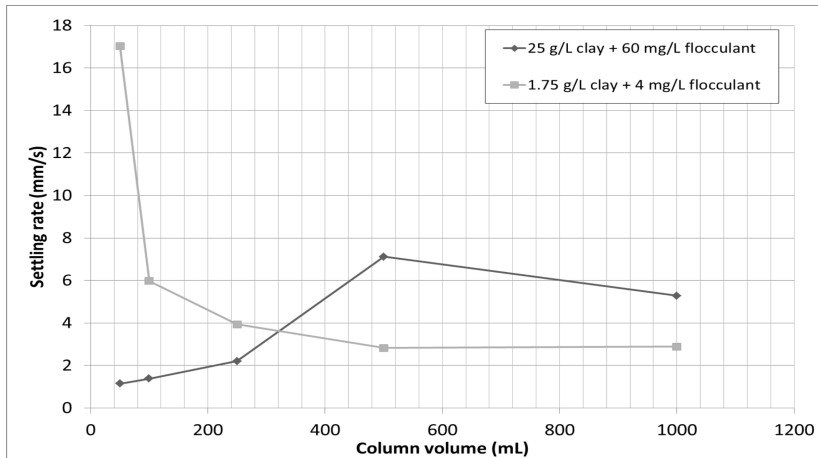


**Figure 5.19** – Settling rate of 2.4 mg/g concentration cationic flocculant to clay ratio in different column sizes.

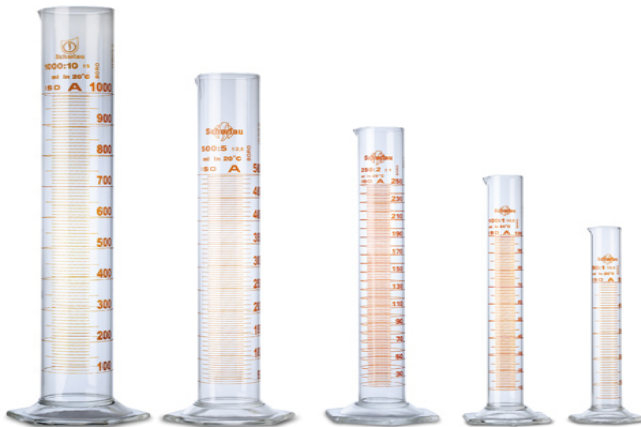


**Figure 5.20** – Picture of the different columns used to study the influence of settling due to different diameter. From left to right the sizes are 1000 mL, 500 mL, 250 mL, 100 mL, and 50 mL. [Labotienda, 2015]

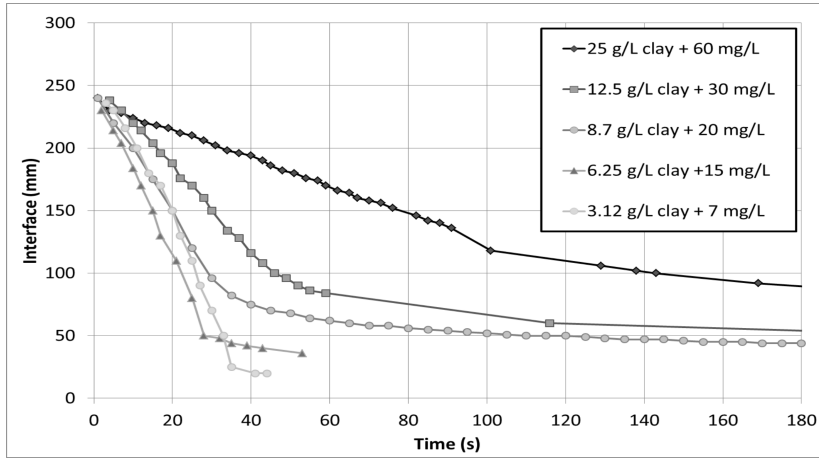


**Figure 5.21** – The concentration of cationic flocculant to clay ratio of 2.4 mg/g in different portions in 250 mL column (same diameter)

### Anionic flocculant

The influence of the column size is shown in figure 5.22. Two suspensions with two different clay concentrations, both at optimum flocculant to clay ratio are shown in figure 5.22. For both 5 g/L and 25 g/L the initial settling rate increases with increasing column size. For the smallest column sizes, small settling velocities are observed, due to hindered settling, caused by the interaction between the walls of the column and the large flocs. For larger column sizes this hindrance is minimal leading to the observed large initial settling velocities.

In figure 5.23 the hindered settling effect on settling rate at different clay concentrations for the same flocculant to clay ratio was studied. As shown in this graph the lower concentrations of clay settle slower than the higher. This might be due to the lack of efficient mixing and homogeneity since the anionic flocculation is very sensitive to mixing as discussed earlier.



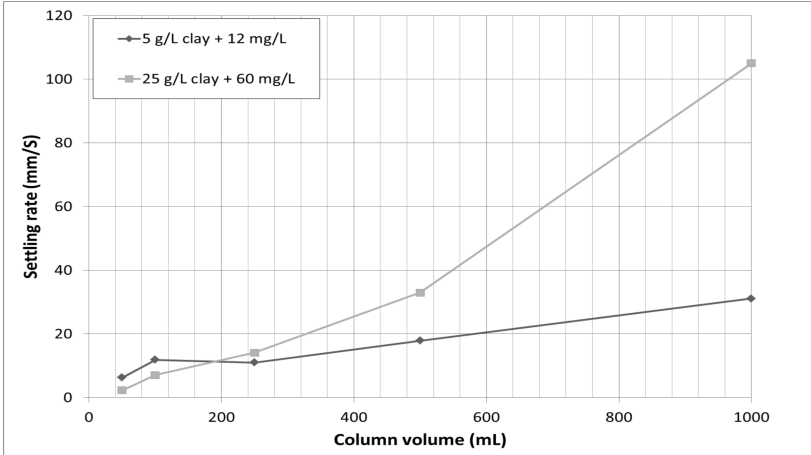


**Figure 5.22** – Settling rate as function of column size for the same anionic flocculant to clay ratio of 2.4 mg/g (corresponding to the optimum flocculant dose) but two different clay concentrations indicated in the figure.

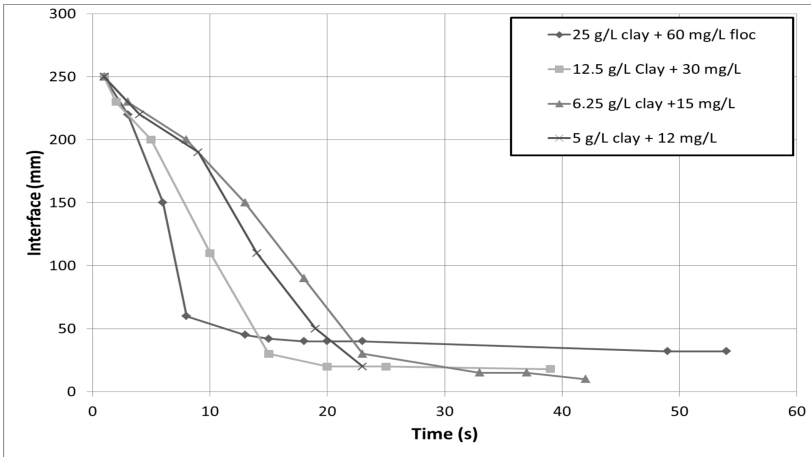


**Figure 5.23** – Influence of the clay concentration on the settling rate. All curves are for the anionic flocculant to clay ratio 2.4 mg/g (optimum dose) for clay concentration given in the figure.

## 5.6 Conclusions

In this chapter a systematic investigation of the flocculation and settling behavior of clay suspensions in presence of either cationic or anionic ployelectrolyte is presented. A summary of the main findings is presented in figure 5.24, where the relation between optimum flocculant dose and clay concentration is given for both anionic and cationic flocculants.

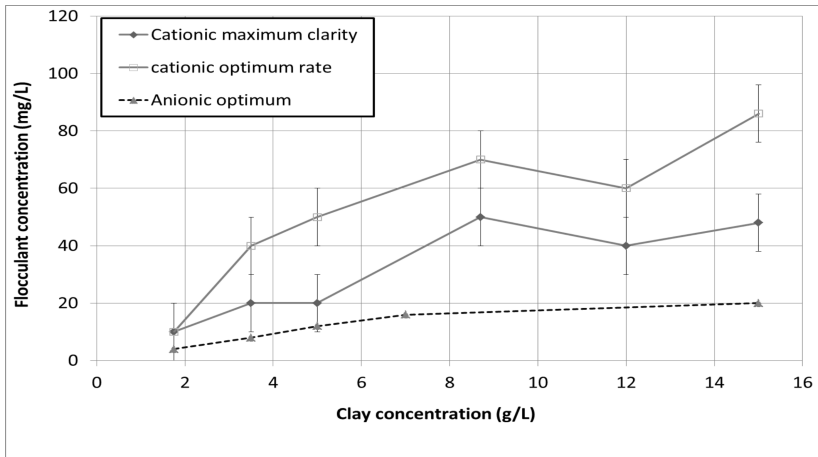


**Figure 5.24** – Optimum flocculant dose as function of clay concentration for both anionic and cationic flocculant. For cationic flocculant a distinction is made between fastest settling rate (defining the optimum dose) and maximum supernatant clarity (defining the maximum clarity dose). No maximum clarity was observed for the anionic flocculant due to hindered settling.

The experiments were done with the standard mixing procedure, i.e. hand mixing. This optimum for cationic flocculant was roughly 5 mg/g for 1 g/L clay. This value is in agreement with the value found in chapter 4, even though the shear rate was different. In chapter 4 it was found that the relation between clay concentration and the optimum cationic flocculant dose is linear for clay concentrations below 1 g/L. For higher clay concentrations, the optimum cationic flocculant dose increases in a non-linear way with clay concentration until an optimum value of 14

mg/g. In figure 5.24 the "maximum clarity" flocculant dose as a function of clay concentration is also plotted. The optimum dose corresponds to the flocculant dose needed to achieve fastest settling rate. At this optimum rate the supernatant clarity was not optimum. At the maximum clarity dose, optimal surface coverage of the particle by polyelectrolyte is achieved. This corresponds to flocs with a zero electrophoretic mobility as shown in chapter 4. The link between zero electrophoretic mobility and supernatant maximum clarity was also found by Narkis *et al.* [Narkis et al., 1991] in the case of montmorillonite. The variation of flocculant dose as function of clay concentration is however the same for optimum dose and maximum clarity dose. This variation is attributed to environmental conditions such as mixing method, mixing time and column size that were discussed in detail in the previous sections.

The variation of optimum flocculant dose with clay concentration is less pronounced for the anionic flocculant than for cationic flocculant. The anionic optimum concentration is roughly 2.2 mg/g for all clay concentrations. As explained in the previous sections this is due to the fact that the amount of cations present in the water are the limiting factor. The flocculation process in presence of anionic flocculant is therefore very limited. Good supernatant clarity was never observed.

The difference between the flocculation mechanisms for the anionic and the cationic flocculants can best be seen in figure 5.25. Two samples were left to be stirred in a 1 L jar. The shear rate was  $25 \text{ s}^{-1}$  in both cases and the pictures were taken 10 minutes after the start of the experiment. As discussed in the previous sections and in chapter 4, cationic flocculant acts through charge neutralization while the anionic flocculant through bridging mechanism. This leads to the different floc shapes observed in the jars. Since the amount of cations present in the water is insufficient to lead to optimal flocculation in the case of anionic flocculant, the water remains turbid and the overall negative charge of the flocs prevents the re-conformation of the flocs, as is observed for the cationic flocs. These different flocculation mechanisms influence the optimum flocculant dose, settling rate and consolidation properties as can be seen in figure 5.26. With cationic flocculant the formed bed was always thicker and has a more open structure than with anionic floccu-

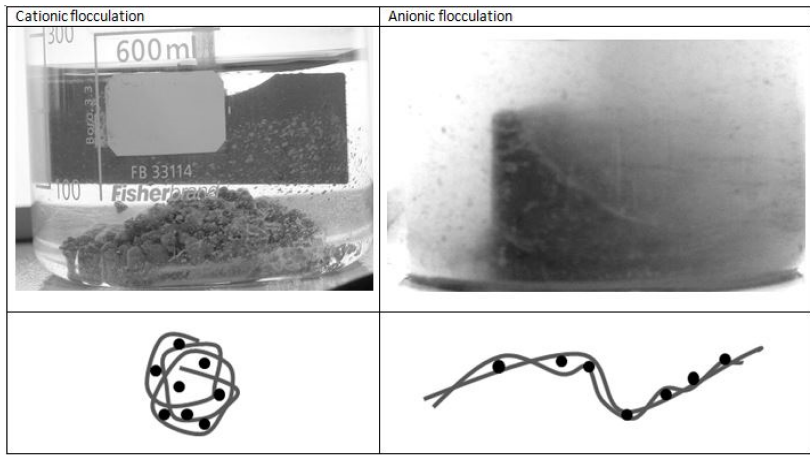


**Figure 5.25** – Influence of the flocculant type on the shape of the formed flocs. Cationic polymer forms spherical and open flocs while anionic polymer creates more thin and compacted flocs. It is showed also how cationic polymer promotes clear water after flocculation and fast settling. Anionic polymer on the other hand forms a turbid water column.

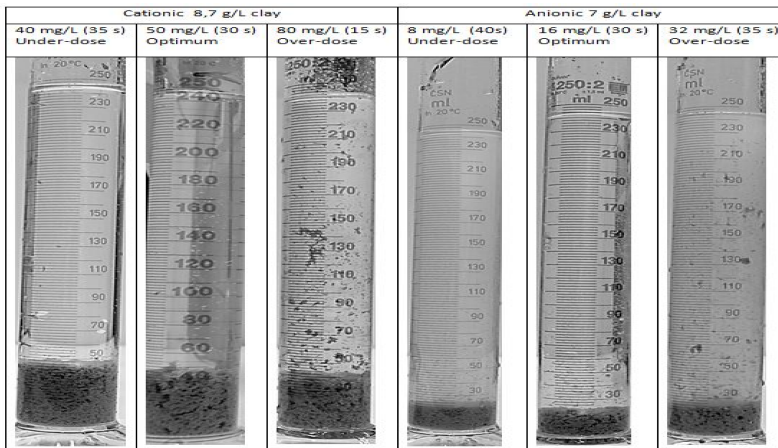


**Figure 5.26** – Settling columns for flocculant under, at and above the optimum doses. All the pictures were taken at the end of the tests. Note that in the case of cationic flocculant over-dose, some flocs remain attached to the column wall. In the case of anionic flocculant over-dose the few flocs observed in the column are not attached to the wall but are settling down extremely slowly.

lant. Anionic flocculant therefore appear as the most efficient flocculant with regard to compaction. This results are confirmed and explained more in detail in chapter 6.



## References

- [Bergaya and Lagaly, 2013] Bergaya, F. and Lagaly, G. (2013). *Handbook of clay science*, volume 5. Newnes.
- [Bolto and Gregory, 2007] Bolto, B. and Gregory, J. (2007). Organic polyelectrolytes in water treatment. *Water research*, 41(11):2301–2324.
- [Chen et al., 1996] Chen, G., Chang, I., Hung, W., and Lee, D. (1996). Regimes for zone settling of waste activated sludges. *Water Research*, 30(8):1844–1850.
- [Concha Arcil, 2009] Concha Arcil, F. (2009). Settling velocities of particulate systems. *Kona Powder and Particle Journal*, 27(0):18–37.
- [Dankers and Winterwerp, 2007] Dankers, P. and Winterwerp, J. (2007). Hindered settling of mud flocs: theory and validation. *Continental shelf research*, 27(14):1893–1907.
- [Fargues and Turchiuli, 2003] Fargues, C. and Turchiuli, C. (2003). Structural characterization of flocs in relation to their settling performances. *Chemical Engineering Research and Design*, 81(9):1171–1178.
- [Goodwin, 2009] Goodwin, J. (2009). *Colloids and interfaces with surfactants and polymers*. John Wiley & Sons.
- [Jarvis et al., 2005] Jarvis, P., Jefferson, B., and Parsons, S. A. (2005). Measuring floc structural characteristics. *Reviews in Environmental Science and Bio/Technology*, 4(1-2):1–18.
- [Ji et al., 2013] Ji, Y., Lu, Q., Liu, Q., and Zeng, H. (2013). Effect of solution salinity on settling of mineral tailings by polymer flocculants.



- Colloids and Surfaces A: Physicochemical and Engineering Aspects*, 430:29–38.
- [Labotienda, 2015] Labotienda (2015). Laboratorio website. <http://http://www.labotienda.com>. Accessed: 2015-04-30.
- [Latif et al., 2005] Latif, M., Eldin, M., and Kady, M. (2005). Settling of high concentrations of clay suspended in water by nonionic polyacrylamide flocculants. *Alexandria Engineering Journal*, 44(2):325–338.
- [McFarlane et al., 2006] McFarlane, A., Bremmell, K., and Addai-Mensah, J. (2006). Improved dewatering behavior of clay minerals dispersions via interfacial chemistry and particle interactions optimization. *Journal of colloid and interface science*, 293(1):116–127.
- [Mierczynska-Vasilev et al., 2013] Mierczynska-Vasilev, A., Kor, M., Addai-Mensah, J., and Beattie, D. A. (2013). The influence of polymer chemistry on adsorption and flocculation of talc suspensions. *Chemical Engineering Journal*, 220:375–382.
- [Narkis et al., 1991] Narkis, N., Ghattas, B., Rebhun, M., and Rubin, A. (1991). Mechanism of flocculation with aluminium salts in combination with polymeric flocculants as flocculant aids. *Water supply*, 9(1):37–44.
- [Owen et al., 2008] Owen, A., Fawell, P., Swift, J., Labbett, D., Benn, F., and Farrow, J. (2008). Using turbulent pipe flow to study the factors affecting polymer-bridging flocculation of mineral systems. *International Journal of Mineral Processing*, 87(3):90–99.
- [Petzold et al., 2003] Petzold, G., Mende, M., Lunkwitz, K., Schwarz, S., and Buchhammer, H.-M. (2003). Higher efficiency in the flocculation of clay suspensions by using combinations of oppositely charged polyelectrolytes. *Colloids and Surfaces A: Physicochemical and Engineering Aspects*, 218(1):47–57.
- [Sutherland et al., 2014] Sutherland, B. R., Barrett, K. J., and Gingras, M. K. (2014). Clay settling in fresh and salt water. *Environmental Fluid Mechanics*, 15(1):147–160.

- [Tan et al., 2012] Tan, X.-L., Zhang, G.-P., Hang, Y., FURUKAWA, Y., et al. (2012). Characterization of particle size and settling velocity of cohesive sediments affected by a neutral exopolymer. *International Journal of Sediment Research*, 27(4):473–485.
- [Tripathy and De, 2006] Tripathy, T. and De, B. R. (2006). Flocculation: a new way to treat the waste water.
- [Wen et al., 1997] Wen, H., Liu, C., and Lee, D. (1997). Size and density of flocculated sludge flocs. *Journal of Environmental Science & Health Part A*, 32(4):1125–1137.
- [Winterwerp and Van Kesteren, 2004] Winterwerp, J. C. and Van Kesteren, W. G. (2004). *Introduction to the physics of cohesive sediment dynamics in the marine environment*. Elsevier.
- [Yoon and Deng, 2004] Yoon, S.-Y. and Deng, Y. (2004). Flocculation and reflocculation of clay suspension by different polymer systems under turbulent conditions. *Journal of colloid and interface science*, 278(1):139–145.
- [Young and Smith, 2000] Young, S. and Smith, D. (2000). Effect of mixing on the kinetics of polymer-aided flocculation. *Aqua*, 49:1–8.
- [Zhao, 2004] Zhao, Y. (2004). Settling behaviour of polymer flocculated water-treatment sludge i: analyses of settling curves. *Separation and Purification Technology*, 35(1):71–80.



## Chapter 6

# Consolidation of flocculated clay as function of polyelectrolyte charge.

### Abstract

In this chapter the consolidation process of flocculated clay in the presence of polyelectrolyte is studied. In this study large settling columns are used (0.12 m diameter and height of 1 m) to minimize wall effects. Difference between anionic and cationic polyelectrolytes are studied. The consolidation is studied from floc formation through settling until full consolidation is reached. The differences in flocs and structure of the bed are discussed. The cationic polyelectrolyte creates open flocs that settle a bit slower than the flocs formed by anionic polyelectrolyte. The flocs formed by addition of cationic polyelectrolyte produce a fully porous bed with low strength. Flocs formed by addition of anionic polyelectrolyte settle faster and produce a more compact bed.

## 6.1 Introduction

The consolidation of soft soils is a complex phenomenon that is not fully understood, as it bridges several aspects of science: soil mechanics, hydraulics, colloid science, and chemistry. Biology is not mentioned here as only (synthetic) organic matter with no biological activity is considered in the present thesis. More and more soft soils are used in land reclamation projects [Indraratna et al., 2011, Lee et al., 1987, Terashi and Katagiri, 2005]. An other application concerns the tailings from industry. Large tailing ponds are produced by these industries, where fine particles are left to settle, with the objective to be able to reclaim the water supernatant. Ideally, these tailing ponds should be converted in land at long term. Requirements for the consolidation of soft soils are:

- They should dewater quickly.
- The bed made from the settled soil should be strong enough to sustain human activity.

The dewatering of slurries is a major issue in mining industry where process water should be separated from fines for reuse [COSIA, 2016, centre for Policy Alternatives, 2016]. Different technologies are used to accelerate the settling phase in mining industries, e.g. the use of centrifugal force and polymers to speed removal of process water from the tailings; a filtering technology to dewater tailings and increasing the proportion of solid content [COSIA, 2016]. The importance of the material composition, amount and type of clays, and its evolution over time has been recognized, which led to a large increase in research in this area over the past years. Numerous studies headed in the direction of understanding the optimal use of chemical additives (coagulants, flocculants) to enhance process water clarity, dewatering and strength development [Novak and Langford, 1977, Mpofo et al., 2003]. In this chapter we correlate the results found on flocculation from chapter 4 and settling from chapter 5 with settling and consolidation experiments in large columns. From the interface against time curves the following parameters can be studied:

- Settling velocity and gelling concentration [Dankers and Winterwerp, 2007].
- Permeability and fractal dimension [Merckelbach and Kranenburg, 2004b, Merckelbach, 2000].
- Effective stress at the end of the consolidation test [Merckelbach and Kranenburg, 2004b, Merckelbach, 2000].

In particular the impact of two different types of flocculant on the settling and consolidation properties of flocculated natural fine sediments are investigated.

## 6.2 Materials

### 6.2.1 Clay

The clay used in the experiments is the same clay used in chapter 2. The clay was always dispersed in tap water the obtained suspension having conductivity of 0.5 mS/cm.

### 6.2.2 Flocculant

Flocculants used were anionic and cationic polyacrylamide-based polyelectrolytes. These flocculants are the same that the flocculants used in chapter 4. The specifications of both flocculants are given in chapter 4.

### 6.2.3 Water

The relevant tap water specifications are listed in chapter 2. These specifications were obtained from the local drinking water company Evides for the months during which the experiments were performed.

## 6.3 Methods

### 6.3.1 Experimental set-up

The experiments were carried out in Perspex columns with an inner diameter of 0.12 m and a height of 1 m, placed in a temperature-controlled room. At the start of an experiment, each column is filled with the desired sediment suspension. The starting time of all columns is synchronized by re-stirring with a rod (gently) all columns for a short while after the last column has been filled. After the water has come at a standstill the camera recording is started. Pictures are taken automatically at fixed time intervals for the entire duration of the experiment (i.e. 4 to 6 weeks). From the images, the interface between clean water and settling/consolidating sediment as function of time is obtained. Table 6.1 shows an overview of these experiments, indicating the clay concentration and the flocculant concentration.

## 6.4 Results and discussions.

### 6.4.1 Hindered settling

Hindered settling of flocs originates from the influence of neighboring particles on the settling velocity of individual particles within a mixture [Winterwerp, 2002]. Consolidation begins when the gelling concentration is reached. The gelling concentration is defined as the concentration at which particles touch each other, thereby forming a clay fabric. Figure 6.1 shows the settling interface for three different concentrations of clay. The effective settling velocity  $\omega_s$  is the time derivative of the settling interface. From figure 6.1 it can be seen that the settling velocity decreases with concentration of clay. This is usually attributed to flocculation, differential settling, hindered settling and complex hydrodynamic effects. When flocculants are used, the effective settling velocity increases see figure 6.2 and 6.3. The settling velocity of individual flocs  $\omega_{s,0}$  and the gelling concentration  $c_{gel}$  can be calculated

**Table 6.1** – Overview of experiments. Clay concentration and flocculant concentration and type.

Sediment concentration [g/L]	Flocculant concentration [g/L]	Flocculant
30	-	-
50	-	-
70	-	-
30	0.04	cationic (Zetag 7587)
30	0.07	cationic (Zetag 7587)
30	0.16	cationic (Zetag 7587)
30	0.025	anionic (Zetag 4110)
30	0.1	anionic (Zetag 4110)
30	0.15	anionic (Zetag 4110)

from Eq. 6.4.1 [Dankers and Winterwerp, 2007].

$$\omega_s = \omega_{s,0} \frac{(1 - \phi)^m (1 - \phi_p)}{1 + 2.5\phi} \quad (6.4.1)$$

Where  $\phi$  is the floc volumetric concentration and is equal to  $c/c_{gel}$ ,  $c$  is the mass concentration,  $\phi_p$  is the volumetric concentration of primary particles it is equal to  $c/\phi_s$ , in which  $\phi_s$  is the density of sediments, and  $m$  is an empirical parameter used to account for possible non-linear effects. [Dankers and Winterwerp, 2007] found a  $m$  value of 2. The data can be fitted with Eq. 6.4.1 to obtain  $\omega_{s,0}$  and  $c_{gel}$ , assuming  $c$  equal to the initial mass concentration [Dankers and Winterwerp, 2007] and using  $m = 2$ . To solve the equation with two unknowns, least square fitting from



Matlab is used. The data from the height evolution as function of time from the whole consolidation test is given in the figures below. Figure 6.5 shows three clay concentrations 30 g/L, 50 g/L, and 70 g/L. Figure 6.6 shows the data of 30 g/L and three different concentrations of anionic flocculant and figure 6.7 shows 30 g/L clay and three concentrations of cationic flocculant.

The values of effective settling velocity and  $c_{gel}$  are shown in table 6.2. Figure 6.4 shows the fitting of the three points and values of settling velocity of individual flocs and the  $c_{gel}$ . The individual floc settling velocities are: for the clay  $\omega_{s,0} = 0.00012$  m/s, clay with cationic flocculant  $\omega_{s,0} = 0.006$  m/s and clay with anionic flocculant  $\omega_{s,0} = 0.007$  m/s. The floc settling velocity of clay with anionic is the largest. This is due to the fact that these flocs have a larger density (being more compact) and larger size. This is in line with the results found in chapter 4 and chapter 5.  $C_{gel}$  in the presence of flocculant is calculated from the graph of height versus time. The  $c_{gel}$  is estimated at the point of inflection in which the slope for the settling interface change to the consolidation phase, in this point and due to mass conservation, between initial time of the experiment and the time in which the settling phase ends, we get a concentration  $c_{gel}$  value. All the values of  $c_{gel}$  in the presence of flocculant are over-estimated due to the way in which they have been calculated in this chapter. The gelling concentration decreases when flocculant is added, as expected. As the flocs formed by the addition of cationic flocculant have a more open structure than flocs formed by addition of anionic flocculant, the  $c_{gel}$  is smaller for cationic flocculant.

## 6.4.2 Initial phase of consolidation

Consolidation of soft mud layers can be described by the classical Gibson's consolidation equation [Gibson et al., 1967]. Relations for the bulk permeability  $k$  and the vertical effective stresses  $\sigma_{zz}^{sk}$  must be known to solve the Gibson's equation. Merckelbach and Kranenburg [Merckelbach and Kranenburg, 2004b] proposed constitutive equations for effective stress and permeability on the basis of scale invariance. These

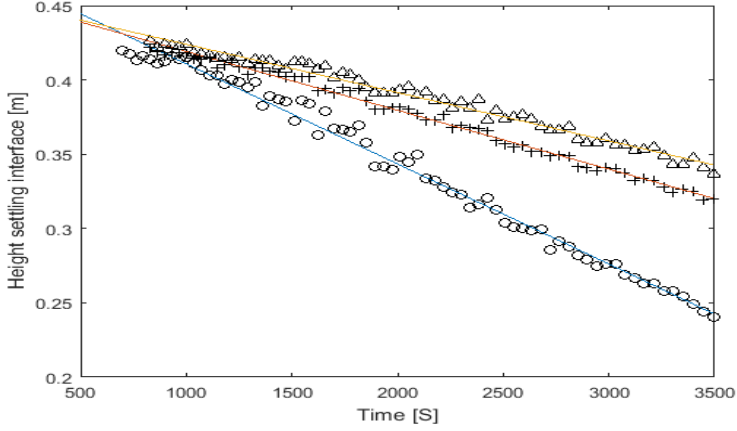


**Figure 6.1** – Evolution of clay interface at function of time during the settling phase. Circles represent 30 g/L concentration clay, crosses represent 50 g/L concentration clay and triangles represent 70 g/L clay concentration respectively.

equations read:

$$\sigma_{zz}^{sk} = k_p \left( \frac{\phi_s^m}{1 - \phi_s^{sa}} \right)^{\frac{2}{3-n_f}} - k_{p,o} \quad (6.4.2)$$

$$k = k_k \left( \frac{\phi_s^m}{1 - \phi_s^{sa}} \right)^{\frac{-2}{3-n_f}} \quad (6.4.3)$$

Where  $k_p$  is the effective stress parameter,  $k_{p,o}$  is a parameter that represents effects due to creep,  $n_f$  is the fractal dimension of flocs,  $k_k$  is the permeability parameter,  $\phi_s^m$  is the volume concentration of solids from the mud fraction and  $\phi_s^{sa}$  is the volume concentration of solids from the sand fraction. The material functions can be determined directly by measurements, but Merckelbach and Kranenburg [Merckelbach and Kranenburg, 2004a] propose a method in which these parameters can

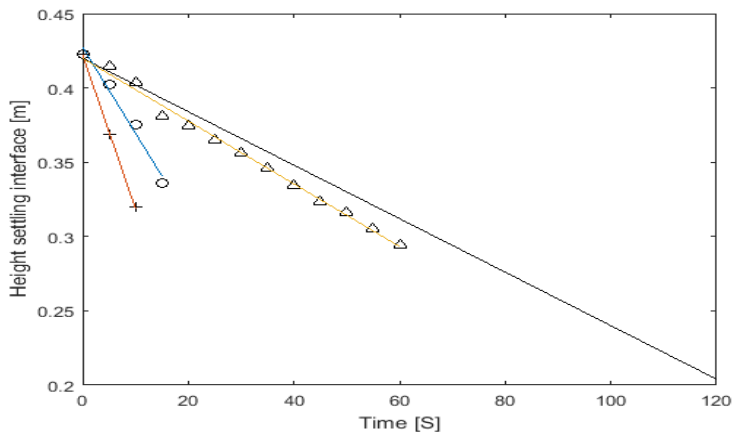


**Figure 6.2** – Evolution of height settling interface of three 30 g/L clay samples with anionic flocculant. Black line represents 30 g/L clay, triangles represent 0.15 g/L anionic flocculant, circles represent 0.1 g/L anionic flocculant concentration, and crosses represent 0.025 g/L anionic flocculant (close to optimal dose).

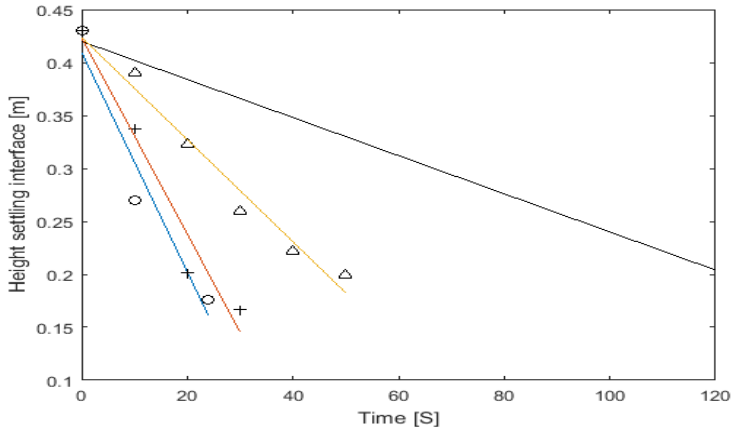


**Figure 6.3** – Evolution of height settling interface of three 30 g/L clay samples with cationic flocculant. Black line represents 30 g/L clay, triangles represent 0.04 g/L cationic flocculant, crosses represent 0.07 g/L cationic flocculant (close to optimal dose), and circles represent 0.16 g/L cationic flocculant concentration.

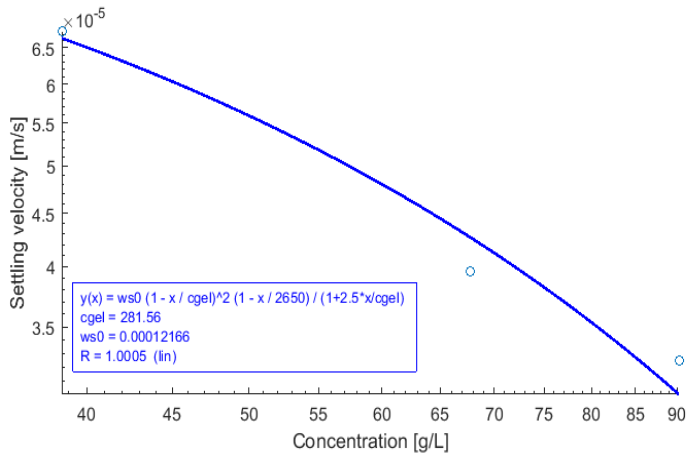


**Figure 6.4** – Fitting of three points obtained from the data of concentrations and settling velocities of clay used to calculate the individual settling velocity of a floc and the gelling concentration.

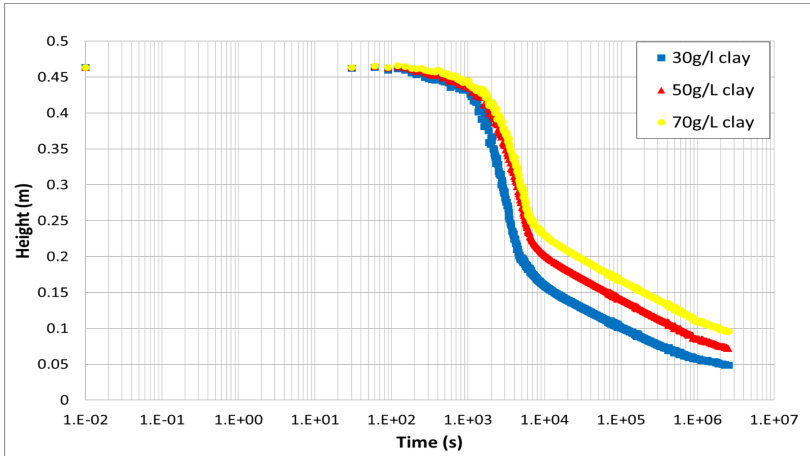


**Figure 6.5** – Evolution of clay interface at function of time during the consolidation test. Blue represent 30 g/L concentration clay, red represent 50 g/L concentration clay and yellow represent 70 g/L clay concentration respectively.

be determined by measuring the evolution of the mud-water interface through the consolidation process.

The initial phase of consolidation is the phase governed by the permeability of the soil. The fractal dimension and permeability parameter can be obtained from the mud-water interface as function of time data [Merckelbach, 2000]. The equations 6.4.2 and 6.4.3 are only valid for cohesive-consolidation behavior. The boundary between cohesive and non-cohesive consolidation behavior is found at 10% clay content [Winterwerp and Van Kesteren, 2004, Te Slaa et al., 2013]. In all tests performed in this chapter, the clay used has a clay content (percentage of particles smaller than  $2 \mu\text{m}$ ) of 13%, therefore we can assume a cohesive behavior.

Following the procedure used by Merckelbach [Merckelbach, 2000] plotting the sediment-water interface versus time on double logarithmic scales, the fractal dimension and the permeability parameter can be

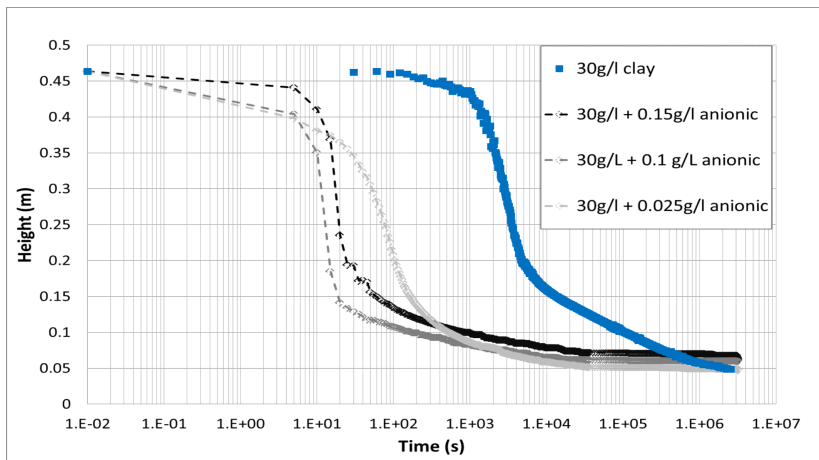


**Figure 6.6** – Evolution of clay interface at function of time during the consolidation test. Blue represent 30 g/L concentration clay, from black to light grey the samples contains 30 g/L clay with 0.15 g/L, 0.1 g/L and 0.025 g/L of anionic flocculant (close to optimal dose) respectively.

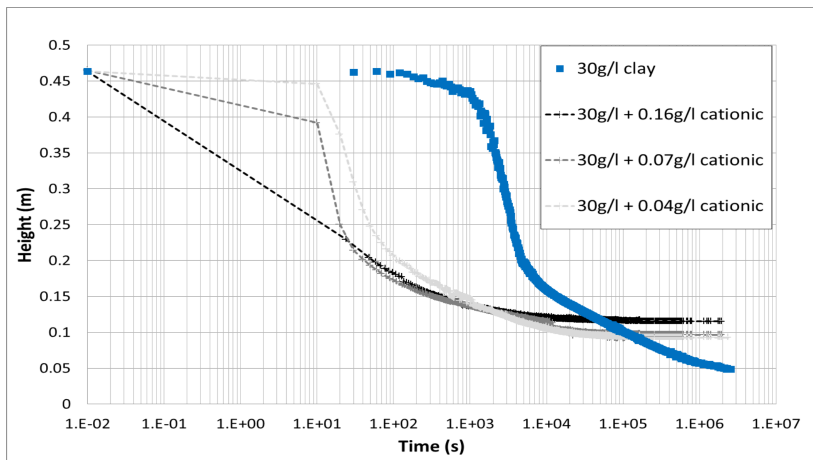


**Figure 6.7** – Evolution of clay interface at function of time during the consolidation test. Blue represent 30 g/L concentration clay, from black to light grey the samples contains 30 g/L clay with 0.16 g/L, 0.07 g/L (close to optimal dose) and 0.04 g/L of cationic flocculant respectively.

**Table 6.2** – Overview of  $\omega_s$  and  $c_{gel}$  results. Clay concentration, flocculant concentration,  $\omega_s$  and  $c_{gel}$ .

Clay[g/L]	Flocculant[g/L]	$\omega_s$ (m/s)	$\omega_{s,0}$ (m/s)	$c_{gel}$ (g/L)
30		$6.7 \times 10^{-5}$	$1.2 \times 10^{-4}$	281
50		$3.9 \times 10^{-5}$	$1.2 \times 10^{-4}$	281
70		$3.2 \times 10^{-5}$	$1.2 \times 10^{-4}$	281
30	0.04 cationic	0.004	$6 \times 10^{-3}$	53
30	0.07 cationic	0.0075	$6 \times 10^{-3}$	54
30	0.16 cationic	0.008	$6 \times 10^{-3}$	60
30	0.025 anionic	0.002	$7 \times 10^{-3}$	70
30	0.1 anionic	0.015	$7 \times 10^{-3}$	80
30	0.15 anionic	0.011	$7 \times 10^{-3}$	100

obtained by fitting the equation 6.4.4:

$$h(t) - \varsigma_s = \left( \frac{2-n}{1-n} \varsigma_m \right)^{\frac{1-n}{2-n}} \left( (n-2) k_k \frac{\rho_s - \rho_w}{\rho_w} \right)^{\frac{1}{2-n}} t^{\frac{1}{2-n}} \quad (6.4.4)$$

where  $\varsigma_m$  is the Gibson height defined for the total clay and silt solids,  $\varsigma_s$  is the Gibson height defined for sand only,  $h$  is the height of the sediment-water interface,  $\rho_w$  is the density of water,  $\rho_s$  the density of solids and

$$n = 2/(3 - n_f) \quad (6.4.5)$$

For the first phase of consolidation, the results of  $k_k$  and  $n_f$  are shown in table 6.3. In figure 6.8 the fitting for 30 g/L clay concentration is shown. The permeability parameter decreases when flocculant is added into the clay, at the same time that the fractal dimension of the flocs increases. The permeability parameter and fractal dimension for the clay used are  $2.2 \cdot 10^{-13}$  m/s and 2.63. The permeability parameter with cationic flocculant varies from  $4.6 \cdot 10^{-18}$  m/s to  $6.0 \cdot 10^{-17}$  m/s and fractal dimension from 2.79 to 2.76. With anionic flocculant permeability



parameter varies from  $1.4 \cdot 10^{-19}$  m/s to  $5.6 \cdot 10^{-15}$  m/s and the fractal dimension from 2.82 to 2.74.

The larger the fractal dimension, the more compact flocs are formed [Gregory, 1997]. From the structure of the flocs, see figures 6.9 and 6.10, it was observed that the flocs created with anionic flocculant were indeed more compact than the flocs created with cationic polymers. The permeability parameter values are very small when anionic and cationic flocculant are added to the system. This is in line with the increase in fractal dimension. Flocs formed with cationic polymers are subjected to diffusion-limited aggregation (DLA), which implies that each collision leads to aggregation. On the contrary when flocs are formed with anionic polymers there is an inter-particle repulsion, therefore collision efficiency decreases and aggregation is more reaction-limited [Klein and Meakin, 1989]. Reaction-limited aggregation (RLA), implies more dense flocs like in the case of flocs formed with anionic flocculant.

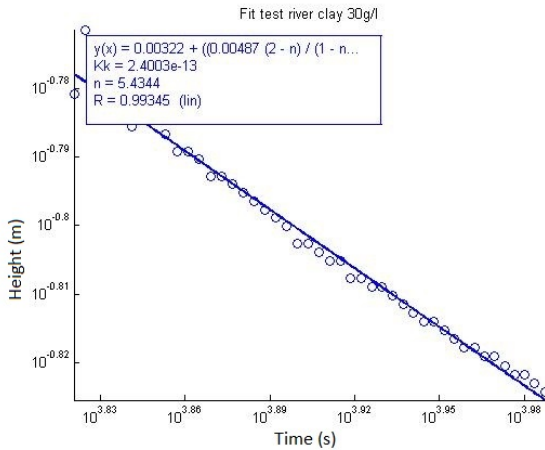


**Figure 6.8** – Permeability parameter obtained from the fitting of the data of the 30 g/L clay sample.

The permeability parameter shows in both cases, for cationic and anionic polymers, a decrease in permeability with respect to the clay sample. Therefore the amount of water trapped into the bed is larger,

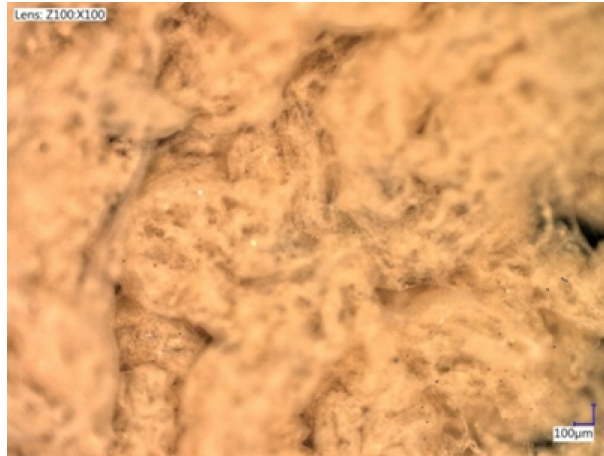


**Figure 6.9** – Flocs formed by clay and anionic polyelectrolyte.

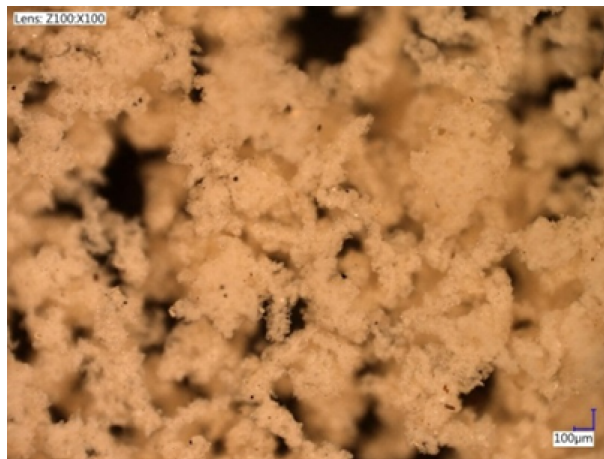


**Figure 6.10** – Flocs formed by clay and cationic polyelectrolyte.

creating a more fluffy bed. Figure 6.11 shows the permeability of 30 g/L clay, 30 g/L clay with 0.02 g/L anionic (optimal dose for anionic) and 30 g/L clay with 0.07 g/L cationic (optimal dose for cationic) as function of  $\phi$  (volumetric concentration). The optimal dose found in these experiments is line with the results found in chapter 4 and chapter 5. The permeability shown in figure 6.11 is calculated from the permeability parameters and fractal dimension with equation 6.4.3. At the end of the tests,  $\phi_s$  is between 0.1 and 0.12. In this range the permeability of the bed with cationic polymer is always the lowest. In the range of low  $\phi_s$  (volume fraction of sediments) the permeability of clay bed and clay with anionic bed are similar, confirming again that anionic polymers create more compact flocs than cationic.

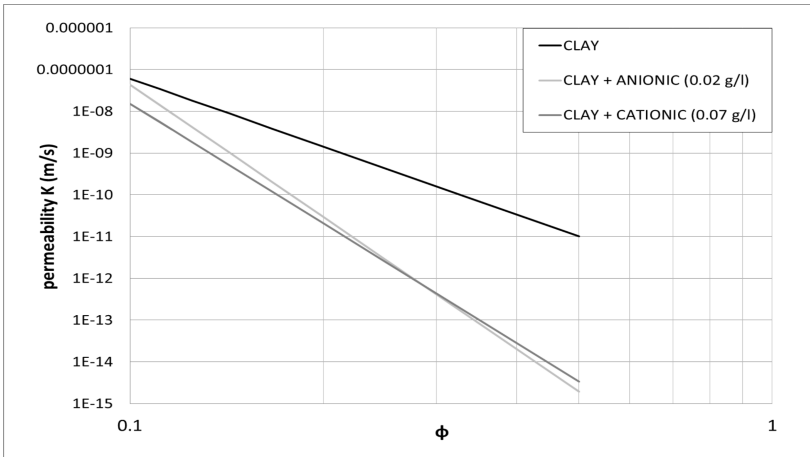


**Figure 6.11** – Permeability as function of  $\phi$  of 30 g/L clay and optimal dosage of cationic and anionic polyelectrolyte.

### 6.4.3 Final phase of consolidation

The final consolidation phase is characterized by small deformations of the bed. The effective stress parameter ( $K_p$ ) can be calculated by equa-

**Table 6.3** – Overview of  $k_k$  and  $n_f$  results. Clay concentration, flocculant concentration,  $k_k$  and  $n_f$ .

Clay [g/L]	Flocculant [g/L]	$k_k$ (m/s)	$n_f$
30	-	$2.4 \cdot 10^{-13}$	2.63
50	-	$1.9 \cdot 10^{-13}$	2.63
70	-	$2.2 \cdot 10^{-13}$	2.64
30	0.04 cationic	$6.0 \cdot 10^{-17}$	2.76
30	0.07 cationic	$4.6 \cdot 10^{-18}$	2.79
30	0.16 cationic	$5.3 \cdot 10^{-17}$	2.77
30	0.025 anionic	$5.6 \cdot 10^{-15}$	2.74
30	0.1 anionic	$1.3 \cdot 10^{-18}$	2.81
30	0.15 anionic	$1.4 \cdot 10^{-19}$	2.82

tion 6.4.6 [Merckelbach and Kranenburg, 2004a]:

$$h_\infty = \varsigma_s + \left( \frac{n}{n-1} \right) \frac{k_p}{g(\rho_s - \rho_w)} \left( \frac{g(\rho_s - \rho_w)}{k_p} \varsigma_m \right)^{\frac{n-1}{n}} \quad (6.4.6)$$

Where  $h_\infty$  is the final height of the bed. The results of effective stress parameter and shows in table 6.4.

The effective stress parameter calculated by equation 6.4.6 increases with polymers concentration. This increase of  $k_p$  indicates a larger effective stress of the bed. The effective stresses are defined by equation

To check whether the effective stress parameter values are correct, some quantitative measurements were done in the sediment bed. The sediment bed at  $h_\infty$  had to be used for further test, therefore a vane test was not possible as it would have disturbed the bed. Hence small weights of copper of known weight were placed on the top of the bed. A thread is attached to the weights to lower them down to the bed. No tension is induced on the thread once is deposited on the bed. The test starts with the smallest weight (1 g). The weight was increased each time when it was observed that the previous weight was stable on the

**Table 6.4** – Overview of  $k_p$  results. Clay concentration, flocculant concentration,  $k_p$ . The first three values of  $k_p$  for clay are not correct because at the experiment the equilibrium was not reached.

Clay [g/L]	Flocculant [g/L]	$k_p$ (Pa) at $h_\infty$
30	-	(9.92 $10^{+06}$ )
50	-	(6.91 $10^{+06}$ )
70	-	(8.06 $10^{+06}$ )
30	0.04 cationic	$1.26 \cdot 10^{+13}$
30	0.07 cationic	$2.27 \cdot 10^{+13}$
30	0.16 cationic	$9.7 \cdot 10^{+11}$
30	0.025 anionic	$8.97 \cdot 10^{+13}$
30	0.1 anionic	$1.26 \cdot 10^{+13}$
30	0.15 anionic	$2.48 \cdot 10^{+09}$

surface of the mud bed. Using the same principle as Van Kessel and Fontijn [van Kessel and Fontijn, 2000] a value for the vertical effective stress is obtained. Figure 6.12 shows a sketch of the weight on top of the mud bed. The sum of forces on the weight when it is stable on the mud bed is zero, hence:

$$m_p g = \sigma_{eff} A_p \quad (6.4.7)$$

where  $A_p$  is the area of the weight,  $m_p$  is the mass of the weight, and  $g = 9.81 \text{ m/s}^2$ . This gives:

$$\sigma_{eff} = \frac{m_p g}{A_p} \quad (6.4.8)$$

The results are plotted in figure 6.13. The measurements done with the weights give lower effective stresses than the model for clay. Larger stresses are found for the sample with anionic flocculant and smaller effective stresses for the cationic sample which is the one with more open flocs.

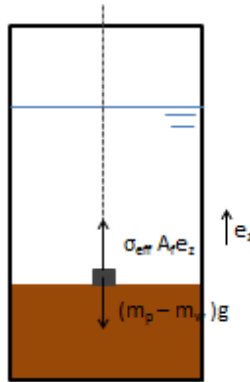


**Figure 6.12** – Drawing of the weight into the columns to measure the effective stress.

## 6.5 Conclusions

This chapter presents the behavior in consolidation of the same material (same granulometry) due to the addition of polymers. In this chapter, we focussed on the properties of the formed bed. It has been already explained in chapters 4 and 5 how polymers affect flocculation and settling of the sediments. A conceptual picture of the conclusions is shown in figure 6.14. The conclusions found from the study are:

- The gelling concentration decreases when polymers are used, as expected. The sediment bed is formed faster with polymers. For

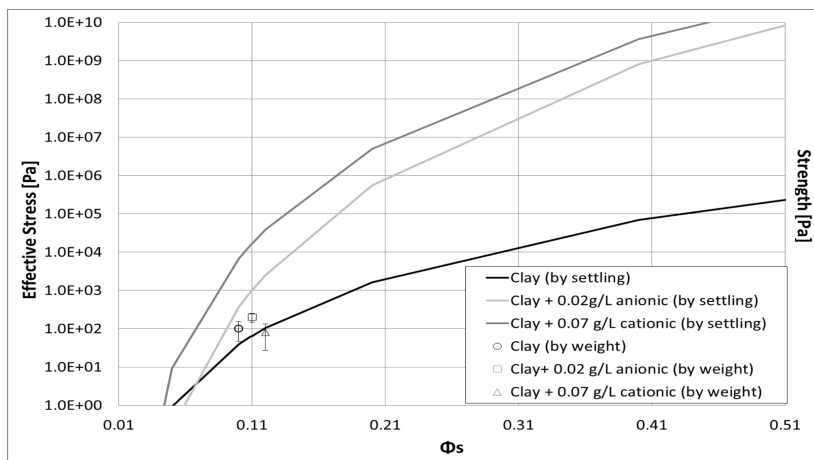


**Figure 6.13** – Effective stresses [Pa] as function of  $\phi$  for 30 g/L clay, 30 g/L clay and 0.02 g/L anionic flocculant, and 30 g/L clay and 0.07 g/L cationic flocculant (optimal doses). Symbols are the effective stress as the samples at the end of the test measured by weights. The lines are the mean effective stresses calculated by the model.

the optimal doses a smaller gelling concentration is found for the cationic flocculant than for the anionic.

- Settling velocities increase when polymers are used. The settling velocity is larger for the flocs formed by anionic polymer because they have a larger density than cationic flocs. The settling velocities found in this chapter have the same trend than the settling velocities found in chapter 5. Although, the settling velocities found in this chapter are ten times smaller than the ones obtained in chapter 5. The difference in velocities are due to hindered settling effect. The clay concentrations studied in chapter 5 are smaller therefore, settling velocities are larger.
- Fractal dimensions increased with the concentration of polymers. Flocs formed by cationic polymer and clay have smaller fractal dimensions than flocs formed by anionic polymer. The flocs formed by anionic polymer are less porous, so denser.
- In general, the hydraulic permeability decreases when polymers are used. The largest permeability is found for clay. The lowest value of permeability is found for samples containing anionic flocculant. This is confirmed by the final bed height, which is higher for bed containing flocculant.
- The effective stress parameter for anionic flocculant based flocs is large when calculated with Merckelbach and Kranenburg model [Merckelbach and Kranenburg, 2004a]. The effective stress was calculated in two ways. First, we used the approach developed by Merckelbach and Kranenburg [Merckelbach and Kranenburg, 2004a]. It appears that this model predict an effective stress that is higher for the bed formed by clay and cationic polymer than the bed formed by clay and anionic polymer and only clay beds. This result is counter-intuitive, as one would expect the open, fluffy flocs formed by clay and cationic polymer to form a bed with lower effective stress. By performing weight measurements on the top of each bed, we found on the other hand, what we expected: the clay bed has a higher effective stress than the bed formed by



clay and cationic polymer, but a lower effective stress than the bed formed by clay and anionic polymer. Clearly, the Merckelbach and Kranenburg model [Merckelbach and Kranenburg, 2004a] should be revised for the situation when flocculant is used. This will be of importance for the investigation of natural sediment, where organic matter plays the role of flocculant.

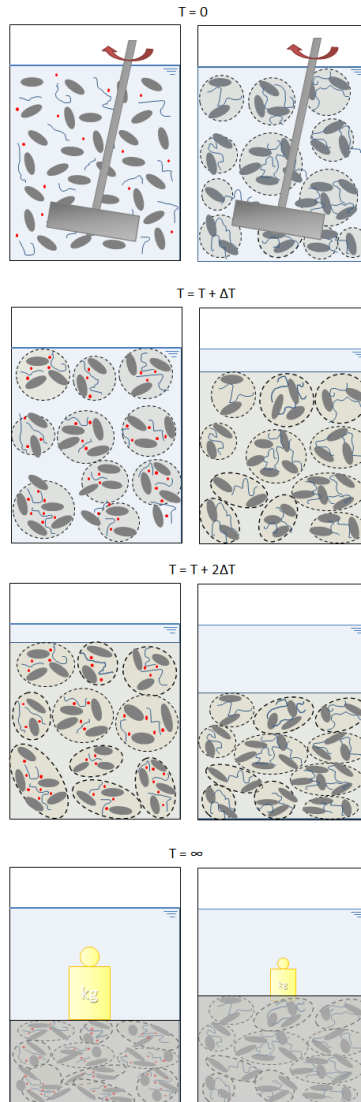


**Figure 6.14** – Conceptual picture of the consolidation test. The left column shows anionic polymers (blue), cations (red dots) and clay (grey particles) and the right column represents cationic polymer (blue) and clay (grey particles). The first row represents the beginning of the test, i.e. the mixing of the samples. The second row shows the flocculation and delay mechanism at the beginning of settling for the flocs created by anionic polymers, and beginning of settling for the flocs formed by cationic polymers. Third row is the settling phase. And fourth row represents the consolidation and the strength of each bed.



## References

- [centre for Policy Alternatives, 2016] centre for Policy Alternatives, C. (2016). cppa website.
- [COSIA, 2016] COSIA (2016). COSIA website. <https://www.cosia.ca/>. Accessed: 2015-04-30.
- [Dankers and Winterwerp, 2007] Dankers, P. and Winterwerp, J. (2007). Hindered settling of mud flocs: theory and validation. *Continental shelf research*, 27(14):1893–1907.
- [Gibson et al., 1967] Gibson, R., England, G., and Hussey, M. (1967). The theory of one-dimensional consolidation of saturated clays. *Geotechnique*, 17(3):261–273.
- [Gregory, 1997] Gregory, J. (1997). The density of particle aggregates. *Water Science and Technology*, 36(4):1–13.
- [Indraratna et al., 2011] Indraratna, B., Rujikiatkamjorn, C., Ameratunga, J., and Boyle, P. (2011). Performance and prediction of vacuum combined surcharge consolidation at port of brisbane. *Journal of Geotechnical and Geoenvironmental Engineering*, 137(11):1009–1018.
- [Klein and Meakin, 1989] Klein, R. and Meakin, P. (1989). Universality in colloid aggregation. *Nature*, 339(3).
- [Lee et al., 1987] Lee, S., Karunaratne, G., Yong, K., and Ganeshan, V. (1987). Layered clay-sand scheme of land reclamation. *Journal of geotechnical engineering*, 113(9):984–995.
- [Merckelbach and Kranenburg, 2004a] Merckelbach, L. and Kranenburg, C. (2004a). Determining effective stress and permeability equations for soft mud from simple laboratory experiments. *Géotechnique*, 54(9):581–591.

- [Merckelbach and Kranenburg, 2004b] Merckelbach, L. and Kranenburg, C. (2004b). Equations for effective stress and permeability of soft mud–sand mixtures. *Géotechnique*, 54(4):235–243.
- [Merckelbach, 2000] Merckelbach, L. M. (2000). *Consolidation and strength evolution of soft mud layers*. TU Delft, Delft University of Technology.
- [Mpofu et al., 2003] Mpofu, P., Addai-Mensah, J., and Ralston, J. (2003). Investigation of the effect of polymer structure type on flocculation, rheology and dewatering behaviour of kaolinite dispersions. *International Journal of Mineral Processing*, 71(1):247–268.
- [Novak and Langford, 1977] Novak, J. T. and Langford, M. (1977). The use of polymers for improving chemical sludge dewatering on sand beds. *Journal (American Water Works Association)*, pages 106–110.
- [Te Slaa et al., 2013] Te Slaa, S., He, Q., van Maren, D. S., and Winterwerp, J. C. (2013). Sedimentation processes in silt-rich sediment systems. *Ocean Dynamics*, 63(4):399–421.
- [Terashi and Katagiri, 2005] Terashi, M. and Katagiri, M. (2005). Key issues in the application of vertical drains to a sea reclamation by extremely soft clay slurry. *Elsevier Geo-Engineering Book Series*, 3:119–143.
- [van Kessel and Fontijn, 2000] van Kessel, T. and Fontijn, H. L. (2000). Miniature sounding tests on soft saturated cohesive soils. *GEOTECHNIQUE-LONDON-*, 50(5):537–546.
- [Winterwerp, 2002] Winterwerp, J. (2002). On the flocculation and settling velocity of estuarine mud. *Continental shelf research*, 22(9):1339–1360.
- [Winterwerp and Van Kesteren, 2004] Winterwerp, J. C. and Van Kesteren, W. G. (2004). *Introduction to the physics of cohesive sediment dynamics in the marine environment*. Elsevier.

## Chapter 7

# Application: use of electrophoretic mobility measurements to understand the stability of fine tailings suspensions

### Abstract

This study aims at understanding the role of specific ion types (monovalent/divalent) present in the water on the flocculation behavior and hence settling of sediments of interest for the oil sand industry. These sediments consist of thin fine tailings (TFT) and besides mineral sediment, contains traces of bitumen and organic matter. Kaolinite is investigated as well in this chapter, because between 40 to 70% of the oil sand sediments consist of kaolinite. The flocculation behavior of both TFT and kaolinite can be linked to the electrokinetic mobility (EM). The EM values were smaller in the case that divalent salt was used compared to the case where monovalent salt was used. As a consequence, both kaolinite and fine tailings flocculate faster in a divalent electrolyte dur-

ing settling columns experiments. The influence of pH was also studied. It was found that the flocculation of fine tailings in an electrolyte where divalent ions are predominant is not influenced by pH. No noticeable influence of bitumen on flocculation was observed during this study.

Most of the contents of this chapter have been published in:

- Ibanez, M., Wijdeveld, A., Chassagne, C. (2014). The role of mono-and divalent ions in the stability of kaolinite suspensions and fine tailings. *Clays and Clay minerals*, 62(5), 374-385.

## 7.1 Introduction

Canada has the third largest oil reserves in the world, and 97% of these reserves are in oil sands. The Athabasca oil sands located in northeast Alberta (Canada) are the largest known crude bitumen deposits in the world. Oil sands known also as bituminous sands are a type of petroleum deposit. Oil sands are a mixture of sand, clay, water and viscous bitumen. The current study focuses on the fine tailings from Athabasca oil sands. These fine tailings are a by-product of the oil sand extraction process, and contain suspended silts, clays, and hydrocarbon residues. In the Clark hot water extraction process, bitumen is separated from the slurry, and tailings are pumped into tailing ponds [Clark, 1939, Clark and Pasternack, 1932]. Upon deposition, the tailings segregate about one-half of the fines drop out with sand to form dikes and beaches. The large remaining waste volumes are composed of water, traces of bitumen, and fines which are discharged into tailings ponds as thin fine tailings (TFT). The existing tailings ponds cover 176 km<sup>2</sup>, and were formed by active mining over 30 to 40 years. The Canadian government requires that all lands disturbed by oil sands operations should be reclaimed as solid surface (Canadian Government). Currently COSIA (Canada's Oil Sands Innovation Alliance) works together with universities, companies, government and research institutes to improve the management of oil sand tailings. A major issue for the oil sand industry is the settling of the fines. After a few years the suspended fines are referred to as mature fine tailings (MFT). The MFT remain in a fluid-like state for decades because of their very slow consolidation rate [Kasperski, 1992, MacKinnon, 1989].

Different technologies are used to accelerate TFT/MFT settling, like: 1) the use of centrifuge force and polymers to speed up removal of process water from the thin fine tailings, 2) a filtering technology to dewater tailings before they deposit in the ponds; 3) addition of CO<sub>2</sub> into the tailings line to increase dewatering [COSIA, 2016].

Several studies [Liu et al., 2002, Zhu et al., 2011] have been devoted to the investigation of the interfacial properties and electrokinetic charge of TFT in relation with their flocculation behavior, induced by



the addition of polymers, the presence of salts, and the reduction of pH by CO<sub>2</sub> bubbling.

This chapter shows how the electrophoretic mobility theory studied in chapter 3 can be applied. In particular:

- A link is to be established between the electrophoretic mobility of TFT and of kaolinite of which the TFT is mostly composed of. Electrophoretic mobility experiments give access to the electrokinetic charge of suspended particles. These results are compared to the flocculation and settling properties of TFT.
- The effect of lowering the pH by bubbling with CO<sub>2</sub>, as often done in oil sands industry to improve flocculation is critically analyzed.

## 7.2 Materials

### 7.2.1 Thin fine tailings

The thin fine tailings were sampled from Athabasca oil sands ponds, north of Edmonton (Alberta, Canada) are hereafter referred to as "SP02" samples. The samples are representative of tailings that are deposited in ponds. The suspensions were prepared at the desired concentration by addition of demi-water with a resistivity of 18 MOhm-cm. The original ionic concentration is lowered until 0.03 mS/cm, so that ionic strength dependence measurements could be performed. The sample contains kaolinite/muscovite, dickite, quartz, and NaCl. This composition has been obtained from XRD measurements. The D<sub>50</sub> of the SP02 sample obtained from static light scattering was similar to that of the kaolinite sample; it was around 17 μm, see figure 7.1.

### 7.2.2 Kaolinite

The kaolinite sample was polywhite-E kaolinite from deposits in the South West of England. The material has a surface area of 8 m<sup>2</sup>/g and a specific density of 2.6 g/cm<sup>3</sup>; these values were given by the manufacturer. The kaolinite sample composition was analyzed by XRD measurements and found to contain kaolinite, muscovite, and dickite. The D<sub>50</sub>

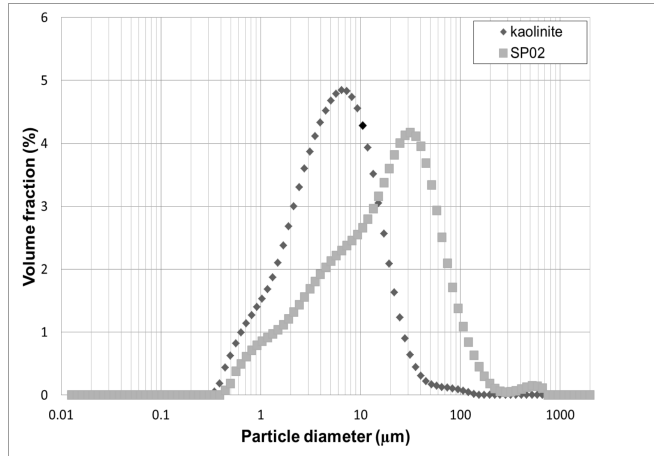


**Figure 7.1** – Particle size distribution of kaolinite (black) and TFT sample SP02 (gray) samples.

of the kaolinite sample was  $5.7 \mu\text{m}$  obtained from static light scattering see figure 7.1.

Two samples of kaolinite were prepared to study their zeta potential. One was dialyzed; the dialyzing procedure was as follows: a suspension of kaolinite in water of 20% wt was prepared. After settling, the water remaining at the supernatant (at the top) was replaced by ultrapure water (18 MOhm-cm) every day until the conductivity of the supernatant reached a value of  $3 \mu\text{S}/\text{cm}$ . The non-dialyzed sample was a solution of kaolinite dispersed as received in ultrapure water, 20% wt. The sample had a conductivity of  $0.63 \text{ mS}/\text{cm}$ . The salts used during the experiments were provided by the manufacturer MERK. The element composition of the SP02, kaolinite and kaolinite dialyzed samples was also analyzed by ESEM. The bulk sample is a sample from the stock taken after it has been mixed thoroughly. The composition showed in particular a difference in Si element between SP02 supernatant and bulk, denoting a predominance of silica-based particles ( $\text{SiO}_2$ ) in the bulk (table 7.1).

**Table 7.1** – Composition (wt%) of kaolinite and SP02 samples.

	SP02 bulk	SP02 supernatant	Dialyzed kaolinite	Non-dialyzed kaolinite
C	20.0	23.7	-	-
O	41.6	39.8	50	46.6
Na	1.2	-	4.7	-
Mg	0.6	1.0	-	-
Al	4.6	9.6	21.2	21.5
Si	29.1	14.5	24.9	25.9
S	-	-	1.1	-
Cl	-	2.3	-	-
K	1.3	1.6	2.8	4.3
Fe	1.5	1.7	1.0	1.7

## 7.3 Methods

### 7.3.1 XRD measurements

X-ray is detailed in chapter 2.

### 7.3.2 ESEM measurements

Environmental Scanning Electron Microscope (ESEM) is detailed in chapter 2.

### 7.3.3 Particle size from static light scattering

Particle size distribution experiments were performed according to the protocol defined in chapter 2. The particle size distributions of kaolinite and fine tailings samples were measured at  $\text{pH} = 7$  by Static Light Scattering (7.1). The conductivity of the samples was below 1 mS/cm (no salt added) to prevent flocculation.

### 7.3.4 Electrophoretic mobility measurements

The electrophoretic mobility of the suspensions was measured using a ZetaNano ZS device, see chapter 3. The electrophoretic mobility values (typically in  $\text{m}^2/\text{Vs}$  units) will be given as "apparent" zeta potential values (in mV) as done by many other authors by using the Smoluchowski formula (3.4.1). The "apparent" zeta potential is a qualitative measure and it helps to understand the electrophoretic behaviour of suspensions [Chassagne et al., 2009]. The "apparent" zeta potential measurements were carried out as a function of pH, type and concentration of electrolyte, and concentration of solid in solution. An average of 10 measurements was taken to represent the mean measured potential. The applied voltage during the measurements was 50 V, as was already found out to be an optimal value for these types of measurements [Chassagne and Ibanez, 2014]. The series of measurements in which the salt concentration was varied were always performed following the protocol given in chapter 3.

The SP02 sample was diluted with ultrapure water until a concentration (0.1 g/L) giving a good signal-to-noise ratio in the electrophoresis measurements was obtained. The zeta potential experiments were carried out at different pHs; the pH was adjusted by addition of NaOH or HCl. The pH values were 4, 6, and 8 with divalent salt ( $\text{MgCl}_2$ ) or monovalent salt (NaCl).

The kaolinite samples (dialyzed or not) were diluted with ultrapure water until a concentration of 0.26 g/L, supplying a good signal-to-noise ratio in the electrophoresis measurements. For the non-dialyzed samples, the influence of the particle volume fraction was investigated. The zeta potential experiments were carried out at different pHs; the pH was adjusted by addition of NaOH or HCl. The pH values were 4, 6, and 8 with divalent salt ( $\text{MgCl}_2$ ) or monovalent salt (NaCl). In one of the experiments, the pH was also lowered by increasing the amount of dissolved  $\text{CO}_2$ . The obtained "apparent" zeta potential was compared with the one obtained by changing the pH by adding HCl.

### 7.3.5 CO<sub>2</sub> bubbling

A closed cylinder (a triaxial cell) with a gas inlet and an open gas outlet was used. One liter of water was bubbled with a gas mixture of 90% N<sub>2</sub> and 10% CO<sub>2</sub>, at a flow rate of 200 mL/min. The gas was pre-wetted by using a water-filled container to prevent evaporation in the triaxial cell. Bubbling was stopped when the desired pH (6.3) was reached. A pH check after finishing the measurements showed a maximum pH increase of 0.1 units during the time of measurement. The pH of the kaolinite suspension was reduced by bubbling with 100% pure CO<sub>2</sub> gas until the pH achieved the value of 5. The suspension was then used directly in the zeta nano measurement cell. The measurements were performed immediately.

## 7.4 Results and discussion

### 7.4.1 Particle size

Both kaolinite and SPO2 samples are polydispersed, as confirmed by Static Light Scattering see figure 7.1. Figure 7.2d, 7.2e and 7.2f show the ESEM pictures of the SP02 sample. Flocculated material is apparent in the ESEM picture of the SP02 supernatant (Figure 7.2f). The carbon content is unreliable due to the presence of the carbon-based wafer onto which the sample is deposited. We can only assume that hydrocarbons (bitumen) form the observed matrix in which the smallest colloidal particles are trapped. Figure 7.2a shows the ESEM picture of the kaolinite sample and figure 7.2b and 7.2c show the ESEM pictures of the kaolinite dialyzed sample. It was not possible to measure the supernatant particle size of SP02, because (see figure 7.2f) bitumen was present and the material was aggregated.

The particle size distribution of the kaolinite supernatant was also not measurable by Static Light Scattering because the concentration of the sample was too low. The particle size was therefore measured with the ZetaNano ZS device by Dynamic Light Scattering. The radius of the supernatant particles of kaolinite sample was found to be 92 nm at pH 7.

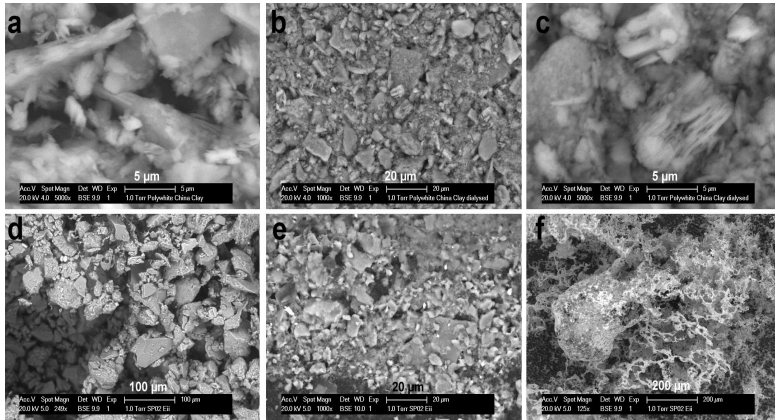


**Figure 7.2** – ESEM pictures: a) kaolinite; b and c) dialyzed kaolinite samples at different magnifications; d, e, and f) SP02 samples at different magnifications.

#### 7.4.2 Electrophoretic mobility

Electrophoretic mobility data gives information about the electrokinetic charge of particles. This electrokinetic charge is related to the surface charge of the particles and its zeta potential, but the relationship between electrokinetic charge and surface charge is only available for simple systems like for example spherical homogeneously charged particles. The kaolinite particles are flat disks, or plate-like in shape, with the disk radius about 5 – 15 times larger than their thickness [Solomon and Hawthorne, 1983]. The kaolinite surface properties are known to be sensitive to both pH and ionic strength and ion type [Kaya et al., 2006, Ma and Pierre, 1999, Ma, 2011, Vane and Zang, 1997]. The platelet particle has pH-dependent edge and surface charges [Mitchell et al., 1976]. Gupta and Miller [Gupta and Miller, 2010] and Zhou and Gunter [Zhou and Gunter, 1992] demonstrated that the point of zero charge of the alumina face of kaolinite is about 6 – 8 which implies that only at pH larger than 8 the kaolinite platelets are fully negatively charged. This should have effects on the flocculation behavior of kaolinite at pH below 8. The "apparent" zeta potential defined above via the Smoluchowski formula (

equation 3.4.1 in chapter 3) is equal to the actual zeta potential when the Debye length,  $1/\kappa$ , is much smaller than the particle size  $L$  ( $\kappa L > 1$ ) for particles of any shape, provided that the contribution of surface conductivity is neglected [Morrison, 1970]. For the smallest particles in this study, which were the kaolinite particles,  $\kappa L$  was roughly equal to 10 for the smallest ionic strength used in case of KCl (monovalent salt) and 16 in case of  $MgCl_2$  (divalent salt). Morrison's condition [Morrison, 1970] is in principle respected for ionic strength above 10 mM where  $\kappa L > 1000$  for both mono and divalent salts. However this condition is only valid for particles with an "ideal" surface implying that the shear plane is located at the particle surface (no Stern layer) and that the electric surface potential is everywhere the same on the surface and equal to the zeta potential. These two last conditions are not true for kaolinite, as demonstrated in [Chassagne et al., 2009] and most probably, neither for SP02, as TFF consists largely of kaolinite. Therefore at small ionic strength the "apparent" zeta potential does not indicate the flocculation behaviour.

Ideally, the electrophoretic mobility of particles should be independent of the particle concentration during the time of the electrophoresis measurements. This means that there are no particle-particle interactions and that the "apparent" zeta potential is representative of the electric potential at the shear plane of one particle. However, at (very) low ionic strength, the double layers around the particles may overlap, leading to inter-particle interactions. The mobility of the particles would then be affected by the presence of neighboring particles.

The "apparent" zeta potential of the dialyzed kaolinite sample did not vary much as function of the solid concentration (figure 7.3), not even without added salt, when the double layers are large. The interaction between particles can therefore be neglected. Besides, the experimental time is short enough (less than 2 minutes) to ensure that even at low pH, attraction between particles will not lead to major flocculation. The electrophoretic mobility measurements performed in the rest of the chapter were done at a volume fraction of about 0.1% (0.26 g/L).

A systematic investigation of the particle concentration dependence of the electrophoretic mobility of fine tailings (SP02) was not done,

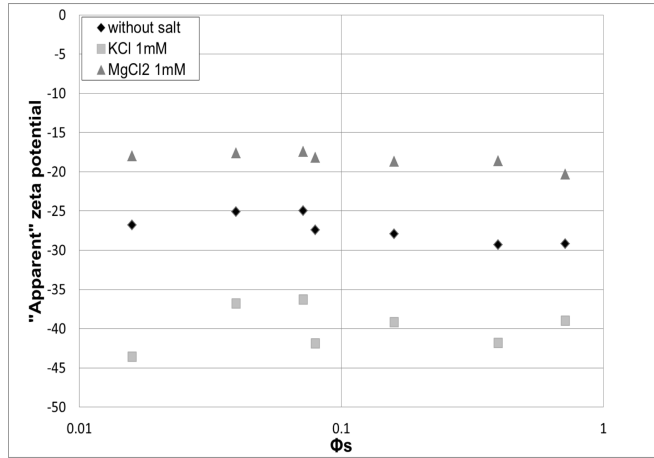


**Figure 7.3** – Zeta potential of the kaolinite sample as a function of solids volume-fraction percentage.

but within the range of volume fraction used (0.1% - 0.3%), the electrophoretic mobility did not vary.

The apparent zeta potential of kaolinite as function of mono- and divalent salts was studied. Monovalent salts affect the compression of the double layer in a different way than divalent salts, as for the same salt concentration the double layer formed by monovalent salt is  $\sqrt{3}$  larger than the double layer formed by divalent salt. Some types of salts are indifferent, in the sense that they only contribute to the double layer and others could react with the particle surface, hereby changing its surface charge. Information about particles' surface charge can therefore be gained by studying the electrophoretic mobility behavior as function of different monovalent and divalent salts.

The samples were dispersed in two types of electrolyte solutions, containing divalent salt ( $\text{MgCl}_2$ ) and monovalent salts (KCl and NaCl) at  $\text{pH} = 6$  (Figure 7.4, 7.5 and 7.6). The potential-determining counter ions are  $\text{Mg}^{2+}$ ,  $\text{K}^+$  and  $\text{Na}^+$ . The electrophoretic mobility experiments reveal that in the ionic strength range investigated, the apparent zeta potential was always negative.



From the particle size distribution of the sample it was found that the supernatant particle' size is about 10 times smaller than the bulk size. The zeta potential of the non-dialyzed kaolinite supernatant was always lower in absolute value than the zeta potential of the kaolinite bulk sample (figure 7.4).

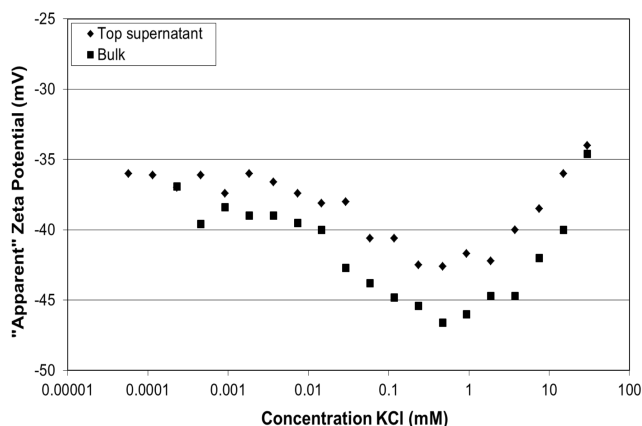


**Figure 7.4** – Zeta potential of bulk and supernatant non-dialyzed kaolinite samples as a function of the concentration of KCl salt.

Even if the surface charge properties of the supernatant and bulk particles are the same, their apparent zeta potential should be smaller for the smallest particle size in the salt concentration investigated (see figure 7.5). The minimum of the curves is therefore shifted towards higher ionic strength. In the theoretical example of figure 7.5 spherical particles of radius  $2.5 \mu\text{m}$  and  $100 \text{ nm}$  with constant charge ( $0.02 \text{ C/m}^2$ ) and no Stern layer were used (chapter 3). The trend observed in figure 7.4 is therefore not surprising.

In figure 7.6 the differences between the apparent zeta potential of dialyzed and non-dialyzed kaolinites for different types of cations ( $\text{NaCl}$  and  $\text{MgCl}_2$ ) are presented. The behavior of the apparent zeta potential of non-dialyzed kaolinite, as function of  $\text{NaCl}$  was different. The magnitude of the apparent zeta potential values is lower in case of  $\text{NaCl}$  as

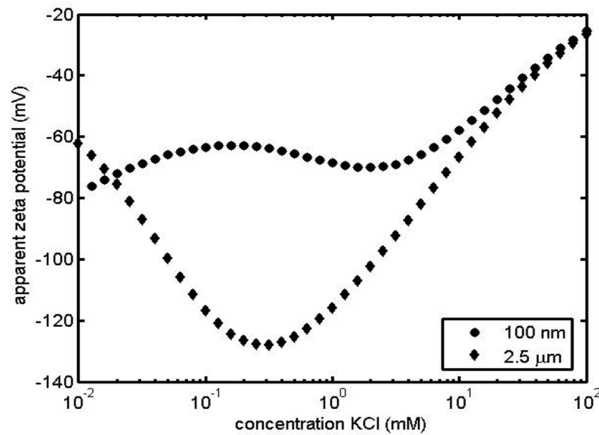


**Figure 7.5** – Theoretical values of zeta potential of the bulk and supernatant kaolinite samples as a function of the concentration of KCl salt.

compared to KCl from its behavior upon addition of KCl. And the apparent zeta potential is less sensitive upon addition of NaCl than KCl in the range of  $[0 - 0.1]$  mM of added salt. Moreover the conductivity variation upon added salt concentration for both NaCl and KCl (not shown here) revealed that, due to the impurities of the non-dialyzed sample, ions were present in the suspension in an amount corresponding to 0.1 mM of added monovalent salt.

### **Monovalent salt**

An explanation for this behavior is that  $K^+$  acts as an indifferent ion for kaolinite: the surface charge of kaolinite is insensitive to the addition of more amount of  $K^+$  ions in the suspension. The addition of an extra amount of  $K^+$  ions contributes only to increase the conductivity and reduce the size of the double layer around the particles. The apparent zeta potentials shown in figure 7.4 and 7.5 correspond to the expected behavior of the apparent zeta potential for a constant charge particle in the presence of indifferent ions.

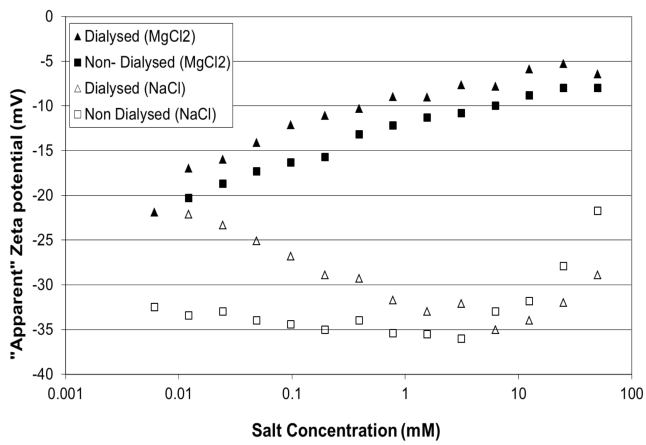


**Figure 7.6** – Zeta potential of a dialyzed kaolinite sample as a function of MgCl<sub>2</sub> salt (filled triangles); zeta potential of a dialyzed kaolinite sample as a function of NaCl salt (open triangles); zeta potential of a non-dialyzed kaolinite sample as a function of MgCl<sub>2</sub> salt (filled squares); zeta potential of nondialyzed kaolinite sample as a function of NaCl salt (open squares).

In case of added  $\text{Na}^+$  ions the apparent zeta potential variation upon addition of salt does not correspond to a constant surface charge behavior. This indicates that  $\text{Na}^+$  ions adsorb on the kaolinite within the time of the experiments (about 2 minutes), making the surface charge less negative. This can explain why the values obtained for the apparent zeta potential are smaller in absolute values than the ones obtained with added KCl (see figures 7.4 and 7.6. At very low concentrations of added salt, the conductivity should in principle vary less than the theoretical conductivity; this could not be measured as the change would be very small for the small particle volume used. In the  $[0.01 - 0.1]$  mM range of added salt, the apparent zeta potential of the dialyzed sample changes much compared to the apparent zeta potential of the non-dialysed sample. In the dialyzed case, the double layer thickness varies much more upon addition of salt because there is no background electrolyte present, giving a larger variation in the apparent zeta potential.

Kaya *et al.* [Kaya et al., 2006] used a washed Georgia kaolinite and found values intermediate between the dialyzed and non-dialyzed values, for the zeta potential as function of NaCl concentration at the same pH. Their kaolinite was first saturated with ammonium acetate ( $\text{CH}_3\text{COONH}_4$ ) and then thoroughly washed with demi-water until the electrical conductivity of the supernatant was below 100 MOhms.

From the flocculation combined with zeta potential studies of Kaya *et al.* [Kaya et al., 2006] it is expected that samples at low ionic strength (0.1 mM) will not flocculate and samples at high ionic strength (10 mM) will flocculate. As the apparent zeta potential for monovalent salt is roughly the same at 0.1 and 10 mM as expected for constant charged particles, it can be concluded that this parameter alone is not suitable for predicting flocculation.

### Divalent salt

In the case of divalent salt ( $\text{MgCl}_2$  and  $\text{CaCl}_2$  (see figure 7.6 and 7.9)), both dialyzed and non-dialyzed kaolinite display the same behavior upon addition of salt. This behavior is different from what would be expected for constant charged particles (see figure 7.11 in [Chassagne and Ibanez, 2012]). Yukselen and Kaya [Yukselen and Kaya, 2003] and Kaya *et*

*al.* [Kaya et al., 2006] found a similar trend and values with their samples of 96% kaolinite (Evans Clay, Georgia). For any divalent salt, at concentrations above 1 mM of added salt, the zeta potential is so small (around -10 mV) that flocculation is expected. This did probably not occur at the time-scale of the electrophoretic measurements, as the measurements were fast (minutes) and the suspensions were very diluted.

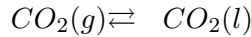
From the work of Kaya *et al.* [Kaya et al., 2006] it is expected that samples at low ionic strength (0.1 mM) in the presence of divalent salt will not flocculate and samples at high ionic strength (10 mM) will flocculate at all pHs. In our experiments, the apparent zeta potential for divalent salt is much smaller (in absolute value) at 10 mM than at 0.1 mM. A quantitative value for the apparent zeta potential at flocculation threshold can be obtained from  $kT/e \sim 25\text{mV}$  at room temperature. This quantitative value is inappropriate for non-spherical particles, as demonstrated in [Chassagne et al., 2009]. From figure 7.6, it can be seen that the apparent zeta potential is below 25 mV in the whole range of ionic strength investigated. The model linking zeta potential and mobility/dielectric response from Chassagne *et al.* [Chassagne et al., 2009] did however not take into account the inhomogeneous distribution of surface charge. As the isoelectric point of the alumina octahedral face lays between pH 6 and 8 [Gupta and Miller, 2010] the surface charges of the kaolinite faces could have opposite signs at pH 6. This could lead to face-face attraction in this pH range and therefore settling.

### 7.4.3 Difference between changing pH with HCl and CO<sub>2</sub>.

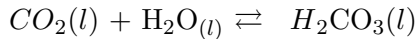
In the Canadian oil sands mining industry the pH of the fine tailings is controlled in situ by adding CO<sub>2</sub>. A systematic study of the pH dependence (adjusted by CO<sub>2</sub> bubbling) on the densification of oil sands tailings has been performed by Zhu *et al.* [Zhu et al., 2011]. In this study, the authors described in particular how bubbling CO<sub>2</sub> into fine tailings improves the supernatant clarity and the initial settling rate of the sediment. They correlated these findings to the fact that the zeta potential decreases in absolute values upon a decrease of pH when either CO<sub>2</sub> bubbling or when HCl is added.

In this section the process leading to flocculation by lowering pH is

studied. In order to lower the pH by CO<sub>2</sub> bubbling, the kaolinite samples were transferred into the jar in which a pH meter and a pressure sensor were installed. The CO<sub>2</sub> was bubbled with 100% pure CO<sub>2</sub> until the pH became 5. The injection of CO<sub>2</sub> bubbles leads to the dissolution of carbon dioxide in water:

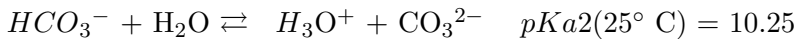
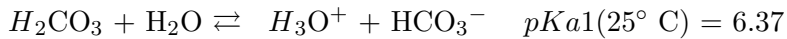


Equilibrium is established between the dissolved CO<sub>2</sub> and H<sub>2</sub>CO<sub>3</sub>, carbonic acid.



(7.4.2)

Carbonic acid is a weak acid that dissociates in two steps:



The injection of CO<sub>2</sub> therefore leads to the production of H<sup>+</sup> (H<sub>3</sub>O<sup>+</sup>) which leads to a pH drop (figure 7.7) for an unbuffered water system with an increasing CO<sub>2</sub> percentage inside the gas bubble from atmospheric (0.4%) to 100% CO<sub>2</sub>. The model used to calculate the evolution of CO<sub>2</sub> fraction in the gas phase of pH, assumes equilibrium between the gas phase and the water phase.

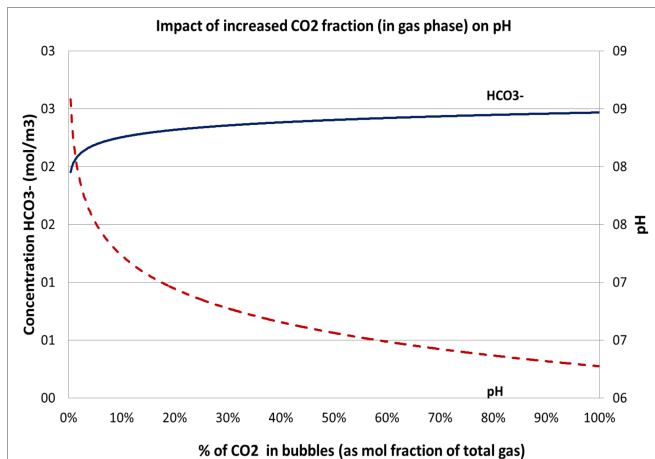


**Figure 7.7** – Model of the impact of increased CO<sub>2</sub> fraction in the gas phase on pH. Red line is the evolution of pH as function of percentage CO<sub>2</sub> gas. And the blue line is the evolution of HCO<sub>3</sub><sup>-</sup> concentration as function of CO<sub>2</sub> gas.

The sample was then quickly injected (less than 5 minutes) in the measurement cell and put into the Zeta Nano device to measure the Zeta Potential. The degassing of CO<sub>2</sub> could not be measured directly due to the small size of Zeta Nano measurement cell. For validation, a glass beaker was used to test the atmosphere/water transfer rate for over/under saturation. An oxygen sensor was used to determine that transfer rate (figure 7.8). The timescale for complete (de)gassing is hours. If the CO<sub>2</sub> loss during the Zeta Potential measurement is comparable to the degassing rate found in figure 7.8, than the pH loss would be less than 0.2 pH units.

We found for kaolinite, like Zhu *et al.* [Zhu et al., 2011] for fine tailings, that for divalent salt there was no difference between changing the pH from 8 to 5 by adding CO<sub>2</sub> gas or HCl (figure 7.9) in the same range of concentration investigated by these authors. Zhu *et al.* [Zhu et al., 2011] investigated samples dispersed in process water which contains less than 25 mg/L of CaCl<sub>2</sub> (equivalent to less than 1 mM of added salt).

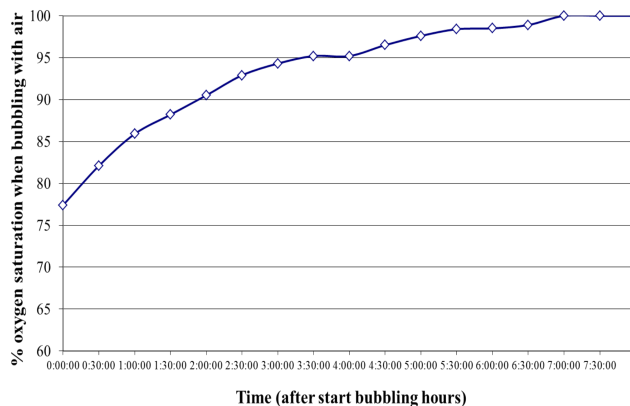


**Figure 7.8** – Evolution of oxygen concentration in water when bubbling with air.

Above 10 mM of added  $\text{CaCl}_2$ , a difference was found between bubbling with  $\text{CO}_2$  or adding HCl (figure 7.9). The fact that the zeta potential became positive at high ionic strengths was also found by Chassagne *et al.* [Chassagne et al., 2009]. Chassagne *et al.* [Chassagne et al., 2009] used a China clay diluted in tap water and found a similar behavior and similar values for the zeta potential as function of pH and added  $\text{CaCl}_2$ . The values were not exactly the same, due to the fact that in this study ultrapure water was used and tap water was used in theirs. Kaya *et al.* [Kaya et al., 2006] found almost the same values as ours for the zeta potential as a function of pH and  $\text{CaCl}_2$  concentration.

However, the measurements at this high ionic strength were very difficult: the apparent zeta potential values increased in time during the measurements as did the conductivity. The apparent zeta potential values given here are the average of the three first measurements. Bubbles were created during the measurements, and the electrodes turned black, so only a few measurements were performed in this concentration range.



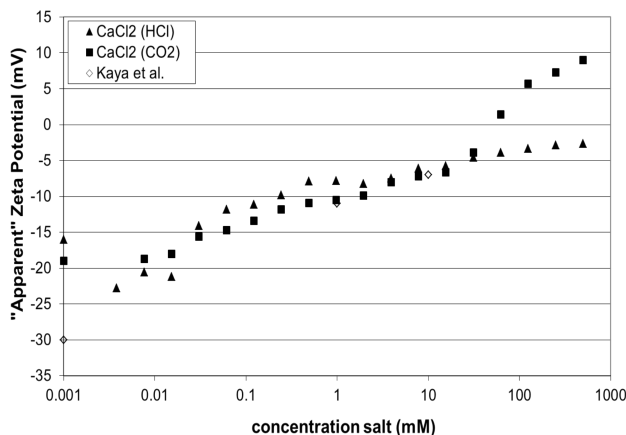


**Figure 7.9** – Zeta potential at pH = 5 of a kaolinite sample as a function of CaCl<sub>2</sub> salt when the pH is adjusted with HCl (triangles) and with CO<sub>2</sub> (squares).

#### 7.4.4 Effect of pH on SP02 and kaolinite in the presence of monovalent and divalent electrolyte.

A different behavior between the zeta potential of SP02 and kaolinite was observed upon addition of monovalent and divalent electrolyte at different pH. In the case of a monovalent electrolyte, like NaCl, the zeta potential varied significantly with pH. The zeta potential of the samples decreased in absolute value when pH decreased. This was true for both kaolinite and SP02 samples (figure 7.10). Kaya *et al.* [Kaya et al., 2006] and Yukselen and Kaya [Yukselen and Kaya, 2003] found similar values as function of pH and NaCl concentration for their kaolinite samples. The zeta potential was always lower in absolute values for the SP02 sample than the zeta potential of kaolinite below 1 mM of added NaCl. For larger ionic strengths, the zeta potentials of the SP02 samples were systematically higher in absolute values compared to the kaolinite samples and the differences between the zeta potentials of kaolinite and SP02 are higher than at low ionic strength. The kaolinite zeta potential decreased at large ionic strength, in line with what is expected from the

shielding of the surface charge by double layer ions [Hunter, 2013] as can be seen in figure 7.9.

The behavior of the SP02 surface charge at large ionic strength appeared to be more complex. An earlier study from Liu *et al.* [Liu et al., 2002] has demonstrated the impact of bitumen on the zeta potential of tailings. They showed in particular that kaolinite samples with bitumen at 1 mM KCl at pH = 8 had an average zeta potential larger in absolute values than kaolinite samples without bitumen at 1 mM KCl at pH = 8. The zeta potential of the bitumen emulsion alone was about  $-70$  mV at pH = 8. As traces of bitumen are present in the SP02 samples, this can be the reason for the large (in absolute values) zeta potentials at ionic strengths above 1 mM of NaCl. This should be confirmed by studying samples in presence and absence of bitumen.

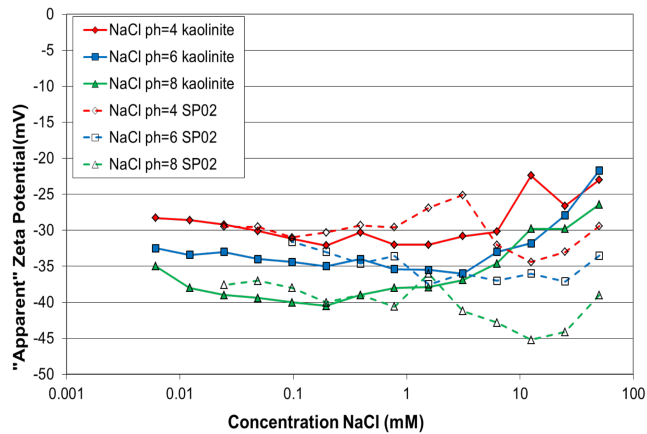


**Figure 7.10** – Zeta potential as a function of the NaCl salt kaolinite sample at pH = 8 (filled triangles); SP02 samples at pH = 8 (open triangles); kaolinite sample at pH = 6 (filled squares); SP02 samples at pH = 6 (open squares); kaolinite sample at pH = 4 (filled diamonds); SP02 samples at pH = 4 (open diamonds).

The zeta potential of kaolinite and fine tailings suspended in a  $MgCl_2$  solution with different values of pH was studied. The zeta potential of the kaolinite immersed in the  $MgCl_2$  electrolyte had a similar behavior

compared to the zeta potential of the fine tailings. In the case that divalent ions were present in the electrolyte, Liu *et al.* [Liu et al., 2002] found that the presence or not of bitumen did not change the zeta potential of kaolinite. The differences between both samples were that the SP02 has slightly higher zeta potentials in absolute value than kaolinite (figure 7.11). The zeta potential behavior was independent of the value of the pH, so a trend could not be found like with monovalent salts (figure 7.10).

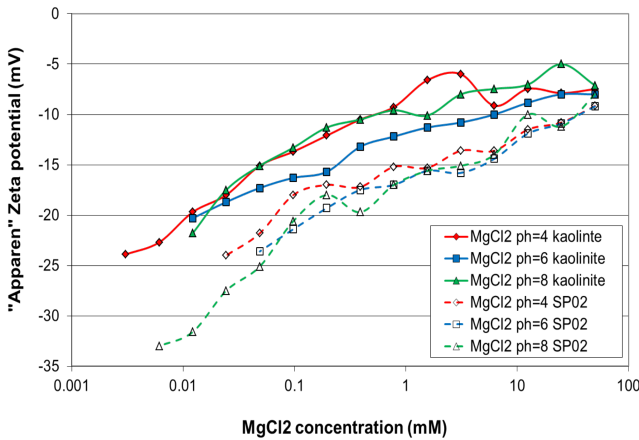


**Figure 7.11** – Zeta potential as a function of MgCl<sub>2</sub> salt kaolinite sample at pH = 8 (filled triangles); SP02 samples at pH = 8 (open triangles), kaolinite sample at pH = 6 (filled squares); SP02 samples at pH = 6 (open squares); kaolinite sample at pH = 4 (filled diamonds); SP02 samples at pH = 4 (open diamonds).

From the apparent zeta potential results, we expected fast flocculation above 5 mM of added salt at any pH in the presence of divalent salt (since the apparent zeta potential becomes very small for these ionic strengths). This conclusion was confirmed by settling column experiments, for which a higher clarity in the supernatant and a faster settlement were observed with the divalent salt (for both kaolinite and SP02) compared to monovalent salt. Kaya *et al.* [Kaya et al., 2006] found similar results when studying the settling of kaolinite in different

aqueous environments.

In an electrolyte where monovalent ions are dominant, the flocculation ability would be more sensitive to pH as the apparent zeta potential is reduced with a decreasing pH (more acidic solution). However, the values of the apparent zeta potential for added monovalent ions at the smallest pH were always larger (in absolute values) than the apparent zeta potential for divalent ions for ionic concentration above 0.1 mM of added salt. The in-situ flocculation of the fine tailings will be greatly influenced by the presence of even a small amount of divalent salt, independently on pH. Zhu *et al.* [Zhu et al., 2011] found a clear supernatant and a faster settling for samples treated with CO<sub>2</sub>. It was observed that when the samples were treated with CO<sub>2</sub> the amount of divalent ions increases in the process water (their Table 2. in ( [Zhu et al., 2011])). In the Syncrude process water used in Zhu *et al.*'s study, the concentration of Ca<sup>2+</sup> is 0.18 mM (7.3 mg/L) whereas it is three times higher (0.57 mM) when the pH is adjusted. It is therefore to be expected that the increase in settling velocity is primarily due to the change in divalent ion concentration.

## 7.5 Conclusions

From the studies presented in this chapter, it can be concluded that:

- Both kaolinite and fine tailings (TFT) exhibited the same electrokinetic behavior as function of pH and ionic strength for added divalent salt and for ionic strengths below 5 mM of added monovalent salt. The kaolinite sample was representative for the behaviour of the TFT sample. Therefore the presence of bitumen or the organic contaminant does not play a dominant role on the flocculation behaviour. Although, the fact that the zeta potential of kaolinite and SP02 differ at ionic strength above 5 mM of added salt might be due to the presence of bitumen in the SP02 samples.
- We confirmed a previous study [Zhu et al., 2011] in which the zeta potential does not depend on pH (controlled by adding HCl and

CO<sub>2</sub>) at reasonable ionic strengths ( < 50 mM of added divalent salt).

- For both kaolinite and fine tailings we found that the apparent zeta potential in an electrolyte containing a majority of monovalent ions decreased in absolute values with decreasing pH.
- Both kaolinite and fine tailings flocculated faster in the presence of a divalent electrolyte compared to a monovalent electrolyte which was in line with the fact that the apparent zeta potential was smaller for divalent salt than for monovalent salt (in absolute values) for any pH at high ionic strength.
- The apparent zeta potential appears to be a good indicator for predicting the flocculation of fine tailings at a reasonable amount of salt (>1 mM). However one should keep in mind that neither the behavior nor the values of this apparent zeta potential (in fact the electrophoretic mobility) as a function ion strength or pH give information about the surface charge of the particles. This could lead to interpretation errors especially in the low ion strength case where the apparent zeta potential indicates flocculation and there is none. Therefore some other formulation (different to Smoluchowski) should be used to calculate zeta potential [Chassagne et al., 2009].

## References

- [Chassagne and Ibanez, 2012] Chassagne, C. and Ibanez, M. (2012). Electrophoretic mobility of latex nanospheres in electrolytes: Experimental challenges. *Pure and Applied Chemistry*, 85(1):41–51.
- [Chassagne and Ibanez, 2014] Chassagne, C. and Ibanez, M. (2014). Hydrodynamic size and electrophoretic mobility of latex nanospheres in monovalent and divalent electrolytes. *Colloids and Surfaces A: Physicochemical and Engineering Aspects*, 440:208–216.
- [Chassagne et al., 2009] Chassagne, C., Mietta, F., and Winterwerp, J. (2009). Electrokinetic study of kaolinite suspensions. *Journal of colloid and interface science*, 336(1):352–359.
- [Clark, 1939] Clark, K. (1939). The hot water method for recovering bitumen from bituminous sand. *Report on Sullivan Concentrator, Alberta Research Council, Alberta Canada*.
- [Clark and Pasternack, 1932] Clark, K. and Pasternack, D. (1932). Hot water separation of bitumen from alberta bituminous sand. *Industrial & Engineering Chemistry*, 24(12):1410–1416.
- [COSIA, 2016] COSIA (2016). COSIA website. <http://www.cosia.ca>. Accessed: 2015-04-30.
- [Gupta and Miller, 2010] Gupta, V. and Miller, J. D. (2010). Surface force measurements at the basal planes of ordered kaolinite particles. *Journal of Colloid and Interface Science*, 344(2):362–371.
- [Hunter, 2013] Hunter, R. J. (2013). *Zeta potential in colloid science: principles and applications*. Academic press.

- [Kasperski, 1992] Kasperski, K. (1992). A review of properties and treatment of oil sands tailings. *AOSTRA Journal of Research*, 8:11–11.
- [Kaya et al., 2006] Kaya, A., Ören, A. H., and Yükselen, Y. (2006). Settling of kaolinite in different aqueous environment. *Marine Georesources and Geotechnology*, 24(3):203–218.
- [Liu et al., 2002] Liu, J., Zhou, Z., Xu, Z., and Masliyah, J. (2002). Bitumen–clay interactions in aqueous media studied by zeta potential distribution measurement. *Journal of colloid and interface science*, 252(2):409–418.
- [Ma and Pierre, 1999] Ma, K. and Pierre, A. C. (1999). Clay sediment-structure formation in aqueous kaolinite suspensions. *Clays and clay minerals*, 47(4):522–526.
- [Ma, 2011] Ma, M. (2011). The dispersive effect of sodium silicate on kaolinite particles in process water: Implications for iron-ore processing. *Clays and Clay Minerals*, 59(3):233–239.
- [MacKinnon, 1989] MacKinnon, M. (1989). Development of the tailings pond at syncrudeâs oil sands plant: 1978–1987. *AOSTRA J. Res*, 5(2):109–133.
- [Mitchell et al., 1976] Mitchell, J. K., Soga, K., et al. (1976). *Fundamentals of soil behavior*. Wiley New York.
- [Morrison, 1970] Morrison, F. (1970). Electrophoresis of a particle of arbitrary shape. *Journal of Colloid and Interface Science*, 34(2):210–214.
- [Solomon and Hawthorne, 1983] Solomon, D. H. and Hawthorne, D. G. (1983). *Chemistry of pigments and fillers*. Wiley.
- [TUDelft, 2015] TUDelft, L. (2015). labs tudelft website. <http://www.labs.tudelft.nl>. Accessed: 2015-04-30.

- [Vane and Zang, 1997] Vane, L. M. and Zang, G. M. (1997). Effect of aqueous phase properties on clay particle zeta potential and electro-osmotic permeability: Implications for electro-kinetic soil remediation processes. *Journal of Hazardous Materials*, 55(1):1–22.
- [Yukselen and Kaya, 2003] Yukselen, Y. and Kaya, A. (2003). Zeta potential of kaolinite in the presence of alkali, alkaline earth and hydrolyzable metal ions. *Water, Air, and Soil Pollution*, 145(1-4):155–168.
- [Zhou and Gunter, 1992] Zhou, Z. and Gunter, W. D. (1992). The nature of the surface charge of kaolinite. *Clays and Clay minerals*, 40(3):365–368.
- [Zhu et al., 2011] Zhu, R., Liu, Q., Xu, Z., Masliyah, J. H., and Khan, A. (2011). Role of dissolving carbon dioxide in densification of oil sands tailings. *Energy & Fuels*, 25(5):2049–2057.





# Chapter 8

## Conclusions

In this chapter we give a general overview of the conclusions from the different chapters of this thesis. Possible applications of the results of this study and some suggestions for further research are also discussed.

### 8.1 Achievements of this research and recommendations

In this thesis we have studied the behaviour of fine grained sediments ( $\leq 10 \mu\text{m}$ ) which is of importance to understand the transport and deposition of clayey material. Fine grained sediments have a dynamic particle size distribution, as the particles can aggregate or break depending on the environmental conditions (salinity, pH, shear stress, organic matter...). We have studied in detail the effect of two polymers in the flocculation processes, and how flocculation affects the following phases of settling and consolidation.

For the flocculants used in this study, anionic polymers together with clay particles form smaller and more compact flocs than cationic flocculants. This does not mean that the flocs formed by anionic polymers are stronger, because they break easily with shear. In the settling phase, the flocs formed by cationic polymers settle faster, with a larger settling velocity. The flocs formed by anionic polymer and clay have a delay in settling phase, as their flocculation depends on the presence of cations

in the system and time is required to form clay/flocculant/cation flocs. When a bed is formed, a difference in the strength of the bed and in its structure is shown. The bed formed by anionic polymers and clay is lower in height than the bed formed only by clay. It has larger permeability and higher effective stresses. A bed formed by cationic polymers and clay is larger in height and has lower permeability and lower effective stress, than the bed formed by anionic polymers, but higher in height and has a lower effective stress than clay bed.

### 8.1.1 Accuracy of the measurements

#### Particle size distribution

Particle size measurements are based on standardized procedures. For instance the BS 1377: Part 2: 1990 standard for sieving and sedigraph, the NEN 5753 standard for sieving, and BS 1377: Part 2: 1990 for hydrometer. Many articles are devoted to the comparison between different devices. It was found that large difference are found in the clay fraction. The difference in fines between sedigraph and Static Light Scattering cause 30%.

In the present thesis, the effect of pre-treatment on Particle Size Distribution measurements was investigated. The recommendation given in this thesis is to not pre-treat natural sediments. Pre-treatment destroys the flocs and the chemicals used are so aggressive that they delaminate the particles (which never happens in situ). Drying the sample and grinding the sample after drying also break the particles and change their structure.

In this thesis, we analyze the differences between the sedigraph, static light scattering (SLS), sieve, and hydrometer. We developed a new protocol for the SLS technique (see chapter 2), that enables to reconcile the values found by sedigraph / hydrometer with those found by SLS. In this new protocol, we have defined how to prepare the sample, and how to separate the different of size ranges to be able to measure the PSD by SLS and obtain similar results than with other techniques. SLS is a very useful tool to assess the dynamics of flocs growth and break-up in time, as explained in chapter 4.

Usually, the accuracy is also based on sampling, and measurement uncertainty. There can be differences in clay concentration, polydispersity in shape and PSD, organic matter content and type, temperature, pH, and salinity at a given location. The accuracy can be assessed by repeating three (or more) times a measurement with three different samples from the same location.

### **$\zeta$ -potential**

There are errors due to the technical limitations of the  $\zeta$ -potential test. For instance, the same sample, measured more than 10 times with the ZetaNano will give a standard deviation of 5 %. The results on the same samples with two different equipments from the same manufacturer give also differences of 5 %. The filling procedure of the cell on the other hand gives significant deviations in the results (30%), as explained in chapter chapter 3. A protocol was therefore devised in order to perform as accurate as possible zeta potential measurements. This protocol consists of filling the cell with the samples always in the same order, starting with the largest salinity and then diluting the samples to lower salinity.

### **8.1.2 Effect of polyelectrolyte on the flocculation, settling and consolidation**

Much work has been done in sanitary engineering to investigate flocculation of sludge through the addition of salts and polyelectrolytes. However, in-situ conditions in a natural environment are different. For instance, shear rates are not constant, as in the case of transport through pipes. In fact shear rates are often cycle in tidal flow and depict seasonal variations. This has a large influence on the floc size and also on the structure of the flocs (see chapter 4 and chapter 5). In particular, flocs created in in-situ conditions have a dynamic size, and we showed that, depending on the type of flocculant used (cationic or anionic), their dynamic behaviour is different.

Salinity is a very important parameter for the flocculation process. Salinity can be low (tap water salinity) whereas in industry the process water is usually compound of ions and poly-ions not representative for in-

situ (poly)ions. Thus we performed new experiments using "low" shears, low ionic strengths, different mixing procedures with demi or tap water in the presence of synthetic polyelectrolytes. Synthetic flocculants were used, to get an idea of the role of positive and negative surface charges on the flocculation, settling and consolidation ability of the samples.

### **Floc size evolution in time ( chapter 4)**

$\zeta$ -potential measurements can be used to predict the optimal flocculant dose when cationic polyelectrolytes are used. Below this optimal dose, flocs formed by cationic polyelectrolyte reconform or erode and their size changes in time. Above this optimal dose, flocs sizes do not vary much in time.

$\zeta$ -potential results give an idea of the surface coverage by anionic polyelectrolytes. The optimal flocculant dose for anionic polyelectrolyte is linked to the cations available in the water.

In a cycle low > high > low shear, flocs formed by cationic polyelectrolyte do not regrow to their original size, whereas flocs formed by anionic polyelectrolyte do. This is most probably due to the fact that the cationic polyelectrolyte is strongly bound to the clay, whereas the anionic polyelectrolyte has a cationic anchoring that can detach/reattach easily upon variations in shear.

### **Settling ( chapter 5)**

The optimal flocculation dose is defined as the dose at which the fastest settling rate is observed and the flocs formed are the densest. Settling column experiments are done to obtain an optimal flocculation dose from this definition. The results of the settling column tests show that the optimal flocculation dose is the same for settling experiments, for SLS and  $\zeta$ -potential experiments.

The influence of mixing methods and mixing time is studied for different polyelectrolytes. It is observed that mixing methods and mixing time have influence on the settling rate. The settling is much lower when the rod method is used in the presence of anionic polyelectrolyte compared to the other mixing method. When cationic polyelectrolyte is

studied, the fastest settling is observed with the jar method. A delayed settling is observed when the hand and jar mixing methods are used in the presence of anionic polyelectrolyte. Summarizing, there is always a delayed setting for anionic poly electrolyte (not for cationic) and for all mixing methods the optimal concentration is the same for anionic polyelectrolyte.

We recommend to be very careful with the mixing procedure used. And we suggest to use always a shear-controlled method to prevent break-up of the flocs. This means to be very careful with the mixing method and calculate the shear used at mixing. Despite the differences in the values of the settling rate, the flocculant to clay ratio that gives the fastest settling velocity for any method is the same. However the size of the flocs obtained is very dependent on the mixing conditions. One should be aware of this fact when doing experiments.

## **Consolidation ( chapter 6)**

The consolidation results confirm the results of chapter 4 flocculation and chapter 5 settling experiments.

We recommend to compare more in detail the settling phase with the bed strength. From the experiments in which polyelectrolytes are used, it is difficult to predict the effective stress from the mud interface data. The structure of bed is open and fluffy due to the polyelectrolyte. Therefore effective stresses should be measured in the sample after the consolidation test is finished. The models used in this thesis need to be improved when polyelectrolytes are used.

Polymers have a large elasticity which makes them very difficult to study and to understand the settling phase. The formation of flocs and the properties of the formed bed should be therefore investigated in relation with chemical engineers.

## **8.2 Application to oil sands**

We showed that  $\zeta$ -potential measurements in the case of oil sand can predict the predominant type of salt (monovalent, divalent) in a sample.

In our study, a majority of divalent salt was found by the  $\zeta$ -potential measurements, and this was confirmed by chemical analysis. The results from chapter 7 shows that kaolinite clay is representative for oil sands samples. The  $\zeta$ -potential and settling measurements show that kaolinite and oil sand samples have a similar behavior. Therefore bitumen and other contaminant do not play a dominant role.

The flocculation ability of a representative oil sand tailing sample was studied as function of pH. We found that varying pH would not increase the flocculation ability, in contrast with a previously published study. We showed that in the previous study changing pH in fact led at the same time to an increase of divalent salt concentration in the system, which in turn led to a better flocculation.

# Summary

This thesis focuses on the coagulation and flocculation processes of cohesive sediments under the influence of polyelectrolyte. For this study clay particles and anionic and cationic flocculants were used. The influence of the shear stresses on the flocculation demonstrated that the shear stress is the parameter that influences the most the break-up and re-grow of the aggregates.

Fine sediment management requires the necessity of understanding what happens between clay particles and flocculant as it affects their flocculation, settling, and the formation of the bed. A good quality soil requires a good de-watering, meaning a quick removal of water, and it should have enough strength at the end of consolidation. This knowledge is of importance for dredging management and end-uses like mining industries, sanitary engineering, dredging engineering will benefit for it and mining industry in which they need to re-use the slurry from their manufacturing.

The understanding of small scale physics helps to predict the flocculation processes. Particle-particle interaction and interaction between particles and flocculants govern these processes. As colloidal particles are responsible for most of the cohesive behaviour of sediment it is important to be able to well estimate the amount of colloidal fraction in a sample. In this thesis a new protocol for determining particle size distributions is developed that reconcile traditional techniques (hydrometer and sedigraph) with Static Light Scattering technique that are currently used. The  $\zeta$ -potential is a very useful tool to better understand flocculation processes. Therefore a detailed  $\zeta$ -potential study of the clay



particles and the flocculant has been done in this thesis. We start with a theoretical study and a comparison between devices. The results from the  $\zeta$ -potential measurements on clay in the presence of flocculant are presented and in the last part of the thesis the  $\zeta$ -potential is used in an application in mining industry.

Flocculation experiments were done by SLS to study first how flocs are growing in presence of flocculants (anionic and cationic). The anionic polymer creates smaller and more compact flocs and the limiting factor of growth was the amount of cations in the water. The cationic polymer creates large and open flocs. The influence of shear stress in the flocculation process was also study. When the flocs formed with anionic polymers were under higher shear stresses they broke, but when the shear was decreased the flocs were able to re-grow almost to the initial size. On the contrary, when the shear was increased in the case of flocs formed by cationic polymers and clay the flocs broke but after decreasing the shear the flocs could not re-grow to their initial sizes.

Settling experiments have been performed as function of column size and different mixing methods. The mixing methods and time have an influence on the settling velocity. The same optimal flocculation dose was obtained from the settling experiments irrespective of the mixing method. Consolidation experiments were performed next. We show that the current models for consolidation should be adapted for studying the consolidation in presence of flocculant. The bed made by clay and cationic flocculant is fluffy and it does not have strength, while the one made by clay and anionic polymer is more compact and it has more strength.

# Samenvatting

Dit proefschrift richt zich op het proces van coagulatie en flocculatie van cohesieve sedimenten onder invloed van een polyelektrolyt. Voor deze studie zijn kleideeltjes en anionische en kationische flocculanten gebruikt. Er wordt in dit proefschrift aangetoond dat het proces van uiteenvallen en opnieuw aangroeien van de aggregaten het meest beïnvloed wordt door de schuifspanningen tijdens het flocculatieproces.

Fijn sedimentbeheer vereist de nodige kennis over wat er precies gebeurt tussen de kleideeltjes en de flocculant, aangezien dit de flocculatie, bezinking, en bodemvorming van het fijne sediment beïnvloedt. Een bruikbaar bodemlaag vereist een goed ontwateringsproces, wat betekent dat het water snel verwijderd kan worden met behoud van voldoende sterkte aan het einde van het consolidatieproces. Deze kennis is belangrijk voor de mijnbouw, sanitaire technieken en in de baggertechniek.

Goede kennis over kleinschalige fysica helpt bij het voorspellen van de flocculatieprocessen. Deze flocculatieprocessen worden namelijk gedomineerd door de interactie tussen deeltjes en de interactie tussen deeltjes en de flocculanten. De colloïdale deeltjes zijn met name verantwoordelijk voor het cohesieve gedrag van het sediment. Het is daarom van groot belang om een nauwkeurige inschatting te kunnen maken van de hoeveelheid colloïdale deeltjes in een monster. In dit proefschrift is een nieuw protocol voor de bepaling van de deeltjesgrootteverdeling ontwikkeld waarbij een combinatie van traditionele technieken (hydrometer en sedimentograph) en Static Light Scattering (SLS) wordt gebruikt.

De zeta-potentiaal is een zeer nuttig hulpmiddel om flocculatiepro-

cessen beter te kunnen begrijpen. Met dit als uitgangspunt is er een gedetailleerde zeta-potentiaal studie van de kleideeltjes en de flocculanten uitgevoerd. Als eerste is er een theoretische studie gedaan en een vergelijking van verschillende apparaten/instrumenten gemaakt. Het resultaat van de zeta-potentiaal metingen op de kleideeltjes in aanwezigheid van flocculanten worden hier gepresenteerd en in het laatste deel van het proefschrift wordt de zeta-potentiaal gebruikt in een toepassing in de mijnindustrie.

SLS experimenten zijn uitgevoerd om te onderzoeken hoe de vlokken groeien in de aanwezigheid van flocculanten (anionisch en kationisch). Het anionische polymeer creëert kleinere en compactere vlokken en de beperkende factor in groei was de hoeveelheid kationen in het water. Het kationische polymeer creëert juist grote en open vlokken. De invloed van de schuifspanning tijdens het flocculatieproces is ook bestudeerd. De vlokken die gemaakt werden van de kleideeltjes en anionische polymeren, onderhevig aan hogere schuifspanning, braken uiteindelijk af. Door de schuifspanning te verlagen konden de vlokken weer opnieuw aangroeien en zich herstellen tot de originele vloggrootte. Daarentegen konden de vlokken die gemaakt werden van kleideeltjes en kationische polymeren bij hogere schuifspanningen zich niet herstellen nadat de schuifspanning verlaagd werd.

Bezinkingsexperimenten zijn uitgevoerd om te bepalen wat het effect is van de kolomhoogte en verschillende mengmethoden. The mengmethode en mengtijd hebben een directe invloed op de bezinkingsnelheid. Dezelfde optimale flocculatie-dosis is bepaald voor ieder bezinkingsexperiment en deze optimale dosis is onafhankelijk van de toegepaste mengmethode.

Daarnaast zijn ook consolidatie-experimenten uitgevoerd. Hier wordt aangetoond dat de huidige modellen voor consolidatie moeten worden aangepast om het consolidatieproces in aanwezigheid van een flocculant te kunnen bestuderen. Het bed dat gevormd wordt door klei en een kationische flocculant is fluffy en niet erg sterk, terwijl het bed dat gevormd wordt door middel van klei en een anionisch polymeer compacter en sterker is.

# Acknowledgments

”Man sacrifices his health in order to make money. Then he sacrifices his money to recuperate his health. And then he is so anxious about the future that he does not enjoy the present; the result being that he does not live in the present or the future; he lives as if he is never going to die, and then dies having never really lived.”

---

Dalai Lama

I would like to thank all the people that have contributed to the fulfillment of this thesis. First I would like to thank my promotor Prof Han Winterwerp. Thanks Han for accepting me as your PhD student when it was still not very clear how could we manage to fund and finalize this work, and also thanks for believing in Claire and me. Special thanks to Claire Chassagne, my daily supervisor, for all her efforts to find the funding for this research work and thanks for believing in me from the beginning. Thanks Claire for everything you have taught me, I have learned a lot with you, and coming from different disciplines, you have shown me how to see the civil engineer world from another perspective (colloidal science) that I think this has been very useful. Thanks also for being there in the bad moments, unfortunately I had a lot of tough periods during my PhD research, but you have been always next to me, being very supportive and as close as a good friend, thanks a lot for everything.

I would like to thank also all my former colleagues from Deltares.

I have worked with several engineers, technicians and scientists from Deltares and I have to thank all of them for what I have learned there. I would like to give special thanks to Walther van Kesteren, it was amazing to work with him and he is one of the persons from who I have learned most. Thanks also to Deltares for allowing me to use its facilities and for making me the engineer I am now due to the professional experience I have gained there.

Many thanks also to all the PhD students from the environmental fluid mechanics lab, thanks to my friend Maria for the time together, and for listening to all my complains. Specially thanks to Victor for all his help solving the problems I had with latex while I was writing this thesis. Thanks also to Zeinab for helping me with some of the tests. I would like to make a special mention to Ad Reniers, who wanted that I would keep a good memory from this research period. And I must say he managed, thanks for being so supportive with Claire and with me and helping us in the financial situation.

On the personal side, first I want to make a special mention to my mother and my brother, they passed away during my research. This work is dedicated to you two. Thanks to them I am the person who I am today, and I have kept fighting in life for everything important as they taught me. They were the two persons that I know would be most proud of me and very satisfied of seeing this thesis finished. Second to my father, that he has been next to me in the difficult moments trying to give me the support that my mum always gave me, of course in a different way, his way. I must say, that is a lot for a character like him, thanks. I want to give special thanks to my husband Miguel, who has also been next to me every day, helping me in the bad and in the good moments. He has trusted me even when I could not keep enough strength to work and to live. Thanks for being my support and my guidance, without you nothing of this would be possible. I cannot forget my little son, he arrives at the end of this research period but he has made me seeing the light and happiness at the end of the path. And also my niece and nephews that make me smile always when I see how easy is to enjoy the childhood.

To finalize, I would like to mention the rest of my family, family in

law and all my friends, my best friend from Soria and the university friends from Madrid in particular, that even though they were not here in the Netherlands, they have been always next to me and they have supported me. And also all the friends that I have made during my time in the Netherlands, thanks for sharing this period of my life and allow me to see life from a different perspective.

I would also like to give special thanks to my Dutch friends Dirk, Tati and Sophie for helping me with the translation of the summary and propositions, to Katherine for checking the English and of course to Pablo Marcos for the design of the cover of this thesis.



# Curriculum Vitae

Maria E Ibanez Sanz was born on 14th June 1983 in Soria, Spain. She completed a scientific high school education at the IES Castilla in 2001. After high school, she started her studies in Civil engineering and a Master degree in Transport and Infrastructure at the Politecnica Universidad in Madrid where she graduated in 2009. After graduating from the Politecnica Universidad of Madrid, Maria started her research on flocculation as a PhD candidate at the section of Fluid Mechanics of Delft University of Technology from 2012 until July 2017. Her work during this period culminated in this thesis. At the same time she was doing her PhD she was also working at Deltares as a consultant engineer in the Ecosystem and Sediment Dynamics department. She is now working at Antea Group Belgium, which she joined in September 2017.

